Design and instrumentation of an experimental system for magnetic refrigeration

Auteur : Parmentier, Justine
Promoteur(s) : Vanderbemden, Philippe; Lemort, Vincent
Faculté : Faculté des Sciences appliquées
Diplôme : Master en ingénieur civil physicien, à finalité approfondie
Année académique : 2016-2017
URI/URL : http://hdl.handle.net/2268.2/3248

UNIVERSITY OF LIÈGE
Faculty of Applied Sciences

Design and instrumentation of an experimental system for magnetic refrigeration

Author:
Justine PARMENTIER

Supervisors:
Vincent LEMORT
Philippe VANDERBEMDEN

Master thesis submitted in partial fulfillment of the requirements
for the Degree of Master of Science in Physical Engineering
Academic year 2016-2017

CONTENTS

LIST OF ABBREVIATIONS

MCM	**M**agneto**C**aloric **M**aterial
MCE	**M**agneto**C**aloric **E**ffect
COP	**C**oefficient **O**f **P**erformance
HEX	**H**eat **EX**changer
CHEX	**C**old **H**eat **EX**changer
HHEX	**H**ot **H**eat **EX**changer
AMR or **AMRR**	**A**ctive **M**agnetic **R**egeneration or **A**ctive **M**agnetic **R**egenerative **R**efrigeration

PHYSICAL CONSTANTS

Magnetic permeability	μ_0	=	$4\pi \cdot 10^{-7}$ $\mathrm{H\,m^{-1}}$
Boltzmann constant	k_B	=	$1.38 \cdot 10^{-23}$ $\mathrm{J\,K^{-1}}$
Gas constant	R	=	8.314 $\mathrm{J\,mol^{-1}\,K^{-1}}$
Planck constant	h	=	$6.626 \cdot 10^{-34}$ $\mathrm{J\,s}$
(reduced)	$\hbar$	=	$1.055 \cdot 10^{-34}$ $\mathrm{J\,s}$

1

INTRODUCTION

For a few years now, people have been aware of the dangers linked to the raise of global warming and to the ozone layer depletion. It is believed that these two are caused by the always growing appetite in power consumption of a population rising way too fast. Refrigeration needs nowadays represent around 15 %, namely a large part, of the global consumption. Steam compression, which is the most widely used refrigeration technology around the globe, is close to reaching its technical boundaries and no longer achieving further improvements. Moreover, in these types of refrigerators, CFCs[1] are utilized, but these gases have an ozone depletion and global warming potential. This is because they are extremely inert and stable due to their strong covalent bonds.

Since the late 1980s protocols have been discussed in order to decrease the use of such nocive gases. The search for alternative, more environmentally-friendly technologies, can no longer be delayed and has become a priority need. A promising replacement candidate is the magnetocaloric effect-based refrigeration. Classical technologies exploit the absorption or release of heat in a working fluid due to a change in its pressure. The magnetocaloric effect, or MCE, is similar but exchanges of heat occur because the material is subjected to a varying external magnetic field.

Refrigerator devices using the MCE have several advantages compared to the classical equipments. First, the absence of CFC allow them to harm much less their environment. They usually involve a solid magnetocaloric material, or MCM, thus the system is more compact and has a higher energy density than one with a gas. Their efficiency is greater than classical devices, with a coefficient of performance whose typical value is 60 %, whereas coefficients for steam compression-based refrigerators cannot overcome 40 %. The MCE devices already existing also show better stability and longevity properties.

Widely studied around the world, this effect was discovered and explained by Weiss and Piccard in 1918. Although lots of people attribute it to Warburg, this latter did not actually observe the effect and the misconception will be explained later on in details. In 1926, Debye and Giauque proposed to use magnetic refrigeration cycles in order to attain very low temperatures. Their technique allowed to reach temperatures below liquid Helium (4 K), and, in 1933, Giauque and MacDougall even experimentally pass the barrier of 1 K for the first time, using paramagnetic salts.

The technology was however not utilized yet for cooling applications until 1976, when Brown managed to build a first prototype based on a magnetic Ericsson cycle. The magnetocaloric material was pure gadolinium and the field was created by a superconducting magnet. In

---

[1]Chlorofluoro-carbons.

1997, another big step was made thanks to the discovery of a material presenting a giant MCE by Percharsky and Gschneidner. Since 2001, permanent magnets have been used instead of superconducting ones, which has increased further the interest for the technology. MCE refrigerator prototypes, especially the ones using active regeneration which will be explained in Chapter 2, are now a real trend around the world.

Nevertheless, two main issues arise: the first one is the fact that a large magnetic field is required for achieving a sufficient temperature span during the cyclic operation of the refrigerator. Typically the magnitude is comprised between 1 and 2 T, but prototypes using slightly smaller (~ 0.5 T) and higher fields (> 5 T) can be found in the literature. The other problem is to find alloys presenting a MCE around room temperature in order to use them for commercial applications. These materials should also be cheap, found in large quantities and be easy to produce. The parent material is indeed pure gadolinium, which is an expensive rare-earth that could not be used for mass production. The best candidates for now are the Fe_2P based compounds.

The present work aims at designing a MCE-based prototype using gadolinium sheets and a 1.05 T cylindrical, Halbach magnet. As it will be described later, usually the variation of the magnetic field is ensured by a relative motion between the MCM and the magnet because a permanent magnet is used such that its values cannot be modified. Electromagnets are not very much widespread since achieving high field values utilizing them yields to many heat losses which are difficult to handle. Two kinds of demonstrators can thus be found: the ones experiencing a reciprocating, linear motion between the magnet and the MCM, and the others in which this motion is rotary. In the present case, the prototype will undergo back and forth movement.

First, the theory related to the MCE will be reviewed in details in Chapter 2, and an example of this one will be applied to gadolinium in order to understand deeper its behaviour. Other possible materials that may be used for magnetic refrigeration will be revised. A brief historical survey will be made, as well as a comparison with other arising, environmentally-friendly technologies. Next, in Chapter 3, a short review of existing prototypes and their main features will be carried in order to fully complete the state of the art.

Chapter 4 then presents a numerical study of the thermal exchanges that should occur during the working of the prototype. Then the fifth chapter studies the behaviour of the force acting on gadolinium plates put inside the Halbach magnet in order to find suitable dimensions for the device. After what the instrumentation needed for performing the measurements during the operation of the demonstrator is presented and tested. At the end of Chapter 5, a summary of all the parts required for the good working of the prototype is performed. The work ends with conclusions on the described topics.

Theoretical calculations, numerical simulations and experimental apparatus are all complementary to each other. The first ones serve in various areas but cannot fully catch the small imperfections of reality. On the other hand, experiments cannot always be carried out easily and the use of numerical tools instead is often of great help. A physicist engineer should be able to make good use of all three of them adequately.

This master thesis is carried in the "Capteurs et systèmes de mesures électriques" lab, at the Montefiore Institute of the University of Liège, under the direction of Philippe Vanderbemden. On the other hand, Vincent Lemort acts as a co-supervisor to bring his expertise concerning the thermal part of the work.

To close this short introduction, one might say that all around the world people have understood they have to face new challenges to replace classical technologies which involve nocive gases. Scientists can no longer rely on past achievements and need to set up new goals. A breath of fresh air is nowadays more than welcome so as to eventually get rid of such harmful technologies.

U - u (J - $J\,kg^{-1}$)   (specific) internal energy

Q - q (J - $J\,kg^{-1}$)   (specific) heat

W - w (J - $J\,kg^{-1}$)   (specific) work

G - g (J - $J\,kg^{-1}$)   (specific) Gibbs free energy

S - s ($J\,K^{-1}$ - $J\,kg^{-1}\,K^{-1}$)   (specific) entropy

S_e - s_e ($J\,K^{-1}$ - $J\,kg^{-1}\,K^{-1}$)   (specific) electronic entropy

S_ℓ - s_ℓ ($J\,K^{-1}$ - $J\,kg^{-1}\,K^{-1}$)   (specific) lattice entropy

S_m - s_m ($J\,K^{-1}$ - $J\,kg^{-1}\,K^{-1}$)   (specific) magnetic entropy

M - σ ($A\,m^{-1}$ - $A\,m^2\,kg^{-1}$)   (specific) magnetization

$\vec{H}$ ($A\,m^{-1}$)   magnetic field

$\vec{B}$ (T)   inductive magnetic field

T (K)   temperature

ΔT_{ad} (K)   adiabatic temperature change

Δs_m ($J\,kg^{-1}\,K^{-1}$)   specific magnetic entropy change

c_H ($J\,kg^{-1}\,K^{-1}$)   specific heat capacity at constant field

2

THE MAGNETOCALORIC EFFECT

In the present chapter will be investigated in details what is the magnetocaloric effect. The basic thermostatic relations describing it will be introduced, after what further investigations will be carried with the help of statistical mechanics. An theoretical example of the MCE in gadolinium will also be presented. Then one will see that several cycles may be utilized in order to build a magnetocaloric effect-based refrigerator. A brief review of the materials that may be used to best exploit this effect will then be made, before going deeper into the history of the MCE. A comparison with other trendy caloric effects will also be realized. Finally, in page 38 one may find a summary of all the important points.

1.   What is the MCE ?

The main characteristics of the magnetocaloric effect will be surveyed in the current section. This effect is an intrinsic property of magnetic materials and can be described in a general manner as *a (reversible) contribution to the thermal response that they exhibit when submitted to an external magnetic field.* Such materials can indeed also experience magnetic hysteresis and eddy currents which may lead to heat losses too.

In this sense, when a regular magnetocaloric material enters the gap of a magnet, it experiences a positive magnetic field variation which results in a heating up of the material, whereas the opposite occurs when the material leaves the gap. There is thus two manners to exploit this effect. One may either use the fact the the material is heated and view it as part of a heat pump, whereas one could think of it as the coolant of a refrigerator. Obviously this latter viewpoint will be considered all along the present work.

1.1   Comparison with a gas compression cycle

In order to conceive e.g. a cooling device based on the MCE, as in every heat engine respecting the second law of thermodynamics, exchanges must be performed through a cycle between a hot reservoir and a cold sink. The typical refrigeration cycle obtained then may be compared with the more classical and well-known gas compression cycle, as depicted in Fig. 2.2.

But first a quick reminder of a refrigeration machine respecting the second law of thermodynamics is presented in Fig. 2.1. The machine operates between a cold sink and a hot reservoir at temperatures respectively denoted T_c and T_h. An amount of work W is used to make the refrigerator extract some heat from the cold source, Q_c, and release Q_h to the hot reservoir.

One sees on the left of Fig. 2.2 a gas compression cycle illustrated with a piston able to compress and relax a gas. A corresponding temperature-entropy $(T-S)$ chart is visible beneath the four stages of the cycle, denoted by letters from (a) to (d). First occurs a compression of the gas by the piston, which heats up the gas by reducing its volume and thus increasing its internal pressure. One assumes that the system during this operation is perfectly thermally insulated from its surroundings and that this step takes place adiabatically.

FIGURE 2.1: Reminder: the classical refrigeration machine.

Next comes a heat transfer between the gas and the hot source, which provokes thus a cooling of the gas. This process occurs at a constant volume, in particular the minimum reached by the piston V_{min}. The third stage consists in an expansion of the gas that is also supposed to occur in an adiabatic manner. This time the gas cools down because its pressure diminishes as its volume increases. Finally, the gas warms up by withdrawing heat from the cold reservoir. This process also takes place in isochoric conditions, but this time the volume reached out by the piston is maximum, namely equal to V_{max}.

The cycle exploiting the MCE may be put in parallel with this gas compression cycle. The main difference lies in the fact that the material exhibiting the MCE replaces the gas, while the action or not of the magnetic field serves as the motion of the piston. The drawings on the right of Fig. 2.2 represent a magnetocaloric material in gray moving in and out of the gap of a magnet (or anything able to produce an inductive field $\vec{B}$) in turquoise.

At first, the MCM is inserted into the magnet yoke and thus submitted to a field which causes a magnetization of the material and an increase in its temperature. This step is assumed to occur without any heat exchange with the surroundings. After that, the material is put in contact with a hot source and its temperature decreases. The magnetic field, however, remains the same all along this stage and equal to H_{max}. Then the MCM is removed from the magnet and thus demagnetized. Its temperature reaches its lowest value. Once again this step is assumed adiabatic. The final step consists in the heat exchange with the cold sink. The material heats up under a constant field H_{min} which is often simply null.

Below the drawings lie two $T-S$ diagrams showing the evolution of the respective cycles. The cycle on the right may serve as a basis for designing a refrigeration demonstrator exploiting the MCE, although it is not the only one, as it will be explained later on. The main components of a device based on the MCE are thus a MCM moving in and out of a magnetic field. One also needs a suitable hydraulic circuit as well as a hot and a cold reservoirs in order to complete the cycle. A few prototypes conceived around the world will be reviewed in the next chapter. But before describing them, the MCE will be detailed in the following sections.
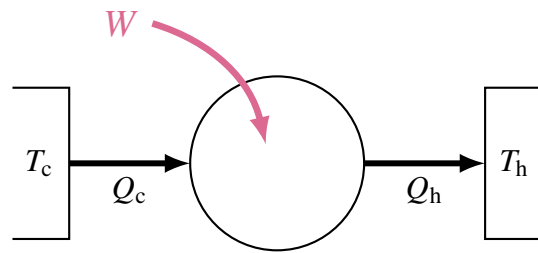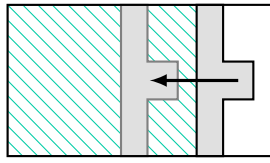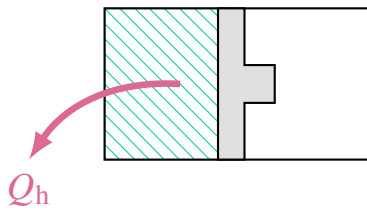
(a) → (b)   adiabatic compression

(a) → (b)   adiabatic magnetization

(b) → (c)   isochoric cooling

Q_h

(b) → (c)   isofield cooling

$\vec{B}$

Q_h

(c) → (d)   adiabatic expansion
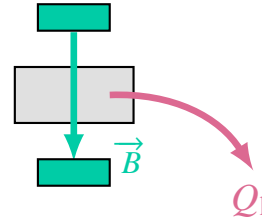
(c) → (d)   adiabatic demagnetization

(d) → (a)   isochoric heating

Q_c
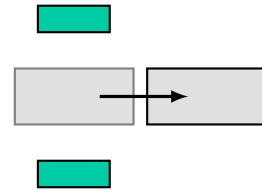
(d) → (a)   isofield heating

Q_c

FIGURE 2.2: Comparison between a classical gas compression cycle (left) and a magnetocaloric cycle (right).

1.2 Phase transitions

Before reviewing the theory describing the MCE, the difference between the phase transitions that materials may experienced should be reminded.

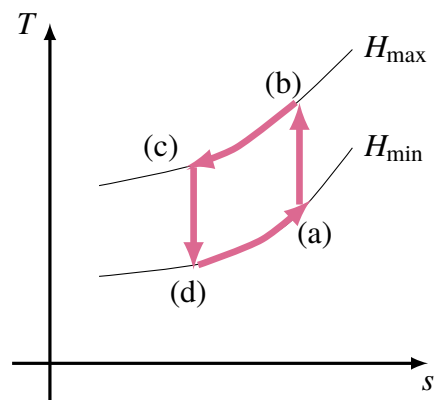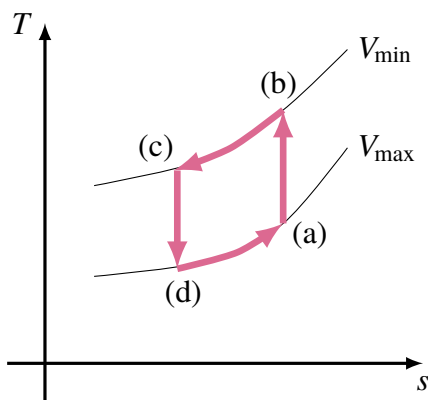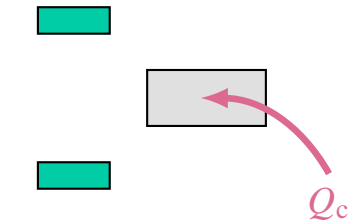A first-order phase transition is not instantaneous and involves two phases of the material in equilibrium as well as a latent heat, whereas the temperature remains constant. Such a transition is accompanied by a discontinuity in the magnetization and entropy with respect to temperature. Therefore, their derivatives display an infinite peak at the transition temperature. In the case of the entropy, this derivative is simply equal to the heat capacity. All three of them are displayed for a typical first-order transition in Fig. 2.3 below.

On the other hand, second-order or continuous phase transitions do not exhibit any discontinuity in thermodynamic variables and do not imply any latent heat. The two phases never both coexist in equilibrium during the transition. Such a behaviour is exposed in the charts of Fig. 2.4 for the specific magnetization, entropy and heat capacity of a material experiencing a second-order phase transition. In all six graphs the Curie temperature, at which the material undergo its phase transition, is represented as T_C.
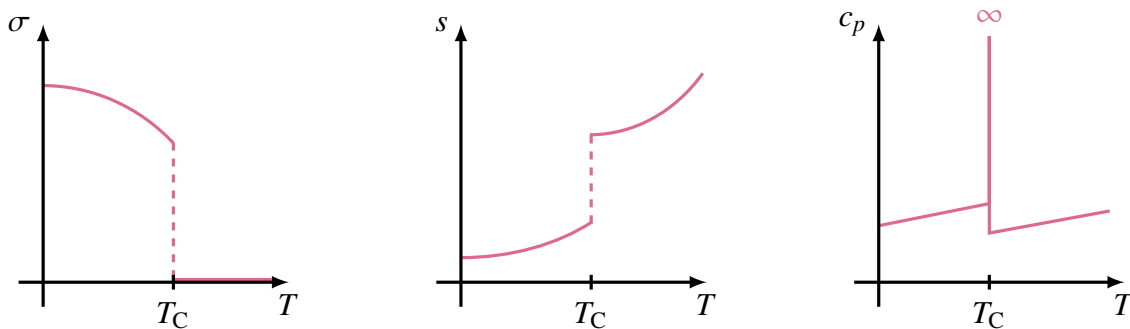
FIGURE 2.3: Specific magnetization σ, heat capacity c_p and entropy s as a function of temperature - typical diagrams for a first-order phase transition.
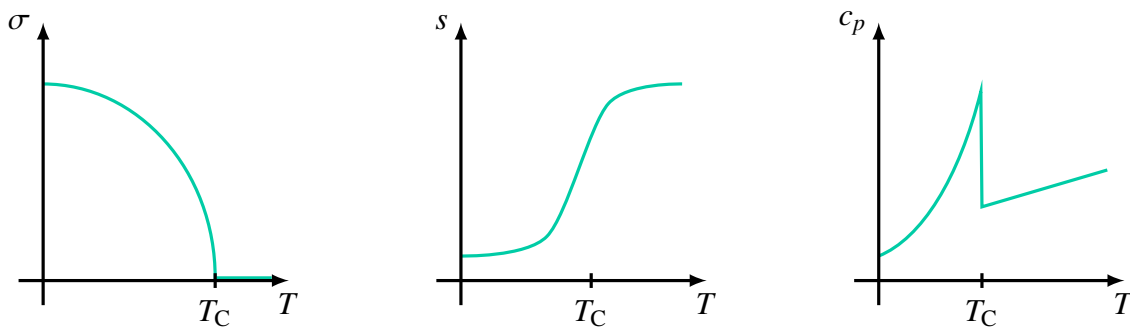
FIGURE 2.4: Specific magnetization σ, heat capacity c_p and entropy s as a function of temperature - typical diagrams for a second-order phase transition.

The MCE might arise at any temperature but it is the most pronounced around the phase transition of the material. In most MCM, this latter mostly consists in the transition from the ferromagnetic, ordered phase towards the paramagnetic phase characterized by disordered, random magnetic moments. Usually ferromagnets are spin-containing materials that are already magnetized or can be magnetized and remain so under the influence of an external field. This definition also holds for e.g. ferrimagnetic and antiferromagnetic materials. Spontaneous

magnetization occurs for instance in iron where there exists a peculiar spin arrangement ; the elementary magnetic dipoles are aligned in a parallel configuration. In paramagnets, there is no particular spin arrangement and the random alignment of the elementary dipoles yields a global null magnetization.

1.3 Thermodynamics[1,2]

Some relations can be derived for understanding better the MCE. This is what will be done is the present section. Due to the fact that the MCE is a reversible process, all the relations below will be written in such a case. It should also be noted that only specific quantities will be used.

1.3.1 Reminders

Before describing in more details the MCE from a mathematical point of view, one should remind some important relations of thermodynamics. The first law states that, for a closed system,

$$\mathrm{d}u = \delta q - \delta w \tag{2.1}$$

with u the internal energy, q the heat and w the work, all expressed per unit mass. The δ symbol represents simply a small variation and accounts for the fact that q and w are not state variables, on the opposite of u, and therefore do not admit a total differential. From the definition of temperature one knows that

$$\mathrm{d}s = \frac{\delta q}{T} \tag{2.2}$$

where s is the specific entropy. In the present case the system considered is a solid, thus the variations of pressure and volume may be neglected. But because this solid will experience magnetic field changes one should write the work variation as

$$\delta W = -\mu_0 \overrightarrow{H} \cdot \mathrm{d}\overrightarrow{M} \tag{2.3}$$

with W the work, $\overrightarrow{H}$ the magnetic field, $\overrightarrow{M}$ the magnetization of the material and μ_0 the magnetic permeability of vacuum. In order to simplify the notations, one may assume the collinearity of vectors $\overrightarrow{H}$ and $\overrightarrow{M}$. If σ designates the specific magnetization, one gets for the work per unit mass

$$\delta w = -\mu_0 H \mathrm{d}\sigma \tag{2.4}$$

The entrance of the material into the magnetic field will cause its magnetization such that the sign of $\mathrm{d}\sigma$ as well as the work contribution $-\delta w$ in Eq. (2.1) will be both positive and bring an increase in the internal energy whereas the demagnetization process will decrease it.

Gathering these relations, one may rewrite the internal energy as

$$\mathrm{d}u = T\mathrm{d}s + \mu_0 H \mathrm{d}\sigma. \tag{2.5}$$

However, the state function best suited for studying phenomena occurring in a material submitted to a magnetic field is the specific Gibbs free energy g, which is defined by

$$g = u + pv - Ts - \mu_0 H \sigma. \tag{2.6}$$

with p the pressure and v the volume per unit mass. Since there are no volume or pressure variations, taking the differential of the former relation yields

$$dg = du - s\, dT - T ds - \mu_0\, \sigma\, dH - \mu_0 H d\sigma \tag{2.7}$$

and one eventually finds by inserting Eq. (2.5) that

$$dg = -s\, dT - \mu_0\, \sigma\, dH. \tag{2.8}$$

1.3.2 Maxwell relation

Because g is a state variable, dg is a total, exact differential. The Schwarz theorem[?] states that a necessary and sufficient condition for the differential of a multiple variables function to be exact is the equality of mixed partial derivatives. One obtains in this case that

$$\frac{\partial}{\partial H}\left(\frac{\partial g}{\partial T}\right)_H = \frac{\partial}{\partial T}\left(\frac{\partial g}{\partial H}\right)_T. \tag{2.9}$$

The differential of g might also writes as

$$dg = \left(\frac{\partial g}{\partial T}\right)_H dT + \left(\frac{\partial g}{\partial H}\right)_T dH. \tag{2.10}$$

Looking at Eq. (2.8) from the previous paragraph, one sees directly that

$$\left(\frac{\partial g}{\partial T}\right)_H = -s \tag{2.11}$$

and

$$\left(\frac{\partial g}{\partial H}\right)_T = -\mu_0 \sigma. \tag{2.12}$$

Therefore, comparing these with Eq. (2.9) above, one finds a Maxwell relation between s and σ as

$$\left(\frac{\partial s}{\partial H}\right)_T = \mu_0 \left(\frac{\partial \sigma}{\partial T}\right)_H. \tag{2.13}$$

1.4 Microscopic understanding of the MCE

Although up to now no distinction was made yet, the total entropy s of a magnetic material can be divided into three contributions: s_e, the electronic entropy of the free electrons inside the material, s_ℓ the lattice contribution coming from the vibrations of the crystal lattice and finally s_m the magnetic entropy due to the magnetization processes. It is assumed that both the

electronic and lattice entropy contributions are only influenced by temperature whereas the third one also depends on the magnetic field. Hence, one gets

$$s(T, H) = s_e(T) + s_\ell(T) + s_m(T, H). \tag{2.14}$$

Thanks to the former relation, the MCE may be understood in the following way. When the material is not submitted to any field, at e.g. ambient temperature, its lattice is ordered in a peculiar manner. The microscopic magnetic moments existing inside the material are not aligned with each other either. But as the MCM is submitted to a positive field variation, these moments align with the main direction of the field, decreasing thus the magnetic entropy. Nevertheless, the process was assumed adiabatic so that there is no possible exchange with the surroundings. The excess magnetic entropy is thus transferred to the two other types of entropy. As the term s_ℓ is increased, the ordering of the lattice diminishes, increasing then the thermal agitation. This is illustrated in Fig. 2.5 hereafter. The same holds for the electronic contribution but the process is mostly governed by the configurational entropy. This thermal agitation being directly related to the temperature of the material, this one raises too.
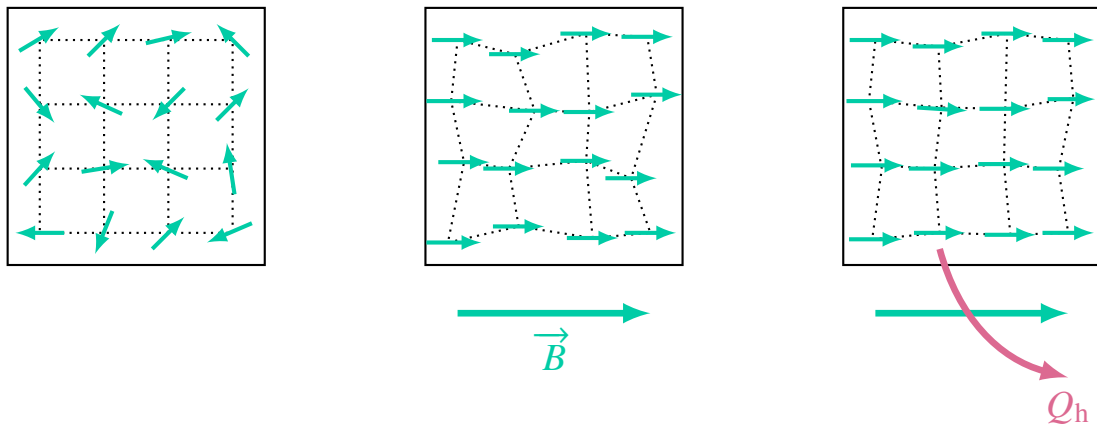

FIGURE 2.5: Scheme of a MCM undergoing a refrigeration cycle: adiabatic magnetization and isofield cooling.
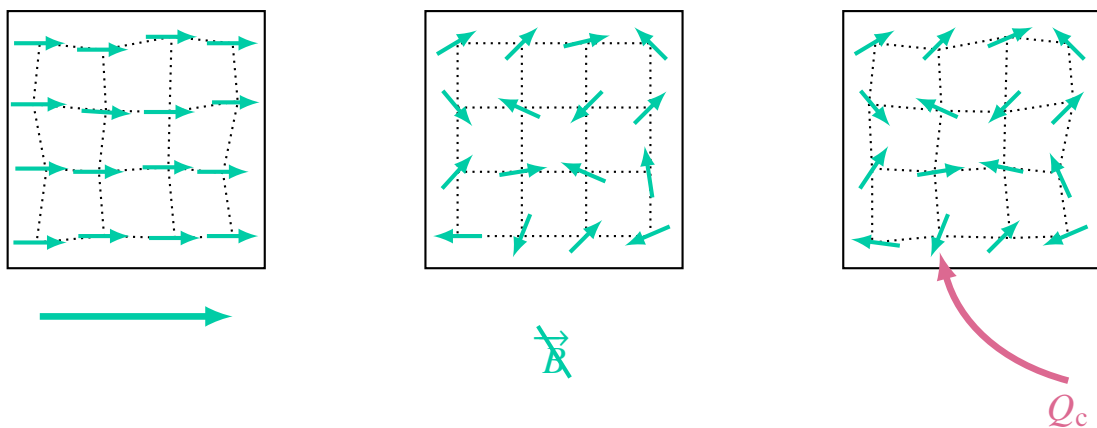

FIGURE 2.6: Scheme of a MCM undergoing a refrigeration cycle: adiabatic demagnetization and isofield heating.

Note that the opposite situation might occur, namely a decrease in temperature as the material is submitted to an increasing field, but it will not be discussed here because it is less usual and will not serve in the following. Such a phenomenon is simply called inverse MCM.

As seen on the right of Fig.2.5 , once the material is put in contact with the hot reservoir, it exchanges heat in such a way that its configurational entropy and hence its temperature both diminish. On the other hand, once the field is removed, the magnetic moments inside the material misalign again, increasing the magnetic entropy. The opposite occurs then: because the process is supposed adiabatic, this additional entropy must come from the material itself. The lattice contribution will thus be reduced in favor of s_m.

When the MCM is put in contact with the cold sink and collects heat from this latter, the thermal agitation inside the MCM rises up and so does the configurational entropy. These two last steps are depicted in Fig. 2.6.

1.5 Characterization of the MCE

There are two ways of characterizing the MCE in a magnetic material. One might either look at its adiabatic change in temperature ΔT_{ad}, or at the isothermal entropy variation Δs, when the material is submitted to a field going from an initial value denoted H_i, and a final one called H_f. This total entropy change reduces simply to the magnetic entropy variation Δs_m because the electronic and lattice entropy parts do not vary in an isothermal process. Both ΔT_{ad} and Δs_m are represented in the chart from Fig. 2.7 on the right.
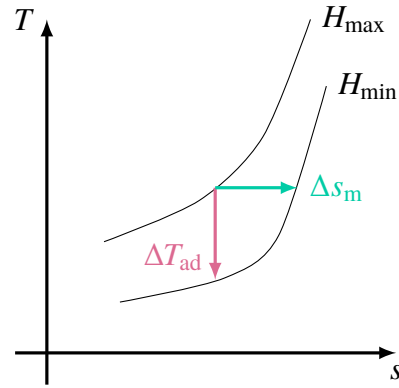
FIGURE 2.7: $T - s$ diagram: representation of ΔT_{ad} and Δs_m.

The total entropy being also a state variable, its differential ds is written in a general manner as

$$\mathrm{d}s = \left(\frac{\partial s}{\partial T}\right)_H \mathrm{d}T + \left(\frac{\partial s}{\partial H}\right)_T \mathrm{d}H. \tag{2.15}$$

Consequently, if the system is submitted to magnetic field variations but kept at a constant temperature, the first term of the former relation cancels out. Taking into account the aforementioned Maxwell relation of Eq. (2.13), it yields

$$\mathrm{d}s = \mathrm{d}s_m = \mu_0 \left(\frac{\partial \sigma}{\partial T}\right)_H \mathrm{d}H. \tag{2.16}$$

Integrating this between the initial and final field values, it becomes

$$\Delta s_m = \int_{H_i}^{H_f} \mu_0 \left(\frac{\partial \sigma}{\partial T}\right)_H \mathrm{d}H. \tag{2.17}$$

In the case of a temperature variation made under adiabatic conditions, ds cancels out in Eq. (2.15) and one finds that

$$\left(\frac{\partial s}{\partial T}\right)_H dT = -\left(\frac{\partial s}{\partial H}\right)_T dH. \tag{2.18}$$

If one reminds that the specific heat capacity c is defined as follows,

$$c = \frac{\delta q}{dT}, \tag{2.19}$$

in the case of an isofield process, one gets

$$c_H = \left(\frac{\partial s}{\partial T}\right)_H T \tag{2.20}$$

with c_H the specific heat capacity of the material under constant field and where Eq. (2.2) in page 9 was utilized. Therefore, Eq. (2.18) turns into

$$dT = -\frac{T}{c_H}\left(\frac{\partial s}{\partial H}\right)_T dH. \tag{2.21}$$

Integrating once again between H_i and H_f, one gets

$$\Delta T_{ad} = -\int_{H_i}^{H_f} \frac{T}{c_H}\left(\frac{\partial s}{\partial H}\right)_T dH. \tag{2.22}$$

For understanding deeper the MCE from a quantum mechanics point of view, the reader is referred to the report[3] from de Oliveira and von Ranke.

1.6 About the entropy term[4,5,6,7]

In this particular section the entropy S rather than the specific entropy s will be used. As a reminder, in Eq. (2.14) from page 11 the total entropy was decomposed in three different contributions as

$$S(T, H) = S_e(T) + S_\ell(T) + S_m(T, H). \tag{2.23}$$

These three terms may all be computed using well-knwon relations from statistical mechanics as well as the Weiss molecular field theory.

First the electronic contribution to the total entropy is given by

$$S_e(T) = \gamma T, \tag{2.24}$$

with γ ($J\,K^{-2}$) the electronic heat capacity coefficient. This relation is obtained by applying the model of an ideal non-relativistic Fermion gas to the conduction of electrons in a metal. Because the spacing between the conduction bands in such a case are very small compared to $k_B T$, k_B being the Boltzmann constant, the bands may be approximated as a quasi-continuum. Hence, the probability that a level of energy ε is occupied by two electrons, $f(\varepsilon)$, is computed

using the Fermi-Dirac statistics as

$$f(\varepsilon) = \cfrac{1}{1 + \exp\left(\cfrac{\varepsilon - \varepsilon_{\mathrm{F}}}{k_{\mathrm{B}}T}\right)}, \tag{2.25}$$

where ε_F designates the Fermi level. After some calculations, one finds for the temperature dependence of the entropy the relation of Eq. (2.24). The γ coefficient that appears in it is obtained as

$$\gamma = \frac{\pi^2}{2}\frac{Nk_{\mathrm{B}}}{T_{\mathrm{F}}} \tag{2.26}$$

with N the total number of particles and T_F the Fermi temperature. This one is a reference temperature for the material defined as

$$T_{\mathrm{F}} = \frac{\varepsilon_{\mathrm{F}}^0}{k_{\mathrm{B}}}, \tag{2.27}$$

where $\varepsilon_{\mathrm{F}}^0$ states for the Fermi level at a temperature of 0 K. However, the contribution from the conduction electrons is weak and may be neglect compared to the configurational entropy.

The lattice contribution, on the other hand, can be calculated using

$$S_\ell(T) = R\left[-3\ln\left(1 - \mathrm{e}^{-\frac{T_{\mathrm{D}}}{T}}\right) + 12\left(\frac{T}{T_{\mathrm{D}}}\right)^3 \int_0^{\frac{T_{\mathrm{D}}}{T}} \frac{y^3}{\mathrm{e}^y - 1}\mathrm{d}y\right] \tag{2.28}$$

with R the universal gas constant, and T_D the Debye temperature given by

$$T_{\mathrm{D}} = \frac{\hbar\omega_{\mathrm{D}}}{k_{\mathrm{B}}}. \tag{2.29}$$

In the former definition, $\hbar$ is the reduced Planck constant and ω_D denotes the Debye frequency relative to the material. These relations come from the Debye model for the total number of phonons propagating in a crystal of N atoms at thermal equilibrium. In this case the number of phonons corresponding to a given ω and thus an energy $\hbar\omega$ is obtained through the Bose-Einstein distribution law for a null chemical potential, namely

$$n_{\mathrm{ph}} = \cfrac{1}{\exp\left(\cfrac{\hbar\omega}{k_{\mathrm{B}}T}\right) - 1}. \tag{2.30}$$

Based on this as well as an assumption made by Debye, the internal energy of the system can be derived, and from that the heat capacity. After some more calculations the configurational entropy of Eq. (2.28) may be found easily.

It should be noted that the Debye temperature characterizes the limit above which the Dulong and Petit's law is acceptable.[8] This law states that the heat capacity evolves linearly with respect to temperature. Under T_D, this approximation is no longer valid and one should take into account the Debye contribution predicting that the heat capacity increases as the cube of the temperature.

In a subsequent section the MCE will be derived graphically for a peculiar material and this restriction should not be forgotten at that point.

Last but not least, the magnetic entropy might be computed as follows

$$S_{\mathrm{m}}(x) = R \left[\ln \left(\frac{\sinh \left(\frac{2J + 1}{2J} x \right)}{\sinh \left(\frac{1}{2J} x \right)} \right) - x B_{\mathrm{J}}(x) \right]. \tag{2.31}$$

This equation comes from the Weiss molecular field theory. Based on the theory already developed for paramagnetism, Weiss provided a model for explaining ferromagnetism[1]. He suggested that the alignment of the magnetic moments inside a domain occurred spontaneously, and that the alignment of each of these moments was due to an internal magnetic field arising from all the other moments existing inside the domain.

Ferromagnetic phases are indeed characterized by distincts domains arising in the material, where all magnetic moments are aligned with each other, compared to e.g. paramagnetic phases where no spontaneous magnetization occurs. For paramagnets, only an external field may yield a magnetization because the magnetic moments are all misaligned whereas this magnetization appears naturally in ferromagnets. However, in soft ferromagnets the domains themselves are arranged randomly which causes the global magnetization of the material to cancel, while in strong ferromagnets this does not occur and these material may thus serve as permanent magnets.

The extra field, called B_{int}, is supposed proportional to the magnetization of the sample. The total inductive magnetic field B_{tot} experienced by a material is then given by the sum of any external field B_{ext} and this internal field as

$$B_{\mathrm{tot}} = B_{\mathrm{ext}} + B_{\mathrm{int}} \tag{2.32}$$
$$= B_{\mathrm{ext}} + \mu_0 \lambda M. \tag{2.33}$$

In the former relation, λ is called Weiss molecular field coefficient and is relative to the material. Introducing this into the equations obtained for the paramagnetism through quantum mechanics, similar relations may be obtained for ferromagnets.

Without any further details, the magnetization M in paramagnets is given by

$$M = N g_J \mu_B J \mathcal{B}_J(x), \tag{2.34}$$

where N is the total number of magnetic moments (be careful, this is not the same as in Eq. (2.26)), g_J the Landé factor, μ_B the Bohr magneton, J the total angular momentum, while $\mathcal{B}_J$ is the Brillouin function defined as

$$\mathcal{B}_J(x) = \frac{2J + 1}{2J} \coth \left(\frac{2J + 1}{2J} x \right) - \frac{1}{2J} \coth \left(\frac{1}{2J} x \right). \tag{2.35}$$

---

[1]Even though it was not discussed yet, gadolinium has a ferromagnetic phase and this is the reason this theory appears right here. Above its Curie temperature it is paramagnetic.

On the other hand, the variable x represents the ratio between the Zeeman energy of a magnetic moment into an external field B_{ext} and the thermal energy, and is therefore given by

$$x = \frac{g_J \mu_B J B_{ext}}{k_B T}.$$ (2.36)

For ferromagnets, the results above are adapted simply by introducing the total field of Eq. (2.33) instead of the external field alone into the previous relation, which yields for x

$$x = \frac{g_J \mu_B J}{k_B T} \left(B_{ext} + \mu_0 \lambda M \right) \cdot$$ (2.37)

After some manipulations , one might find that

$$x = \frac{g_J \mu_B J B_{ext}}{k_B T} + \frac{3 T_C J \mathcal{B}_J(x)}{T (J + 1)}$$ (2.38)

where T_C is the Curie temperature of the material, defining its transition between the ferromagnetic and the paramagnetic phases.

2. Main magnetocaloric materials

This section aims at presenting the materials best suited for exploiting properly the MCE, namely the ones called magnetocaloric materials. The most known of them is gadolinium, but its alloys as well as other compounds might be used too.

2.1 The gadolinium

Gadolinium is the 64th chemical element from the periodic table. This metal belongs to the lanthanide series. It shows a lot of interesting qualities such as improving the properties of some metals or having a large neutron absorption capacity. It is therefore used e.g. in radiography or in nuclear reactors.

However, the property the most interesting in this context is certainly the MCE exhibited by gadolinium at 293 K, namely room temperature. It is around this particular temperature that the metal undergoes a phase transition from the ferromagnetic to paramagnetic phase. The temperature at which the transition occurs is named the Curie temperature and corresponds to the one mentioned at the end of section 1.6.

2.2 Giant MCE

Some materials exhibit what is called the giant magnetocaloric effect. The magnetic entropy difference that they exhibit is much larger than for conventional materials. It can be up to between 2 and 5 times bigger than in these materials.

The interest for the MCE-relate technologies has really started thanks to the discovery of such materials working at room temperature by Gschneidner and Percharsky twenty years ago. They found out that the magnetic entropy change in $Gd_5(Si_2Ge_2)$ is 50 % larger than in pure Gd

that occurred at a temperature a bit smaller than in this latter material. Since then, many other alloys have been found to exhibit a giant magnetocaloric effect.

2.3   Other materials and alloys[9,10,11]

Numerous other materials may also exhibit a magnetocaloric effect. The MCE was first discovered in Iron and the most famous MCM is gadolinium ; they both are simple elements, but the research on alloys is much more widely spread. Such materials often present a giant MCE at sub-room temperature.

A first class of magnetocaloric alloys is the $Gd_5 (Ge_{1-x}Si_x)_4$ type, for $0.3 \leq x \leq 0.5$. For all x values these alloys are ferromagnetic at low temperature and all present the same molecular structure. Close to the ambient temperature, depending on the value of x, the compounds take distinct crystallographic phases. The transition temperature depends on the phase of the material and thus on its composition. Such alloys exhibit not only a MCE but also other properties enhancing the coupling between electronic structure and lattice, such as an anomalous electrical resistivity or a large magnetoresistance effect in some cases.

The main issue appearing when using these materials for magnetic refrigeration is first the fact that MCE is usually observed below room temperature. Besides this, impurities inside the material such as carbon, oxygen and iron can influence the crystallographic phase of the material and thus have a direct impact on the MCE experienced by the material or yield a thermal hysteresis. The size of the MCE is thus strongly correlated to the quality and the preparation of the starting material. Such a high sensitivity to impurities plays an important role in the production costs of e.g. a magnetocaloric refrigerator. One might note that compounds such as $R_5 (Ge_{1-x}Si_x)_4$ can also present a MCE, with structural properties similar to that of the alloy with R = Gd.

Another type of magnetocaloric materials are the $La (Fe, Si)_{13}$ (Si can be replaced with Al). The transition temperatures vary with the iron content of the compound, going from 200 K for rich compounds to 262 K when the iron content is lowered. On the opposite of the first family of MCM described above, the phase transition here is not accompanied by a structural change, and the materials keeps its structure above and below its Curie point.

In order to increase the Curie temperature of these alloys, a technique used is to expand the lattice, which yields an increase in ferromagnetic exchanges. This may be achieved by hydrogenation or introduction of other small atoms such as B, C or N. In $La (Fe, Al)_{13}$, an increase of T_C to almost 900 K can be obtained. However, hydrogen is still the most promising interstitial element for these alloys.

Despite its great Curie temperature modulation, the $La (Fe, Si)_{13}$ type of alloy is also interesting from a cost point of view, because La is the cheapest lanthanide available and Fe and Si can be found easily in large amounts. Some precautions need however be taken into account during the process. As en example, when subjected to the hydrogenation process, it may experience some volume changes and if those are performed too frequently the material might end up breaking into small grains.

A third family is the MnAs based compounds, which are similar to the $Gd_5 (Ge_{1-x}Si_x)_4$ from a crystallographic structure point of view. They also experience a structural change when going from the ferromagnetic to the paramagnetic phase, at a temperature of 307 K.

The reverse transition occurs, on the other hand, at 317 K. The material is thus subjected to a thermal hysteresis, and very large magnetic entropy changes are observed during this transition. Concerning the costs, they are quite low but processing of alloys that contain As is tough because of the biological activity of As.

Last but not least, another family that can be mentioned is the Fe_2P based compounds. It is the best candidate for commercial magnetic refrigeration because it has a lot of interesting qualities.

First, this type of alloy show a large MCE because of the field-induce first-order magnetic phase transition which is reversible in both temperature and alternating field. There is thus no hysteresis. Moreover, a tunable temperature span of between 200 and 450 K is achieved with these compounds. Its low cost is another non negligible aspect ; however, as for the MnAs based compounds, the As should be treated with great care.

The most studied series between the possible alloys is the $MnFe(P, As)$ one. The critical temperature varies in this case between 150 K up to well above the room temperature. Such a compound may be synthesized starting from Fe_2P, $FeAs_2$, Mn chips and P powder. It presents a large variety of crystalline and magnetic phases.

All these materials present their advantages and their drawbacks. When one wants to design e.g. a cooling device based on the MCE, the choice of the material used is mostly dictated by the fact that one wants a giant MCE around room temperature at low cost, but other parameters could be taken into account depending on the application. The study of new, affordable materials presenting a large MCE at room temperature is still an active field of research.

2.4 Hysteresis

The materials of interest for magnetocaloric refrigeration thus include rare-earth-based ferromagnets such as Gd or Gd-Fe, with a Curie point close to the room temperature. Other alloys like Gd-Ge-Si present a giant magnetocaloric effect due to a first-order phase change caused by the presence of an external magnetic field. All these materials may however show a hysteresis effect which can affect their physical properties.

In the framework of the classical thermostatics theory explained in previous sections, all material variables can be described, e.g. one can find the adiabatic change of temperature that a MCM undergoes, or its entropy variation as the external field is made to vary. One might also derive the performance of a thermodynamic cycle based on a $T - S$ diagram. However, all these relations hold because the system is considered reversible and thus always at equilibrium. In reality, the $T - S$ diagram should display a hysteresis and it does no longer suffice to describe entirely the material behaviour. Internal entropy production occurs during the (de)magnetization processes, which is the fundamental characteristic of irreversibility.

To take hysteresis effects into account in the formerly developed theory, one should use a peculiar out-of-equilibrium approach, in which the constitutive relation is replaced by the entropy balance equation, namely,

$$\delta s = \delta_i s + \delta_e s, \tag{2.39}$$

where $\delta_e s$ is the usual exchanged entropy but the term $\delta_e s$ is a new entropy production term that represents the underlying irreversibility of the hysteresis. A model accounting for this

phenomenon was developed by Basso et alt.[12] ; Wada et alt. also treated hysteresis in Mn compounds.[10]

3. MCE in gadolinium: graphical representation

In section 1.5 in page 12, the MCE was generally characterized through its adiabatic change in temperature and its isothermal magnetic entropy variation. Each of them is material-dependent and one might ask what are their typical values in the case of gadolinium. Graphical representations of the magnetization versus magnetic field or temperature and other variables will thus be drawn in the present section in order to have a better understanding of the behaviour of this material. In the following, all the graphs expect the one of Fig. 2.8 will be drawn as a function of temperature ; the range covered will always go from 0 K to 450 K, which allows to capture the main physical phenomena occurring inside the material.

T_C (K)	T_D (K)	J	g_J	μ_B (J T^{-1})	N	λ
293	184	−3.5	2	$9.274 \cdot 10^{-24}$	$6.022 \cdot 10^{23}$	59

TABLE 2.1: Material parameters relative to gadolinium which are involved in the MCE mathematical model.

To lay out such diagrams, the theory exposed in section 1.6 will be applied to the particular case of gadolinium. The equations are simply solved with the symbolic calculating tools of MATLAB. Table 2.1 displays the values of the different material parameters involved which come from the literature.[4,5,13]

In Fig.2.8 below is sketched the dependence of specific magnetization σ to the intensity of the magnetic field B. Different curves were drawn for distinct temperatures, varying by steps of $\Delta T = 5$ K between 283 K and 323 K. One should note that because there is no actual sample nor precise quantity of gadolinium to analyze, the magnetization M was divided not by a mass but by the density of the solid material ρ_s.

As one would expect it regarding Eqs (2.34) to (2.38) in page 15, as the field increases, so does the magnetization inside the material. On the opposite, when the temperature is raised, the magnetization decreases. One might note that below $T_C = 293$ K, the magnetization has a finite value at a null magnetic field. This is depicted by the first two curves drawn in turquoise and pink. Such a result emphasizes the ferromagnetic phase of gadolinium. Above T_C there is no spontaneous magnetization at $B = 0$ T and all the curves include the origin of the axes.

The fact that the magnetization decreases with temperature for a given field may be understood in the following way: as the magnetic moments existing inside the material have a greater thermal agitation, namely when the temperature of the material rises, it is then harder for them to remain aligned in a particular direction since they all have a higher energy. Consequently, for
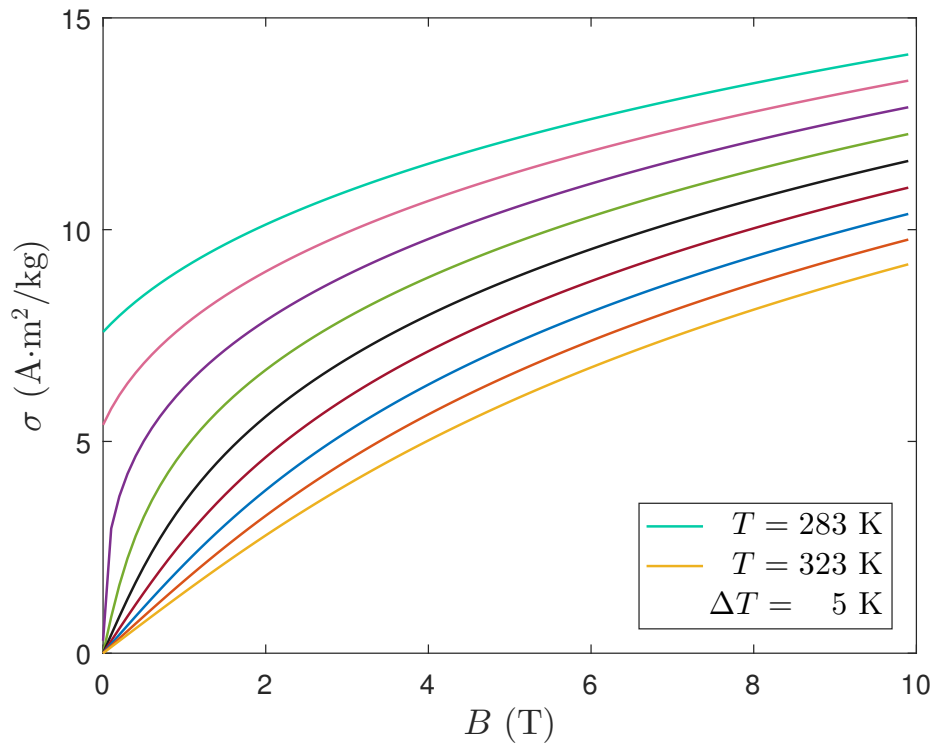
FIGURE 2.8: Magnetization M as a function of the magnetic field B, with the temperature T going from 283 K to 383 K by steps of $\Delta T = 10$ K.
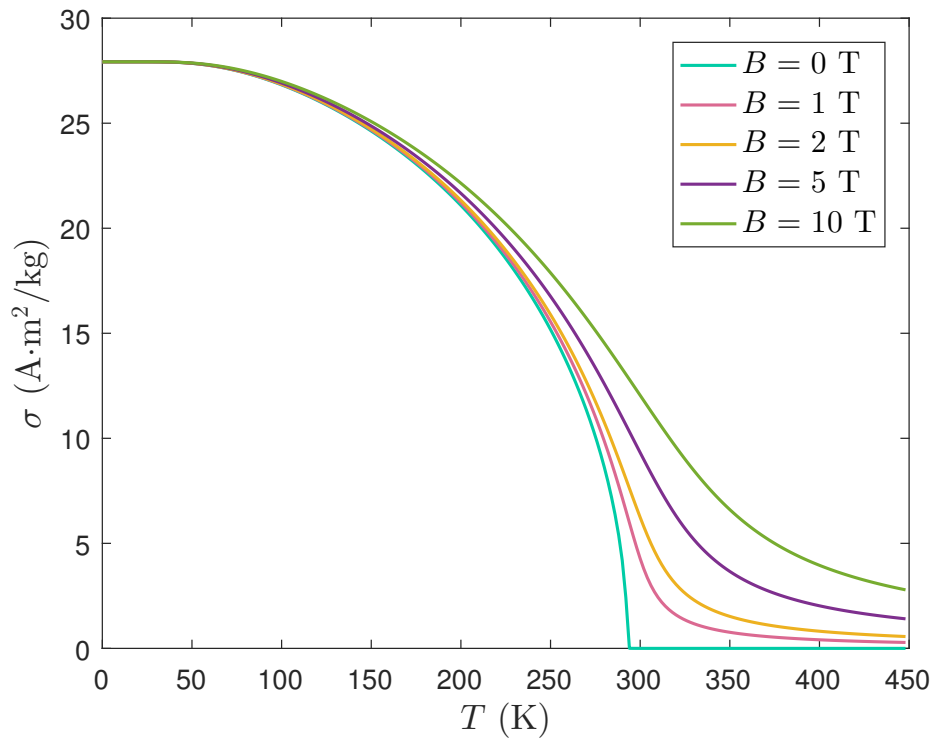

FIGURE 2.9: Specific magnetization σ as a function of the temperature T, for different values of the magnetic field B: $B = 0$ T, $B = 1$ T, $B = 2$ T, $B = 5$ T and $B = 10$ T.
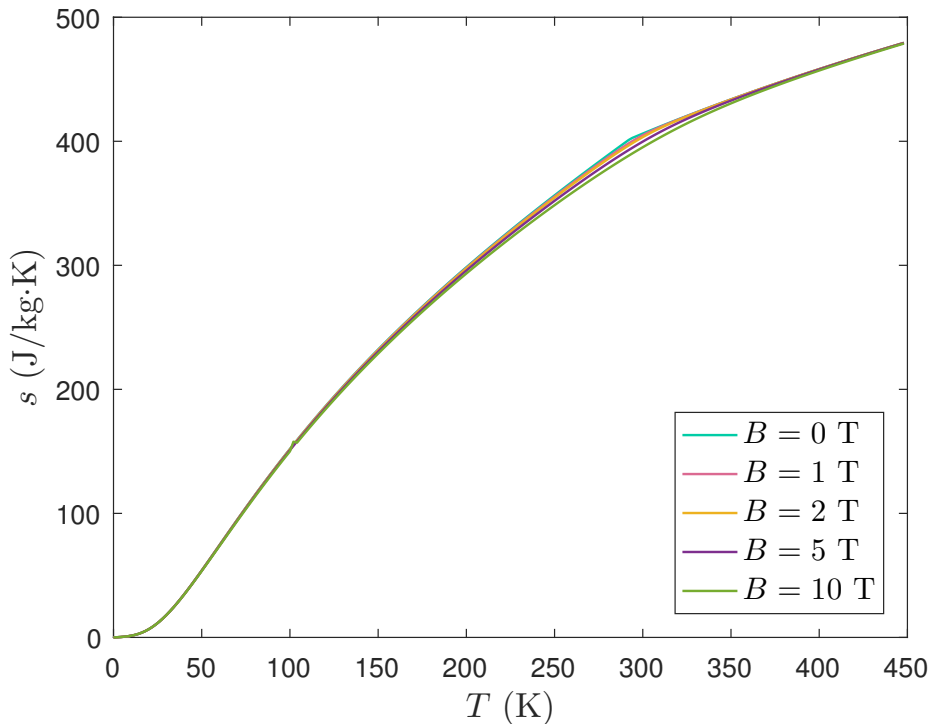
FIGURE 2.10: Total specific entropy s as a function of the temperature T, for different values of the magnetic field B: $B = 0$ T, $B = 1$ T, $B = 2$ T, $B = 5$ T and $B = 10$ T.

a given field, they will less and less tend to align correctly as T increases. This behaviour is also illustrated in Fig. 2.9 showing the specific magnetization as a function of temperature for distinct field values, in particular $B = 0$ T, $B = 1$ T, $B = 2$ T, $B = 5$ T and $B = 10$ T.

In this chart one may once again see that below $T_C = 293$ K, a spontaneous magnetization exists inside the material. This one decreases with temperature and without any external field, as shown by the turquoise line, drops to zero above the Curie point. Such a behaviour corresponds in reality to the transition towards the paramagnetic phase of the gadolinium. Despite this latter, for a finite magnetic field value, σ remains different from zero above T_C.

Fig. 2.10 represents the total specific entropy s with respect to the temperature T, for values of the magnetic field B comprised between 0 T and 10 T. Because the curves are very close to each other, a zoom made onto the behaviour around the Curie point is visible in Appendix **??**.

As a reminder, the total entropy varies in the present case because of three main contributions: the magnetic entropy, the lattice entropy and the entropy related to conduction electrons. This latter is a linear function of temperature and does not have a great influence of the total entropy. The configurational entropy representing the influence of thermal agitation, it logically increases with temperature. The magnetic entropy does too below the Curie point. Such a behaviour is depicted in Fig. 2.11 above. One sees however that above T_C the magnetic contribution remains constant at a null magnetic field and decreases less faster for finite values of B. This is the reason why the total entropy curve presents a discontinuity at T_C for the case $B = 0$ T and a change of slope for the other lines. Finally, one might notice the cubic behaviour of the total entropy at very low temperatures, when $T \to 0$ K, which comes from the configurational contribution and was reminded in page 14 (Debye model of the phonons in a crystal).
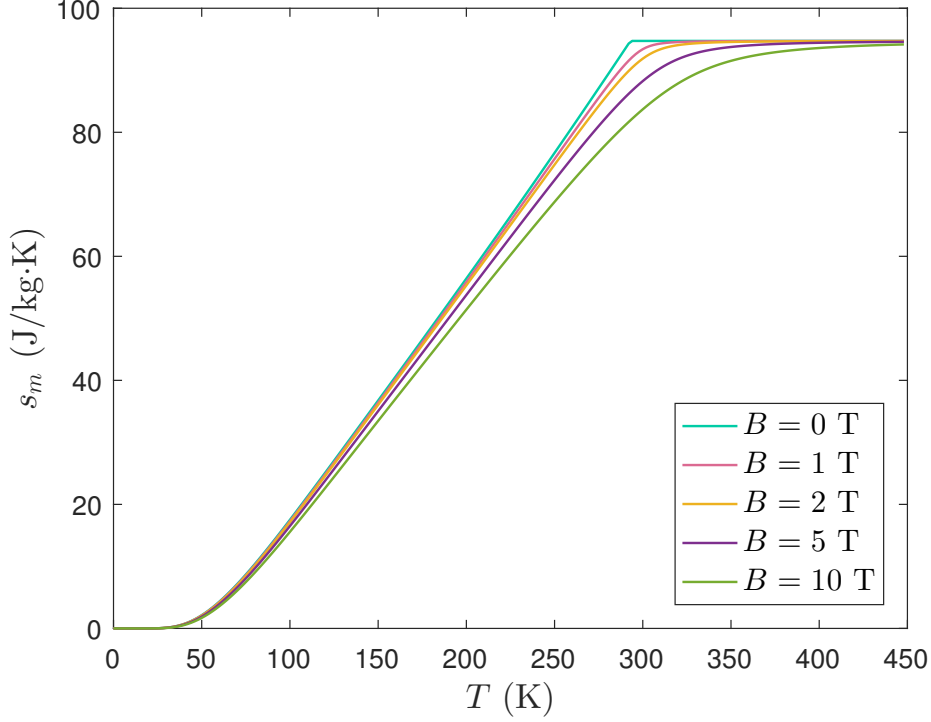
FIGURE 2.11: Specific magnetic entropy s_m as a function of the temperature T, for different values of the magnetic field B: $B = 0$ T, $B = 1$ T, $B = 2$ T, $B = 5$ T and $B = 10$ T.

Talking about the discontinuity of simply the change in the slope of the total entropy, Fig. 2.12 displays the specific heat capacity c_H as a function of temperature, for different field values going once again from $B = 0$ T to $B = 10$ T. The specific heat capacity at constant magneticfield is, as a reminder, given by

$$c_H = \left(\frac{\partial s}{\partial T}\right)_H T,$$

that is, it simply corresponds to the derivatives of the curves from Fig. 2.10 multiplied by the temperature. One sees that below T_C, the heat capacity increases, reaches a maximum then experiences a sudden decrease in the case $B = 0$ T, this variation becoming smoother as the value of the field is augmented. The peak exhibited by the curve in Fig. 2.12 is called a "λ anomaly"[14] due to its resemblance with the Greek letter.

In Fig. 2.13 is drawn the specific magnetic entropy variation Δs_m. This one is computed in an easier manner than by solving Eq. (2.17). One might just take the difference between the curves found in Fig. 2.11 to perform

$$\Delta s_m(T, \Delta B = B_f - B_i) = s_m(T, B_f) - s_m(T, B_i) = s(T, B_f) - s(T, B_i). \tag{2.40}$$

In this relation, the difference between the magnetic entropy values for different fields but at the same temperature is equal to that between total entropy values since the lattice and electronic contributions do not depend on the field. One should note that the value of Δs_m as defined in the previous equation is always negative. Hence one draws instead the opposite of Δs_m. The results obtained in Fig. 2.13 are displayed for B varying between $B_f \in \{1, 2, 5, 10\}$ T and $B_i = 0$ T.
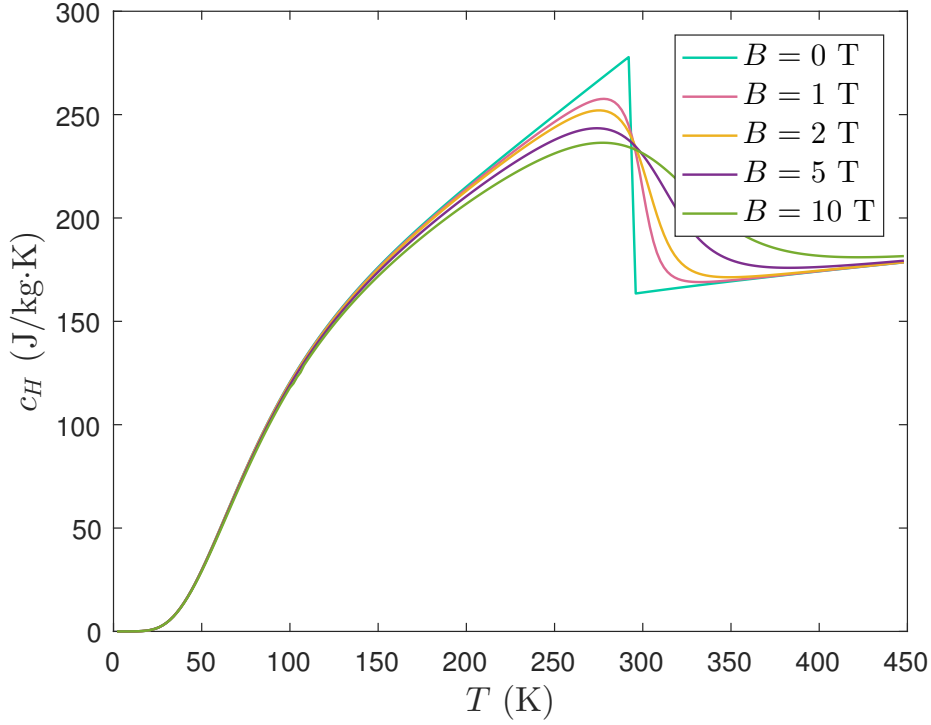
FIGURE 2.12: Total specific heat capacity c_B as a function of the temperature T for different values of the magnetic field B: $B = 0$ T, $B = 1$ T, $B = 2$ T, $B = 5$ T and $B = 10$ T.

As it may be imagined by looking at the graph from Fig. 2.11, at first Δs_{m} increases with temperature because the curves move away from each other. Around the Curie point the variation of entropy is at its maximum, as expected. This is around this temperature that the magnetocaloric effect inside the material is the most pronounced. One T_{C} has been overcome, the lines from Fig. 2.11 start getting close to each other and Δs_{m} decreases.

The last diagram of Fig. 2.14 shows the adiabatic change of temperature experienced by the material versus the temperature. This variation corresponds, for a given entropy value, to the difference between the temperature of any curve drawn for $B \neq 0$ T and the line corresponding to $B = 0$T, namely

$$\Delta T_{\mathrm{ad}}(s, \Delta B = B_{\mathrm{f}} - B_{\mathrm{i}}) = T(s, B_{\mathrm{f}}) - T(s, B_{\mathrm{i}}). \tag{2.41}$$

One might note that compared to the magnetic entropy variation, the change in temperature is always positive.

Gadolinium is not the only material experiencing MCE for which such theoretical graphs might be derived and, for other MCM, parameters should simply be changed accordingly. Measurement methods that will be described afterwards should allow to find experimentally all the curves drawn in this section but on a much shorter range of values because it is not always easy to reach very low temperature or to maintain adiabatic conditions in every cases to perform the measurements. These theoretical curves present the interest of permitting to cover all the possible temperature and field values.
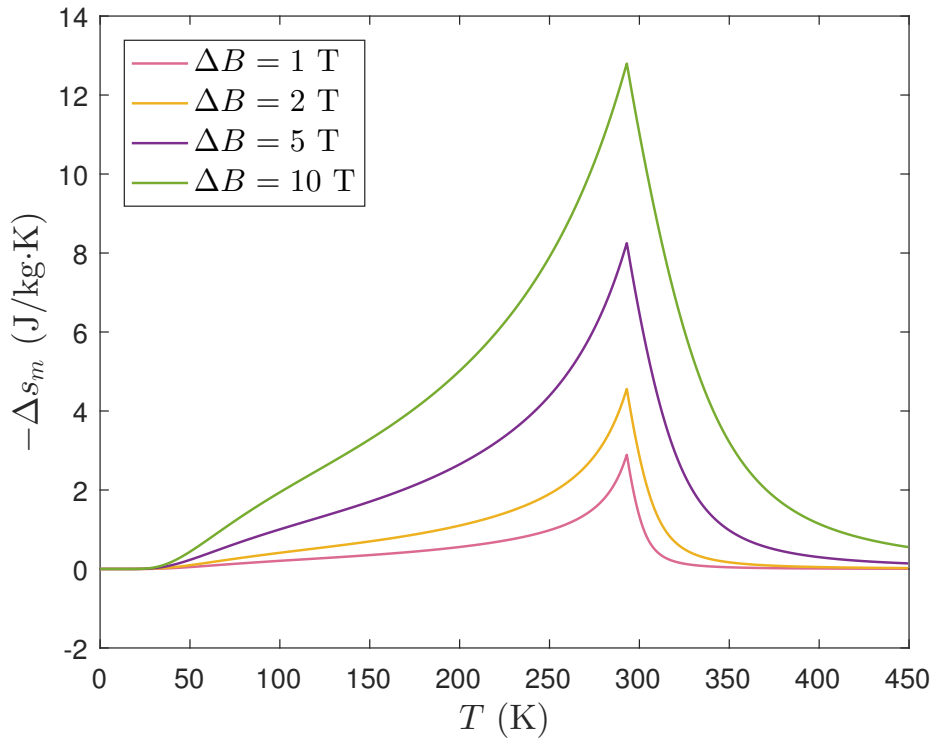
FIGURE 2.13: Variation of the specific magnetic entropy Δs_m as a function of temperature between the magnetic entropy curves of the previous graph (Fig. 2.11). The difference is taken between the lines such that $B \neq 0$ T and the curve for $B = 0$ T.
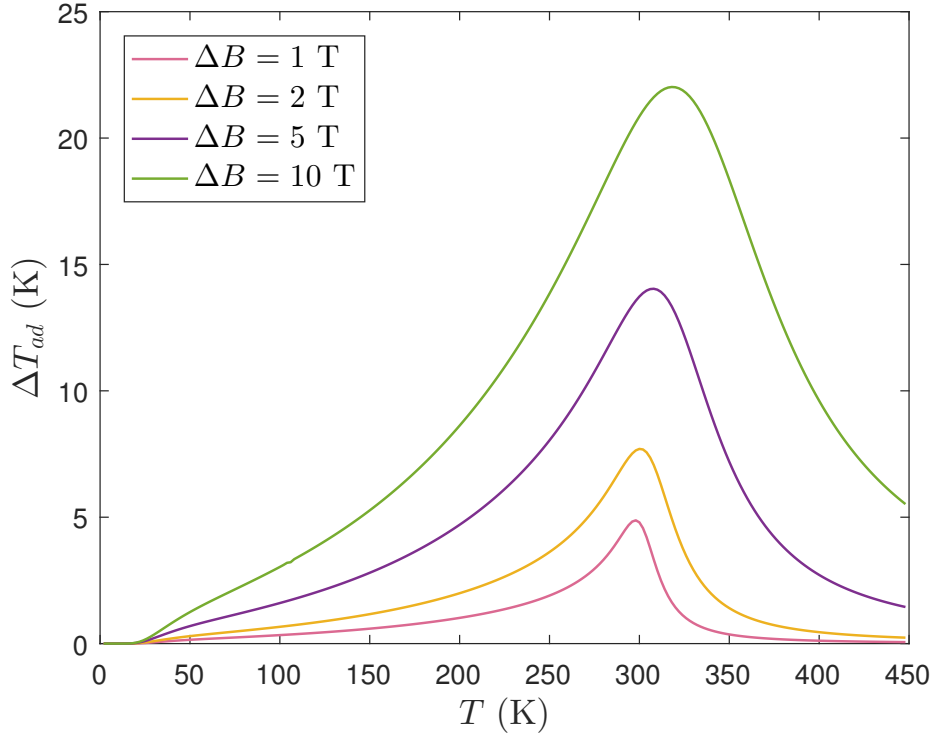
FIGURE 2.14: Adiabatic change of temperature ΔT_ad between the magnetic entropy curves of Fig. 2.11. The difference is taken between the lines such that $B \neq 0$ T and the curve for $B = 0$ T.

4.   Thermodynamic cycles[1]

In order to perform the *magnetization-cooling of the MCM-demagnetization-heating of the MCM*
process, different thermodynamic cycles might be considered and will be reviewed hereafter.
All these cycles will be presented under the form of a $T - S$ diagram in which one sees the path
followed by the material properties between two isofield curves, the first one being drawn for
$H = H_{\text{min}}$ and the second for $H = H_{\text{max}}$, with $H_{\text{min}} < H_{\text{max}}$. The system operates between a
cold temperature T_{c} and a hot one T_{h}, with cold and hot heat exchanges respectively denoted Q_{c}
and C_{h}.

As a reminder, one needs for a refrigerating machine to operate properly to inject an amount
of work W in order to absorb a certain quantity of heat from the cold sink Q_{c}, and to be able
to reject some heat to the hot reservoir Q_{h}. In the charts below, the work W corresponds to the
area surrounded by the cycles.

4.1   Carnot cycle

This well-known thermodynamic cycle simply consists in two adiabatic and two isotherm
(de)magnetization steps. It is illustrated on the upper left of Fig. 2.15 hereafter. First (a-b),
starting from H_{min} and increasing the field, the material is partially magnetized, allowing its
temperature to rise from T_{c} to T_{h}. This step occurs adiabatically.

Then (b-c) the applied field is brought up to H_{max} so that the ultimate magnetization of the
MCM is achieved through an isothermal process. Compared to the first step when the material
had to be thermally isolated, during this stage it should be allowed to exchange with the fluid in
order to keep a constant temperature T_{h}. The heat absorbed by the fluid is then rejected to the
hot reservoir

Thirdly (c-d), the MCM is partly demagnetized by an appropriate decrease of the external
field. In an adiabatic fashion once again, its temperature is reduced back to T_{c}.

The final stage (d-a) consists in the isothermal completion of the demagnetization of the
material. Its temperature being kept at T_{h}, the MCM absorbs the heat from the fluid taken to the
cold sink.

4.2   Brayton cycle

The Brayton cycle is depicted in the upper right of Fig. 2.15 and basically implies two adiabatic
and two isofield processes.

The first stage (a-b) consists in the complete magnetization of the material by increasing
the magnetic field from H_{min} to H_{max}. In the mean time, due to the MCE, the temperature
of the material increases up to T_{h}. It should be noted that, compared to the Carnot cycle, the
temperature at the beginning of the cycle is higher than T_{c}. Because this process is supposed to
occur under adiabatic conditions, the material should be well isolated from its surroundings.

Secondly (b-c), as the field is kept constant at the value of H_{max}, the MCM is put in contact
with the fluid so it can unload its extra heat. The temperature of the material thus diminishes
while the fluid rejects the heat to the hot reservoir.
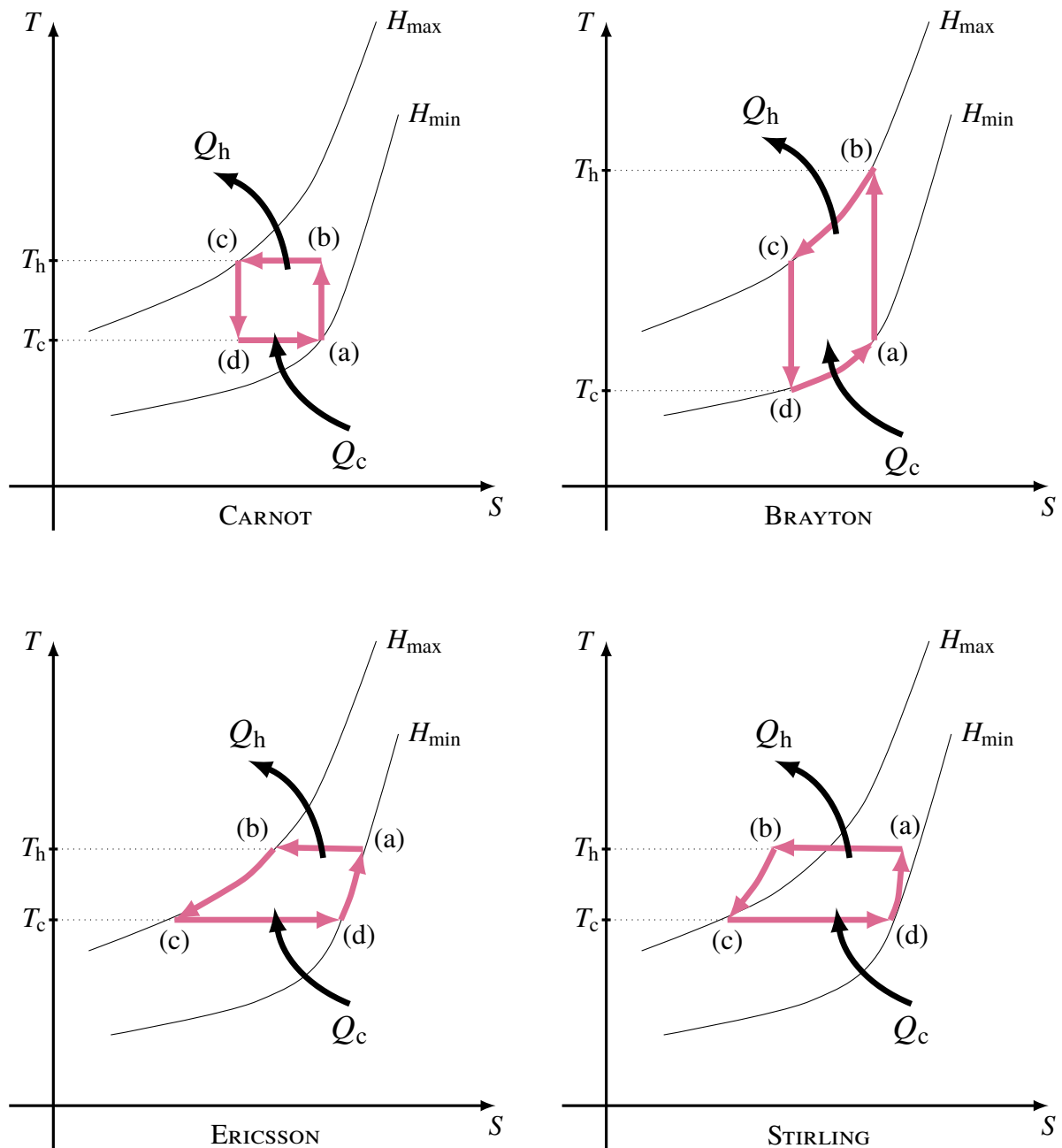
FIGURE 2.15: Comparison between the $T - S$ charts of possible thermodynamic
cycles allowing to exploit the MCE.

The next step (c-d) involves the demagnetization of the material thanks to the reduction of
the applied field back to H_{min}. The temperature of the MCM is decreased to T_c in an adiabatic
manner.

Finally (d-a), at a constant external field of H_{min}, the heat given to the fluid by the cold
source is drained by the MCM, which as a consequence heats up. Compared to the Carnot cycle,
the Brayton cycle allows to achieve a higher temperature span and thus greater heat exchanges

between the fluid and the material.

4.3   Ericsson cycle

This cycle is represented in the lower left corner of Fig. 2.15, and consists in two isotherm and two isofield steps.

The initial stage (a-b) implies the magnetization of the MCM as the applied field is increased from H_{min} to H_{max}. Regarding the Brayton cycle for which this process was performed under adiabatic conditions, in this case it is achieved at a constant temperature T_h. The material thus rejects heat to the hot reservoir because of the MCE occurring at the same time.

Then (b-c), under a constant field, the MCM cools down until T_c by exchanging heat with the fluid which flows from the cold to the hot source.

After what (c-d) the MCM is demagnetized by reducing the external field to H_{min}. This process occurs at a constant temperature in such a way that the material absorbs heat from the cold sink because of the MCE.

The final stage (d-a) is the heating of the MCM up to T_h under the constant field equal to H_{min}. This process is achieved thanks to the fluid which circulates from the hot reservoir towards the cold sink.
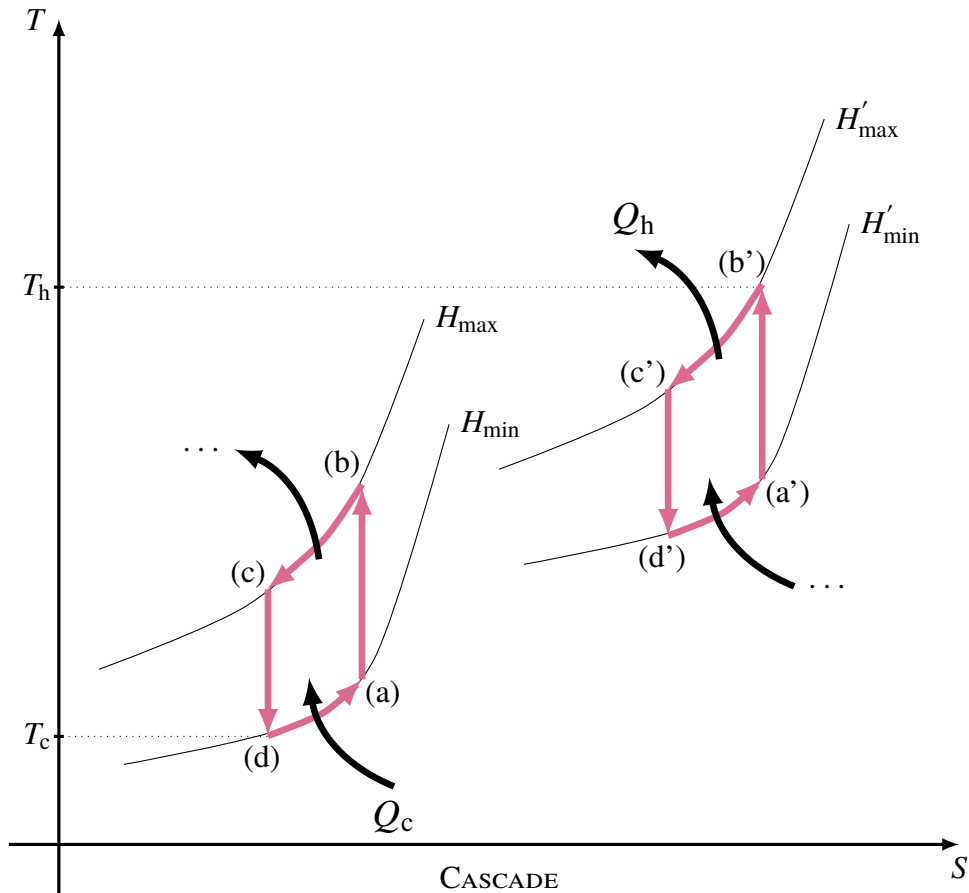
FIGURE 2.16: Example of a cascade cycle constituted of two Brayton magnetic cycles.

4.4 Stirling cycle

The Stirling cycle is very similar to the Ericsson one, except that instead of isofield processes the material undergoes iso-magnetization stages (a-b) and (c-d).

In practice, Ericsson and Stirling cycles are however difficult to achieve because of the isotherm processes which require an accurate control of the magnetic field. It is easier to perform a Brayton cycle where the (de)magnetization stages are performed adiabatically.

4.5 Cascade cycle

An example of a cascade cycle is visible in Fig. 2.16. Since materials experience the most the MCE around their Curie point, once the operating temperatures T_C and T_h get far away from this latter, the effect decreases. As the temperature span of the device becomes larger, the efficiency is lowered. It is thus interesting to work with different MCM possessing distinct Curie temperatures. The magnetic cycles corresponding to these are said to be in cascade and their respective working temperatures are close to the Curie point of each material. The efficiency of the system may in this case be optimized and the global temperature span achieved is higher.

In the diagram below one sees a cascade of two Brayton cycles. It should be noted that the heat extracted from the first one (a-b-c-d) is absorbed by the second (a'-b'-c'-d'). Because magnetocaloric materials are usually solids, such an exchange is easy to achieve since one may use the same fluid between both materials to transfer the heat.

4.6   Active magnetic regenerator cycle[4,15]

In order to increase the efficiency of a thermodynamic cycle, a regenerator may be used. For conventional heat engines, it simply consists in a system gathering the heat from the hot fluid into an additional heat accumulator and then to restore this heat to the fresh, incoming fluid. This kind of system allows to increase the efficiency of the engine.

In the first magnetocaloric refrigeration demonstrators, an external regenerator was used as the fluid flowing between the hot and cold sources. The main issue with such a system was that a constant temperature gradient had to be maintained throughout the moving fluid to ensure this regeneration. It was not easy to implement and a solution allowing to avoid this problem is to use instead the refrigerating material as the regenerator.

In this case the thermal cycle followed by the device is called an active magnetic regenerator cycle. Such cycles allow to reach a higher temperature range around room-temperature. The material is subjected to the variations of the magnetic field and the fluid flows along it to exchange heat with it, in one direction then in the other one. A temperature gradient appears progressively along the active material bed and gets greater as more cycles are performed during the transient regime, then reaches a maximum in the stationary state.

4.6.1   Transient regime

To describe the AMR cycle in details, one might represent simply it by drawing the temperature profile inside the material. In Fig. 2.17 are drawn the first steps of the transient regime. First, in the small chart on top of Fig. 2.17, both the fluid and the material are at the uniform temperature

T_0 before $t = 0$. At $t = 0$, the material is inserted into the magnetic field and gets magnetized as a reaction, whereas the fluid remains at rest. The material subjected to the MCE heats up uniformly and its temperature rises up to $T_0 + \Delta T_{ad}$, as depicted in pink in the picture.

Next, as time passes by ($t > 0$), the fluid is allowed to flow from the cold to the hot source, and carries heat taken from the material. A gradient of temperature thus form along the AMR bed since as the fluid heats up its temperature gets closer and closer to that of the MCM and once it reaches the end of this one, it cannot take as much heat as at the entry. Hence the temperature of the material is strongly decreased on the entrance side and only slightly when the fluid leaves the bed. This is illustrated in the second picture of Fig. 2.17.

After half the cycle length, the material is drawn away from the magnet and demagnetizes whereas the fluid is at rest once again. Its temperature is decreased by ΔT_{ad} in a uniform manner, as depicted in the third part of Fig. 2.17.

Once the fluid flows in the opposite direction, namely from the hot to the cold source, it releases heat to the material which is colder than the fluid. The temperature of the material is mostly increased on the side where the fluids enters the bed and one ends up with the graph of the last picture in Fig. 2.17.

After the fourth step, the previous cycle

FIGURE 2.17: Temperature gradient in MCM during the transient regime of an active magnetic regeneration cycle.

starts over, but a temperature gradient is already existing inside the MCM. It is enhanced further and further as more cycles are performed, until it reaches a stationary value. Of course the case described here is ideal, that is, the heat sources are considered adiabatic. All the energy available is used in order to increase the gradient inside the material ; this cycle is thus performed with a null total work. The main interest is to find the maximum range of temperature achievable by the system ; as power is taken from it, the temperature span gets smaller.
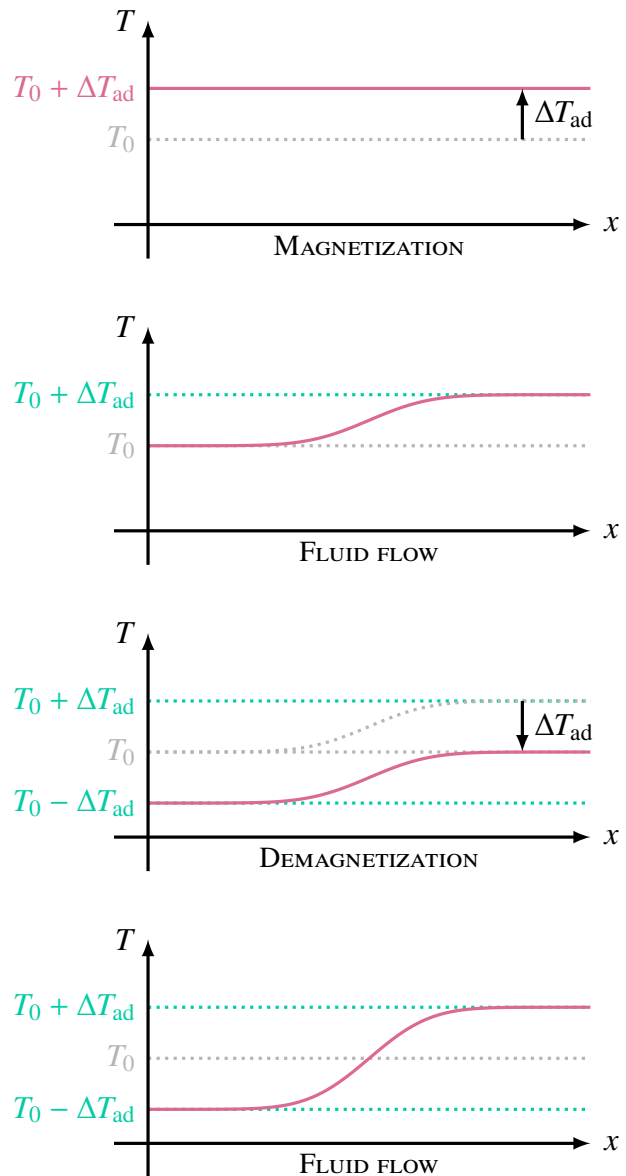
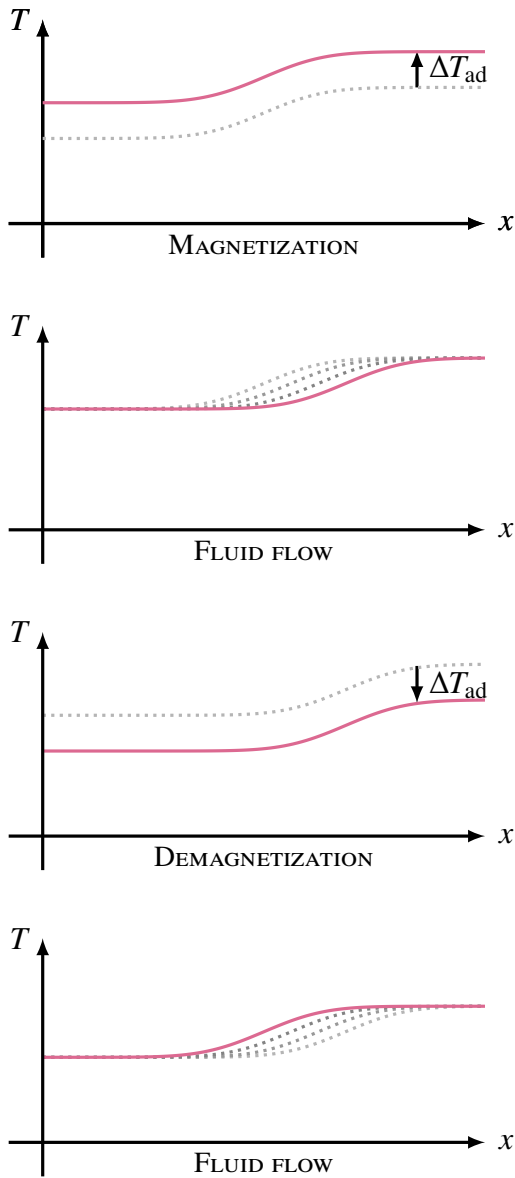FIGURE 2.18: Temperature gradient inside the MCM during the stationary regime of an active magnetic regeneration cycle.

4.6.2 Stationary regime

Once the gradient of temperature inside the material is established, exchanges between the hot and cold heat exchangers at both sources allow to absorb or release energy to the fluid. The regime is now stationary and described in Fig. 2.18.

At first, the temperature gradient inside the material is maximum and both ends of the AMR bed are respectively at temperature T_c and T_h. Inside the first picture from Fig. 2.18, the material is submitted to a magnetic field adiabatically which causes it to magnetize. Its temperature hence rises by ΔT_{ad} in a uniform manner.

Next, the fluid flows between the cold to the hot reservoirs, respectively at temperatures $T_c + \Delta T_{ad}$ and $T_h + \Delta T_{ad}$. Because the fluid absorbs the heat available inside the regenerator, the gradient of temperature is displaced in this latter as depicted in the second picture of Fig. 2.18. The fluid then enters in the hot heat exchanger at $T_h + \Delta T_{ad}$ to leave it discharged from a part of its heat, at the temperature T_h. The excess of energy $\dot{Q}_h$ left by the fluid inside the HHEX corresponds thus to that given by the AMR bed. This step corresponds to an isofield cooling of the material.

After what the material leaves the magnetic field and is demagnetized adiabatically. This yields to a uniform decrease of its temperature by ΔT_{ad}. This situation is drawn in the third illustration of Fig. 2.18.

Finally, an isofield heating is performed throughout the fluid flow between the hot and cold sources. This time the fluid respectively has at first temperatures T_h and T_c, giving its extra energy to the regenerator. This situation is depicted in the fourth picture of Fig. 2.18. The fluid gets out of the AMR bed at temperature T_c to enter the cold heat exchanger and leaves this latter at $T_c + \Delta T_{ad}$. This heat absorbed is the cooling power $\dot{Q}_c$ of the system that one wants to cool, namely this process is the reason why the whole cycle is performed. The performances of a given refrigerator prototype will be assessed in a later section.

4.6.3   Thermodynamic understanding of the AMR cycle

From a microscopic viewpoint, one may understand the AMR cycle as being a succession of Brayton cycles. If one pictures the material as an ensemble of small elements, each element is subjected to its own Brayton cycle. But depending on which side of the bed the material element is situated, this cycle will evolve differently. As time is passing, cycles of the elements located on one side will progressively oscillate between colder temperature whereas on the other end these cycles will vary between hotter temperatures. At the middle, nothing will change. This kind of continuous cascade of Brayton cycles explains the appearance of a temperature gradient inside the AMR bed.

4.7   Assessing the performances of a magnetic refrigeration-based device

As it was just mentioned, the cooling power is the actual value one is interested in when trying to design a refrigerator device. As a reminder, Q_c is the heat injected in the CHEX whereas Q_h is the one rejected by the refrigerator in order for it not to violate the second principle of thermodynamics. On the other hand, W is the work that needs to be injected so that the machine can work properly. Here the total work injected is only constituted of the magnetic work. All the losses are not considered thus this definition is actually theoretical and, in reality, such a coefficient of performance is never achieved by a refrigerating device or heat pump. One indeed needs to use energy for e.g. ensure the motion of the magnet and/or the MCM, which is not taken into account in the following formula.

In order to assess the efficiency of a device, one uses the coefficient of the performance defined for a refrigerator as

$$\text{COP} = \frac{Q_c}{W_{mag}}. \tag{2.42}$$

For an ideal material whose an entropy is a linear function of temperature, the former coefficient is maximal and equal to the Carnot coefficient. It is known that the Carnot coefficient for a refrigeration device is given by

$$\text{COP} < \text{COP}_{\text{Carnot}} = \frac{T_c}{T_h - T_c}. \tag{2.43}$$

5.   Measurement methods[4,15]

In order to evaluate the MCE in a material, one might simply measure the adiabatic change of temperature or perform a measurement of the magnetic change in entropy, which are as previously explained both characteristics of the MCE.

5.8   Direct measurements

The most obvious method is to directly take the temperature of the sample as it is placed in a magnetic field in order to evaluate its heating, with the help of e.g. a thermocouple or any other kind of suitable temperature sensor. However, this only allows to take measurements for small fields and at fixed temperatures. Solutions exist in order to counteract these issues,

such as enhancing the thermal isolation of the material to ensure adiabatic conditions or using differential measuring techniques. In addition to that, electronic circuits can be utilized too to compensate the effect the magnetic field variation may have in response of the sensors. For high field values (≈ 30 T), pulsed techniques are used whereas static measurements can be performed for smaller fields. Measurement errors might be comprised between 5 and 10 %. According to whether the field is applied in a parallel or perpendicular manner to the sample, the MCM response might be affected and so does the measurement.

5.9 Calorimetric measurements

Relations of Eq. (2.20) and (**??**) in page 13 lead to another type of measurements. Calorimetry, namely measurements of specific heat capacity $c_H(T, H)$, allows to deduce the magnetic entropy and its variation as well as the adiabatic variation of temperature. Therefore such measurements permit to directly describe the MCE of a material. The main disadvantage is that this method is quite tricky to implement.

It actually looks like the direct measurement method ; temperature is measured for a sample subjected to a change of magnetic field. This field may be applied in different manners: either by introducing the sample in a magnet and drawing it away from this one or by using pulsed fields, this latter method allowing to reach higher field values.

5.10 Magnetic measurements

Magnetic or indirect measurements allow to only obtain the magnetic entropy variation. They are quite simple to implement because all it takes is a magnetometer to measure the magnetization $M(T, H)$ of the material. The sample is positioned in the field of a variable magnet, e.g. a superconducting coil. The sample is also placed and made to move inside a detection device constituted of two reverse coils mounted in series. The induced flux variation which is proportional to the magnetization of the sample, is measured by integrating the voltage difference at the ends of this sensor. The temperature must be regulated in order for the sample to remain at the same temperature during the magnetic field variations. The results obtained are thus isotherms of $M(T, H)$.

The variation of magnetization as a function of temperature may be linked to the magnetic entropy variation through Eq. 2.17. The results are however taken for discrete temperature values thus one needs to perform a numerical integration of this relation in order to get $\Delta s_m(T, \Delta H)$. One may approximate it simply if the variations of field are small by considering that in this case the derivative of M with respect to T is linear. Hence, one writes for a given temperature T_i

$$\Delta s_m(T_i, \Delta H) = \sum_j \frac{M_{i+1}\left(T_{i+1}, B_j\right) - M_i\left(T_i, B_j\right)}{T_{i+1} - T_i} \delta B_j. \tag{2.44}$$

One can easily deduce from this relation the adiabatic change of temperature and characterize completely the MCE. This method is the most used because it is the fastest and has a better accuracy than the calorimetry near room temperature.

6.   Historical background[16]

A brief historical review on the several discoveries leading to what is known about the MCE today is made in this section. In the 19th century people were already getting interest in the link existing between magnetism and heat effects. The first major discovery happened in 1831 when Faraday realized that a time-varying magnetic flux can induce an electrical current. At that time it was not known that currents could be generated by other means than using a battery. Further investigations allowed Faraday to conclude in 1843 that thess electromagnetically induced currents accompanied by heat loss were indeed the same as any other kind of electrical current.

It was then accepted that cyclic magnetization and demagnetization processes in ferromagnetic materials yield to heat dissipation due to eddy currents, and thus an increase in the temperature of the material. However, scientists at the time found out that a magnetic field can lead to temperature variations inside a materials in other manners. In 1860, Thomson (Lord Kelvin) based his work on the fact that ferromagnetic materials suddenly lose their magnetization when heated above their transition point. He then concluded that iron should experience a heating effect when brought close to a magnet and a cooling one when drawn away from it. He also predicted that nickel and cobalt should experience the same effect, and that this effect will be the largest in the temperature range around its Curie point. He added that this process is reversible but could not observe it experimentally or at least estimate its magnitude. A measurement was performed in iron, which was quite tricky to achieve, only 70 years later by Potter.

It is often misconceived that Warburg unveiled the magnetocaloric effect in 1881, but his contribution is not the actual discovery of the effect. This one goes back to 1917 when Weiss and Piccard found out the apparition of a MCE in nickel. Warburg could indeed not have observed the MCE in iron at room temperature, which is often written in recent papers. Its magnitude is indeed of a few degrees for a field of 1 T at around 770 ° C in such a way that it was very difficult for him to measure it at his time because instrumentation was not precise enough.

FIGURE 2.19: Closed magnetization-demagnetization loop.

The contribution of Warburg is in fact the following: in a now famous paper, he explained that when an iron wire is submitted to an increasing magnetic field going from 0 to H_1, and that the field is then decreased from H_1 to 0, the magnetic moment of the wire is larger in the decreasing case than in the increasing one. If this cycle is repeated, the magnetization of the material follows a closed loop in an $M - H$ diagram, which is well known today to be the hysteresis effect appearing in many materials as shown in Fig. 2.19 above.

After that Warburg computed the work performed on the iron wire during the cycle as the opposite of the line integral around the closed magnetization loop C, namely,
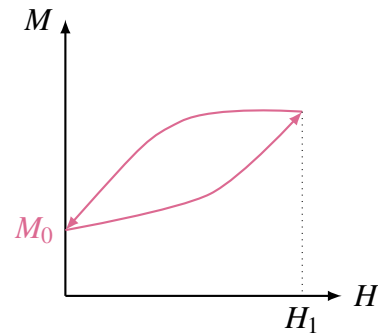
$$-\mu_0 \int_C M \mathrm{d}H, \tag{2.45}$$

34

which is also equal to the area surrounded by this curve. Because after every cycle the wire is in the same magnetic state, this work must be dissipated under the form of heat in the material. The Warburg's law that he derived states that hysteresis is a source of heat dissipation and that for a hysteresis cycle an amount of heat equal to the area surrounded by the loop is lost inside the material. He finally conducted experiments in order to measure this magnetization as a function of the magnetic field. It can be noted that the name "hysteresis" was actually given by Ewing who studied the same phenomenon in 1882.

Then Warburg, with the collaboration of Hönig, wrote about the distinction between the three possible contributions to the thermal response of a magnetic body submitted to a time-varying magnetic field. There is the hysteresis effect which yields to heat losses, as it was described in the former paragraph, the heating or cooling effect due to eddy currents and finally the reversible heat production appearing because of the dependence in temperature of the magnetization. This last contribution is the one that was described for the first time by Thomson.

Both the authors then tried to directly measure the heat in a piece or iron and found out an order of magnitude for what they called the "Thomson heat". Whereas typically the hysteresis heat has an order of 10^{-5} °C, they obtained for the third contribution an size of 10^{-6} °C. They concluded that this heat was small compared to the hysteresis and could not be measured in their experiment. A few years later Delere tried to evaluate this Thomson heat too but failed because he assumed that the hysteresis was a reversible process. It is only around 1930 that it was possible to measure precisely the heat exchanged along individual parts of the hysteresis loop, and until the 1950s people were still searching for ways to separate experimentally the irreversible an reversible parts of this total heat.

A major advance in the understanding of the physical properties of ferromagnets is due to Weiss and its molecular field theory he exposed in 1907. This one was reviewed in details in former sections. In 1905, Langevin explained the Curie law and explained the behaviour of paramagnets. His theory was extended to ferromagnets by Weiss through the concept of an internal magnetic field existing even when the material is not subjected to an external one.

Continuing his study of ferromagnetism, Weiss wanted to derive precisely how the magnetization was influenced by temperature. In 1917, he and Piccard discovered during their research that nickel was experiencing a reversible heating when a magnetic field was applied close to its Curie temperature (354 °C). They obtained an increase of 0.7 °C for a field of 1.5 T. The reversible nature of this phenomenon allowed them to separate it from the hysteresis heat, and they called it a "novel magnetocaloric phenomen". The coworkers also found out a thermodynamic relation describing the effect they just discovered, and were able to link it to the molecular field existing in ferromagnetic materials. Weiss and Piccard are thus the first ones to observe reversibility and the peak in magnetization around the Curie point, both characteristic of the MCE.

In the 1920s, Debye and Giauque independently observed that really low temperatures may be achieved by an adiabatic demagnetization of paramagnetic salts. This effect is very similar to the MCE for ferromagnets and the discovery comes really close after the work of Weiss and Piccard on the MCE. However, Debye and Giauque were not aware of this latter at the time and only used the theory developed by Langevin. The magnetic refrigeration based on adiabatic demagnetization has apparently developed without people knowing the MCE at all.

Nevertheless, the MCE was used as a tool for measuring the equilibrium value of the

intrinsic magnetization of ferromagnets. Weiss indeed noticed that under a null external field, the molecular field is such that total equilibrium magnetization of the material cancels even though the spontaneous magnetization does not. This is because of the individual domains existing in ferromagnets that all have their own spontaneous distinct magnetization but globally arrange themselves in order to minimize the total magnetic energy. Hence the spontaneous magnetization cannot be measured directly. But Weiss showed that the adiabatic variation of temperature appearing below the Curie point is

$$\Delta T_{ad} = A \left(M^2 - M_0^2 \right), \quad A > 0. \tag{2.46}$$

In the former relation M is the magnetization for a given magnetic field H, M_0 the spontaneous magnetization already existing in the material for $H = 0$ and A a positive constant. Measuring ΔT_{ad} and M for several values of H then allows to get M_0. Weiss and Forrer performed such measurements for nickel in 1926, after what people kept using the MCE in this context.

The separation between the development of both aforementioned methods, one for achieving very low temperatures and the other for measuring the spontaneous magnetization of ferromagnets, was probably the fact that using MCE in ferromagnets like nickel, iron and cobalt did not yield to any promising application because of their really high Curie points. The properties of pure gadolinium were not well known at this time and the usual material for adiabatic demagnetization was gadolinium sulfate[2]. But in the beginning of the 1930s pure samples of lanthanides could be produced and some years later, a new ferromagnetic element whose Curie point is around the room temperature, pure gadolinium, was discovered by Weiss, Urbain and Trombe. Its magnetocaloric effect was however only studied in the 1950s.

It is only in 1976 that near-room temperature magnetic refrigeration appeared. A first prototype was built by Brown which uses gadolinium and allowed to reach a temperature span of 47 K. Another device was achieved by Steyert two years later. From this years and until today the interest in magnetocaloric material used for making magnetic refrigeration devices has spread widely over the world, especially since the late 1990s.

7.   Other caloric effects[17]

Besides the MCE described in details into the previous sections, it is interesting to emphasize that other caloric effects may be presented by some materials. They will be quickly reviewed in the following paragraphs.

The first effect that will be described is the electrocaloric effect, which rely on a principle very similar to that of the magnetocaloric effect. It indeed consists in the thermal response shown by some materials to the change in an externally applied electric field. The first demonstration of this effect happened in 1930, in Rochelle salt, which contains Sodium and Potassium[3]. This material is also the one in which ferroelectricity was discovered.

The resemblance with the MCE does not stop there since certain materials also present a giant electrocaloric effect near the ferroelectric transition. Compared to the variations of

---

[2] $Gd_2 (SO_4)_3 \cdot 8H_2O$.

[3] $NaKC_4H_4O_6 \cdot 4H_2O$

temperatures achieved with the MCE in for instance gadolinium, materials presenting this effect can undergo a temperature change of around 12 K. But to get such a result, the field used is of the order[4] of $5 \cdot 10^2 - 3 \cdot 10^3$ kV cm^{-1}, at temperatures generally far above the ambient temperature and thus not well suited for commercial refrigeration. The main advantage of the electrocaloric effect is that it is easier to achieve a large electric field than a magnetic field of at least 1 T[5].

On the other hand, mechanocaloric materials exhibit a reversible thermal variation in response to a change in the applied stress field. Two cases may be considered: the elastocaloric materials which respond to an axial stress change, and the barocaloric materials sensitive to the hydrostatic pressure change, that is a variation in the isotropic stress.

The elastocaloric effect was found in 1805 in natural rubber which warms up when suddenly stretched. The barocaloric effect discovery dates only back to 1998. Both elasto- and barocaloric materials can also undergo giant effects. The temperature spans achieved lie between 12 and 40 K for stress variations going from 0.1 to 0.8 GPa in the case of elastocaloric materials. For barocaloric materials, the best temperature change is of 4.5 K for a pressure change of 0.26 GPa. Examples of materials showing giant elasto- and barocaloric effects are respectively Ni-Ti and $Ni_{49.26}Mn_{36.08}In_{14.66}$.

As for the MCE, some scientists around the world also built a few cooling devices based on the electro- and mechanocaloric effects. Despite its recent discovery, the barocaloric effect also shows promising results. However, although the trend remains mostly focused on the magnetocaloric effect, all these effects are active fields of research and prototypes based on them keep being developed.

Many other candidates for replacing the vapor compression refrigeration exist nowadays. An interesting and recent review comparing them was made by Brown and Domanski.[18] Among all these trending technologies, one may cite e.g. the thermoacoustic or thermoelectric cooling methods. Hydraulic potential or chemical techniques might also be used.

The most important point is that, as it is the case for instance for the development of electric cars, people are now aware of the upcoming changes they have to face. Through the whole world scientists are very concerned about finding environmentally-friendly cooling technologies in order to replace the classical, steam compression one which uses harmful, nocive gases with high global warming potential. Maybe one day the MCE or one of these other technologies will replace refrigerating devices around the globe.

---

[4]Dielectric breakdown occurs in the atmosphere close to 30 kV cm^{-1}.

[5]The magnetic field at the Earth's surface is comprised between 30 and 60 μT and the current world record is of 91.4 T.

Summary

- The search for new technologies has stormed out throughout the world during the past years in order to avoid the use of non environmentally friendly refrigerants and reduce the electricity consumption devoted to refrigeration. For these reasons, the magnetocaloric effect has been widely studied because refrigerators (and heat pumps) exploiting it are thought to be interesting potential alternatives.

- Thermodynamic relations may be derived in order to describe and understand the MCE. The entropy in materials presenting a MCE arises from three contributions but the preponderant one is the magnetic part. This latter allows to understand microscopically why MCMs experience a heating when subjected to a magnetic field and vice versa. More specifically, the mean field theory developed by Weiss allows to derive an equation for this magnetic entropy. It is then possible to draw a graphical representation of the theoretical behaviour of gadolinium using appropriate parameters.

- Besides the fact that gadolinium is the ultimate MCM for room-temperature, studying new alloys presenting a MCE is an active field of research. The compounds containing gadolinium as well as other rare earths are numerous, but the most promising alloys for commercial application are the Fe_2P based family, which show a lot of interesting qualities.

- In order to utilize the MCE and conceive e.g. a cooling device based on it, one should perform a cycle in which (de)magnetization processes are followed by heat exchanges with a fluid flowing between a cold and a hot reservoirs. Such a cycle can be put in parallel with the well-known, classical gas compression one. The type of cycle may differ but the prevailing ones are the Carnot, Brayton and Ericsson cycles. One also wants to achieve regeneration inside the magnetic material bed in order to enhance the effect and optimize the efficiency of the prototype.

- Besides the MCE, other caloric effect may arise in materials and represent nowadays active fields of research. As for the MCE, these materials present a temperature variation but in response to an external electric field or a mechanical driven stress. They show quite similar performances but prototypes based on the MCE remain the most widespread.

References

[1] J. R. Gómez, R. Garcia, A. M. Catoira, and M. R. Gómez, "Magnetocaloric effect: A review of the thermodynamic cycles in magnetic refrigeration," vol. 17, pp. 74–82, 2013.

[2] A. Kitanovski, J. Tušek, U. Tomc, U. Plaznik, M. Ožbolt, and A. Poredoš, *Magnetocaloric Energy Conversion*. Switzerland: Springer, 2015.

[3] N. de Oliveira and P. von Ranke, "Theoretical aspects of the magnetocaloric effect," vol. 489, pp. 89–159, 2010.

[4] F. Allab, *Étude et conception d'un dispositif de réfrigération magnétique basé sur l'effet magnétocalorique géant*. PhD thesis, Institut National Polytechnique de Grenoble, May 2008.

[5] H. R. Bouchekara and M. Nahas, *Trends in Electromagnetism - From Fundamentals to Applications*. InTech, 2012.

[6] W.-N. Huanga and C.-C. Teng, "A simple magnetic refrigerator evaluation model," vol. 282, pp. 311–316, 2004.

[7] B. Leyh, "CHIM9308-1 : Physical chemistry," 2015-2016. Course from the master in Physical Engineering, University of Liège.

[8] "Debye Temperature." http://encyclopedia2.thefreedictionary.com/Debye+Temperature. The Great Soviet Encyclopedia website, accessed 21-May-2017.

[9] E. Brück, "Developments in magnetocaloric refrigeration," vol. 38, pp. R181–R191, 2005.

[10] H. Wada, T. Takahara, K.Katagiri, T.Ohnishi, K.Soejima, and K. Yamashita, "Recent progress of magnetocaloric effect and magnetic refrigerant materials of mn compounds," vol. 117, 2015.

[11] M. Liu and B. Yu, "Development of magnetocaloric materials in room temperature magnetic refrigeration application in recent six years," vol. 16, 2009.

[12] V. Basso, C. P. Sasso, G. Bertotti, and M. LoBue, "Effect of material hysteresis in magnetic refrigeration cycles," pp. 1358–1365, 2006.

[13] M. Balli, D. Fruchart, D. Gignoux, S. Miraglia, E. Hlil, and P. Wolfers, "Modelling of the magnetocaloric effect in $Gd_{(1-x)}Tb_x$ and MnAs compounds," vol. 316, pp. e558–e561, 2007.

[14] Y. Mnyukh, "Lambda- and Schottky-anomalies in solid-state phase transitions," 2011.

[15] Legait, *Étude et conception d'un dispositif de réfrigération magnétique basé sur l'effet magnétocalorique géant*. PhD thesis, Institut National Polytechnique de Grenoble, May 2008.

[16] A. Smith, "Who discovered the magnetocaloric effect? warburg, weiss, and the connection between magnetism and heat," 2013.

[17] S. Crossley, N. D. Mathur, , and X. Moyaa, "New developments in caloric materials for cooling applications," vol. 5, 2015.

[18] J. Brown and P. Domanski, "Review of alternative cooling technologies," vol. 64, pp. 252–262, 2014.

[19] V. Franco, J. Blázquez, B. Ingale, and A. Conde, "The magnetocaloric effect and magnetic refrigeration near room temperature: Materials and models," vol. 42, pp. 305–3042, 2012.

[20] K. A. Gschneidner Jr and V. K. Pecharsky and A. O. Tsokol, "Recent developments in magnetocaloric materials," vol. 68, pp. 1479–1539, 2005.

[21] K. L. Engelbrecht, G. F. Nellis, S. A. Klein, and C. B. Zimm, "Recent developments in room temperature active magnetic regenerative refrigeration," vol. 13, no. 4, pp. 525–542, 2007.

[22] http://www.rsc.org/periodic-table/element/64/gadolinium. Royal Society of Chemistry website, accessed 16-May-2017.

3

ALREADY EXISTING PROTOTYPES

In this chapter will now be presented some of the prototypes designed and built during the past forty years. It all started in 1976 when Brown proposed a first demonstrator constructed by the NASA. Later on, some other American devices were built but the interest in magnetocaloric technology has mainly been spreading around the world since the beginning of the new millennium.

First, the major differences found between the existing prototypes will be briefly reviewed, after what the early demonstrators will be presented in more details. Then a small survey of the devices built during the last years will be performed, from the oldest to the most recent ones.

1. Major characteristics

Every refrigerator/heat pump exploiting the MCE requires some mandatory components, namely a MCM, a (high-field) magnet, and a fluid to perform heat exchanges between the MCM and the surroundings.

The prototypes built up to now may be classified in two main categories: the reciprocating (linear) and the rotary ones. In the first case, either the magnet or the MCM moves in a linear, back and forth manner, and in the second, one of them is in a rotary motion. Another common feature is the form under which the MCM is found in the prototype: one can use either thin plates or a packed-bed. A packed-bed consists e.g. of powder, small spheres or even cylinders. In any case, though, there should always be some room for the fluid to flow through the device.

Due to its ideal properties for near-room temperature refrigeration, exposed in Chapter 2, the material used the most often is gadolinium. However, other compounds presenting a MCE have been found in the past years. The main reason is that, the gadolinium being a really expensive rare earth (around 2500$ for 400 g), it will never be utilized for commercial purpose.

Usually, the magnets used for building the demonstrators have a field of at least 0.8 T. Permanent magnets are nowadays the most widely utilized ones, with typical strength of 1-2 T. However, in the very beginning superconducting magnets were mostly employed, with much higher field values, typically of 7-8 T. Electromagnets may also be used but their major issue is that, for achieving a sufficiently high field, the Joule effect becomes very important. One must therefore ensure that they are efficiently cooled in order not to alter the physical properties of the conductive wires.

In order to enlighten the performances of a refrigerating prototype, one ordinarily measures its no-load temperature span ΔT, its zero-temperature-span cooling power $\dot{Q}_C$ and its COP (coefficient of performance). The "no-load" means with a null cooling power, whereas $\dot{Q}_c$ is the maximum cooling power that can be achieved by the device, with a vanishing temperature span. The coefficient of performance is defined as the ratio between the cooling power produced by and the magnetic power given to the prototype. Depending on the definition, some authors also include for instance the power injected to drive the flow.

In both sections hereafter the demonstrators built up to now will be depicted in details. Based on all these aforementioned characteristics, they will be split into two categories: the linear and the rotary ones. Each of them will then be described using the following list of features:

1. Which MCM is used ? Under which form (plates or packed-bed) ? In which quantity ?

2. Which type of magnet is employed ? What is the value of its field ?

3. Which fluid is used ?

4. What are the dimensions of the prototype ?

5. At which frequency (range) can it operate ?

6. What are its performances (ΔT, $\dot{Q}_C$, COP) ?

7. How does it work ?

8. What are its pros and cons ?

Obviously not all information may be found for every prototype that will be described afterwards.

2. The forerunners of the past century

In this section the first few prototypes built in the end of the past century will be described, starting by the oldest one. This one was of the reciprocating type ; it was conceived by Brown and built by NASA in 1976.

2.1 Brown, 1976

Brown was the first one to think about using regeneration to enhance the temperature span achieved by his prototype. He also suggested a cascade system for improving the temperature span of his demonstrator. The characteristics of the latter are listed hereafter.[1,2]

1. The magnetic working body used consists of 157.2 g of Gd, under the form of 1-mm-thick plates separated by stainless-steel wires of 1 mm diameter.

2. A field of 7 T is provided by a superconducting magnet.

3. 40 cl of fluid composed of 80% of water and 20% of ethyl alcohol is used. The vertical column is oriented with the hot end at the top and the cold one at the bottom to ensure thermal stability.

6. The temperature span achieved is of 47 K (between -1 °C and 46 °C).

7. Fig.3.1 illustrates the principle of operation of the prototype. It follows a magnetic Stirling-like thermodynamic cycle, namely a cycle composed of two isofield lines and two isotherms. The device is made up of a vertical column of fluid, which constitutes the regenerator, containing the magnetic working body. The plates of Gd are separated by some space that allows the fluid to flow in between them, enhancing thermal contact. At the top of the device is placed a heat transfer coil allowing to remove heat from the
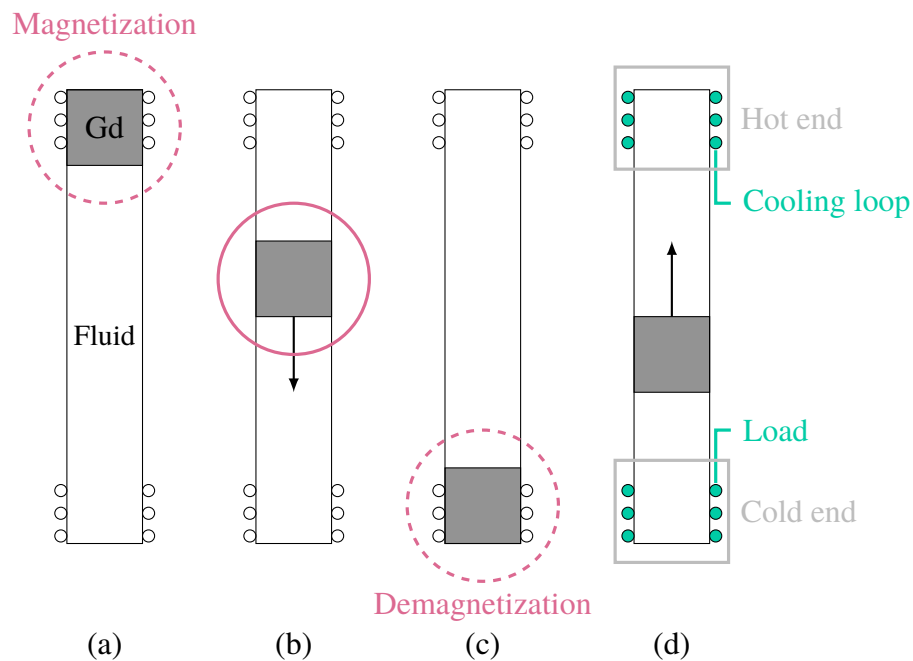

FIGURE 3.1: Brown reciprocating prototype principle of operation.[?]

magnetic material, whereas a cold load is placed at the bottom of the column.

At first (a), the MCM is progressively magnetized at constant temperature. The (de)magnetization processes are depicted in the drawing by dashed pink circles whereas a solid circle represents a constant field. The isotherm magnetization is made possible by the transfer coil that permits heat to go from the material to the surroundings.

Then (b) the magnetic working body is moved to the bottom of the column, at constant field. The column of fluid could be displaced instead but the important point is that there is a linear, relative motion between the regenerating fluid and the MCM. Once it arrives at the bottom of the column, (c) the material is demagnetized isothermally, where its cooling occurs.

Finally, the magnetic body is heated up by the load at the bottom of the column as it is moved back upwards. The load sees thus its temperature decrease, which is the aim of the refrigerative prototype. The heating of the MCM as it is moved to the top creates a temperature gradient along the column of fluid, which is the reason why this column plays the role of regenerator of the device.

As other cycles are performed, the temperature gradient is further increased, and the temperature of the cold end is reduced more and more, until the losses consume the whole cooling effect. The temperature span of 47 K is achieved after around 50 cycles.

8. This device is the first one of a long series. In the beginning prototypes were made using superconducting magnets just as in this case, which did not make so much sense since one needed to achieve very low temperatures to get a high field magnet in order to produce cold around room temperature. However, the discovery of the giant MCE and the first prototype achieved using a permanent magnet instead of a superconducting one allowed to get rid of superconducting magnets in the early 2000s.

2.2 Other devices

The few other devices that were made at the time where the interest for magnetic refrigeration only started to rise are described hereafter.

2.2.1 Green, 1990

In 1990[1], Green et alt. designed at David Taylor Research Center in America the second reciprocating magnetocaloric prototype. It displays some particularities, namely the use of a layered AMR bed under the form of ribbon, and the heat transfers are achieved by a gas instead of a liquid.

1. Two MCM were used under the form of rolled ribbons made with 1/3 of terbium Tb, 1/3 of Gd−Tb alloy and finally 1/3 of Gd, layered along the length of the AMR in the direction of the temperature gradient. The terbium has a Curie point of 235 K, which is lower than that of gadolinium.

2. A superconducting magnet producing a field of 7 T was used.

3. The fluid was nitrogen gas.

4. The AMR was 140 mm long for a diameter of 40 mm and contained a total of 500 g of MCM.

5. A frequency of 0.0143 Hz was achieved by this prototype.

6. The no-load temperature span was 24 K, whereas at 5 K the device had a cooling power of 5 W and at 20.5 K it was reduced to 2 W.

8. Not much information nor any layout can be found easily about the principle of operation of this device. However, it is an example of a prototype made using a layered AMR bed. Such a regenerator allows to increase further the performance of the device, in particular by rising the temperature gradient along the bed. The adiabatic change of temperature will indeed be greater close to the Curie point of the material, and adding in series materials with increasing Curie temperatures allows to benefit as much as possible of this characteristic. However, the idea of using a gas instead of a liquid is not a good one to perform the heat transfers since liquids have the highest heat capacity.

2.2.2 Zimm, 1998

Another prototype using superconducting magnet was built by Zimm et alt. at the Astronautics Technology Center and Ames Laboratory in Iowa State University.

1. Two packed bed AMRs were used, each containing of 1.5 kg Gd spheres.

2. A Nb−Ti superconducting magnet producing a field of 5 T was utilized.

3. The fluid used was simply water.

4. The spheres had a diameter between 0.15 and 0.3 mm.

5. A frequency of 0.0143 Hz was achieved by this prototype.

6. This demonstrator could reach a power of 600 W at a temperature span of 9 K. Using a 1.5 T-field, the cooling power was reduced to 210 W for a temperature span of 9 K.

7. The device consisted in two AMR beds moving reciprocally in and out of the magnet which was kept in place.

8. This device uses gadolinium spheres, which present a higher energy density than plates. However, its is complicated to produce spheres of the exact same diameter. Using so much gadolinium is also very expensive, most prototypes only involve a few hundreds of grams of MCM which is usually enough to get satisfactory performances.

3. From the 2000s until today

It is only at the beginning of the new millennium that prototypes using permanent magnets were achieved. The very first one was made by Bohigas et alt., and will be described hereafter. In the second part of this section, a few reciprocating devices that look like the one designed in this work will be reviewed too. Other rotating devices will not be further investigated since the present work focuses on the linear type.

3.1 Bohigas et alt., 2000

It is only in 2000 that the first room-temperature magnetocaloric prototype using a permanent magnet was created. It is a rotating device designed by Bohigas et alt., in Spain.[3]

1. The magnetic working body consists of a plastic wheel covered with a ribbon of Gd on its lateral surface.

2. A set of permanent magnets are used to constantly provide a field on a section of the device.

3. The fluid in which the container was immersed is olive oil.

4. The dimensions of the wheel were 0.8 cm width and 11 and 7.5 cm diameter ; there were indeed two geometries developed.

5. This device could operate at 0.33 Hz, namely a period of 3 s.

6. For a field of 0.3 T, the temperature span achieved is of 1.6 K, whereas for a field of 0.95 T, it reaches 5 K.

7. The working principle of the device is illustrated in Fig. 3.2. As the wheel is turning, the ribbon of Gd enters the magnetic field provided by the magnet, heats up and exchanges heat with the HHEX. Then once the ribbon leaves the high field area, it cools down and absorbs heat from the CHEX.
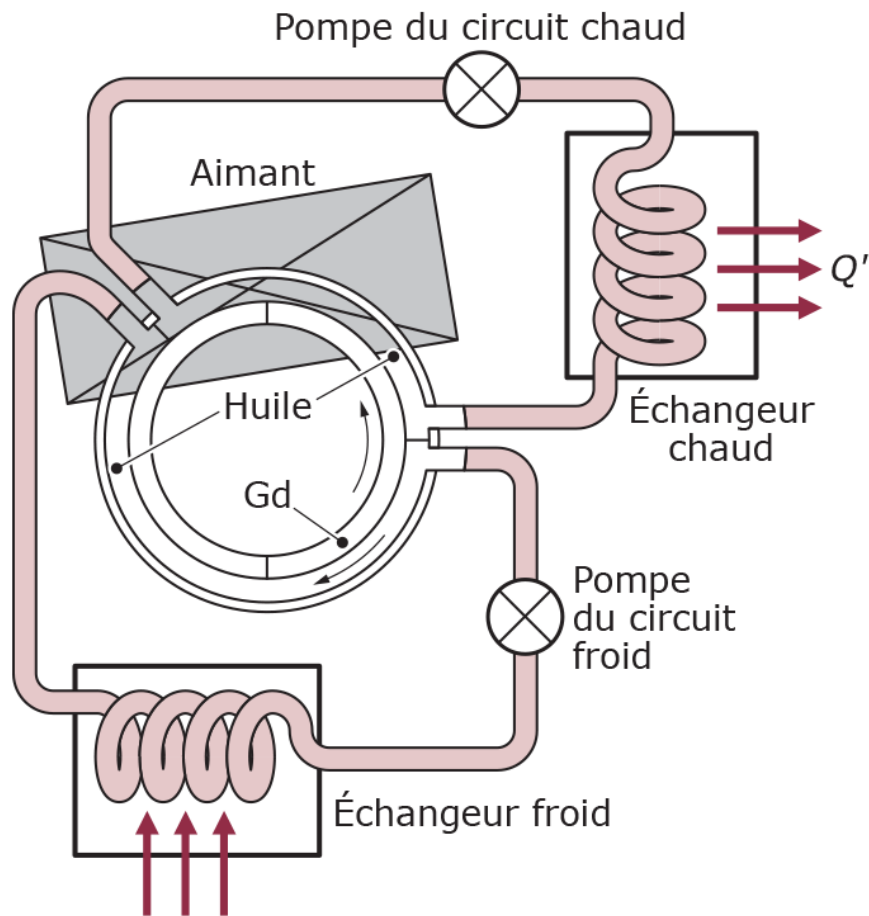

FIGURE 3.2: Bohigas et alt. rotating prototype principle of operation. Picture taken from Lebouc et alt..[4]

8. This device is as already mentioned the first one made using a permanent magnet. Nowadays all magnetic prototypes are created using them. The device made by Bohigas et alt. is hence the first one of a long series of prototypes made around the world.

3.2 Reciprocating devices

A few reciprocating prototypes made during the past years are now presented.

3.2.1 Clot et alt., 2002

A first example of reciprocating prototype is the one achieved by Clot et alt.[5] at the G2Elab[1], which goes back to 2002. At that time, permanent magnets were not already widely used for magnetocaloric-based refrigeration and this demonstrator involving such a magnet. Before that superconducting magnets were still leading the branch.

1. The AMR bed consists in 223 g of gadolinium sheets.

2. A Halbach cylinder generates a 0.8 T permanent magnetic field.

3. The exchange fluid used is simply water, displaced by an external peristaltic pump. Flow values are comprised between 0.5 ml/s and 4.8 ml/s.

4. The sheets are 1 mm thick and are separated by 0.15 mm from each other thanks to spacers.

5. A cycle has a length of 2.4 s thus the frequency is of around 0.42 Hz.

6. For a temperature gradient of 4 K, the mean cooling power equals 8.8 W and has a value of 1.6 W when the temperature span rises up to 7 K. In the first case, the global COP computed (including the total power supplied and not only the magnetic power as described in Chapter 2) has a value of 2.2. The power provided by the pump and the pneumatic drive displacing the whole system is estimated not to overcome 4 W.
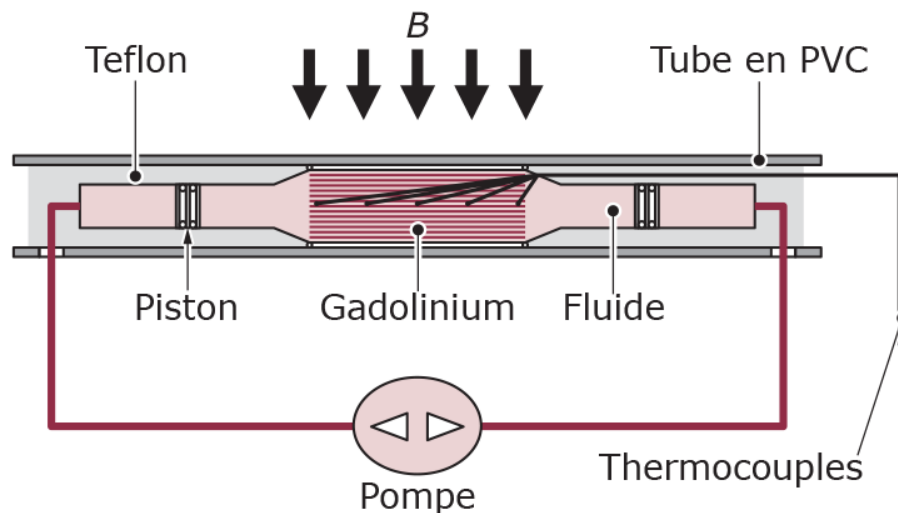

FIGURE 3.3: Clot et alt. linear prototype principle of operation. Picture taken from Lebouc et alt..[4]

---

[1]Grenoble Electrical Engineering Laboratory.

7. The device built is drawn in Fig. 3.3. It consists in a tube containing the gadolinium sheets, between which water can circulate to transport heat. The pump ensures the motion of the fluid through pistons which push and pull water in a forth-and-back movement. On the other hand, a pneumatic drive allows the whole system to move in and out of the cylindrical magnet. A PVC tube permits to guide the hydraulic system and inside this tube is installed Teflon to isolate the fluid from its surroundings. Five T-type thermocouples make temperature measurements inside the AMR bed possible. The working principle of the device is based on the active magnetic refrigeration.

8. This prototype presents the practical interest of being easily tunable: the MCM used, the fluid and even the magnet can be changed easily. One can note that this is the type of device that resembles the most what is studied in the present work.

3.2.2 Engelbrecht et alt., 2011

Another prototype similar to that designed in the present work is the one built by Engelbrecht et alt.,[6] but in their paper they explored different possible AMR beds and compared them.

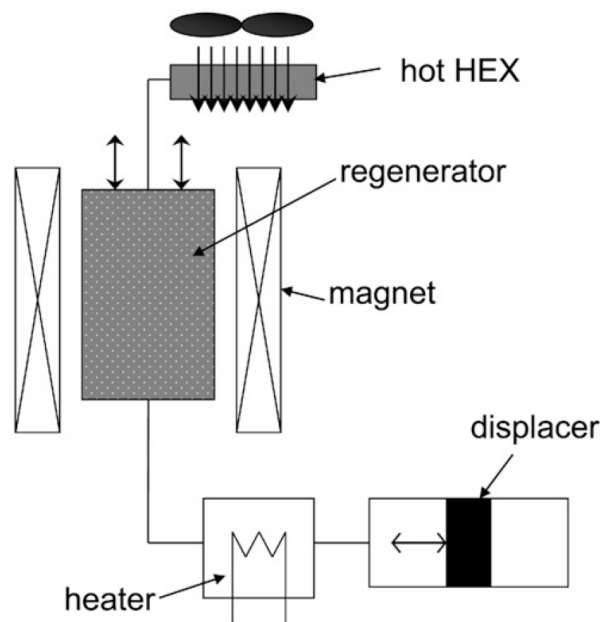FIGURE 3.4: Engelbrect et alt. prototype principle of operation. Picture taken from Engelbrecht et alt..[6]

1. The working body is made of 13 sheets of Gd.

2. The magnet employed is a Halbach cylinder, providing a field of 1.03 T.

3. A fluid constituted of 75% of water added with 25% of antifreeze is used.

4. The sheets are 0.9 mm thick, 25 mm wide and 40 mm long. They are separated by a space of 0.8 mm.

5. The period achieved by the system is of 8 s.

6. The no-load temperature span obtained is of 10.2 K.

7. The principle of operation of the device is illustrated in Fig. 3.4. The regenerator is made to move vertically by a stepper motor in and out of the magnet which is stationary. The AMR cycle is exploited in order to assess the performances of the materials.

   As already mentioned, Engelbrecht et alt. tested several magnetocaloric materials having different Curie temperatures, thus the regenerator was made to be changed easily. Concerning the heat exchangers, their temperature must be made to vary accordingly.

8. The main advantage of this prototype is its interchangeability, which allows to make several tests in order to asses the performances in every case. However, for a commercial purpose such a device is not well suited and mainly serves as a designing prototype.

3.2.3   Balli et alt., 2012

In 2012, the Swiss team of Balli et alt. designed and built a prototype using two AMR beds moving in two magnets. Moreover, each AMR bed is constituted of two sets of plates placed side to side in order to counteract the magnetic force appearing as the MCM is moved in and out of the magnetic field.[7]

1. There are two AMR beds each filled with 400 g of gadolinium plates. Each regenerator is separated in two parts containing each 200 g of Gd.

2. Two Halbach cylinders are used, providing each a field of 1.45 T. They are made of NdFeB.

3. The fluid utilized is silicon oil, and is flowing at 20 g/s.

4. The plates are 1 mm thick, 8 mm wide and 100 mm long. The two parts of each AMR bed are separated by 30 mm.

5. A frequency of 0.5 Hz is reached with such a device.

6. The no-load temperature span achieved is of 32 K. For a temperature span of more than 20 K, a cooling power between 80 and 100 W is obtained.

7. The device shown in Fig. 3.5 is made of two permanent magnets in which two regenerators contain two separated parts containing each gadolinium plates. There are also four heat exchangers, two cold and two hot ones. An actuator allows to control the back-and-forth motion of the AMR beds inside the magnets. In this configuration, the fluid evacuates the cooling energy from the demagnetized part in the AMR bed to the cold source, and releases the heat coming from the magnetized part into the hot reservoir at the same time.

8. The major advantage of the prototype made by Balli et alt. is that the fact that two AMRs are placed side to side allows to decrease the influence of the magnetic force acting on the MCM as they enter the magnet yoke. Moreover, this configuration decreases the demagnetization effect appearing in the opposite direction too.
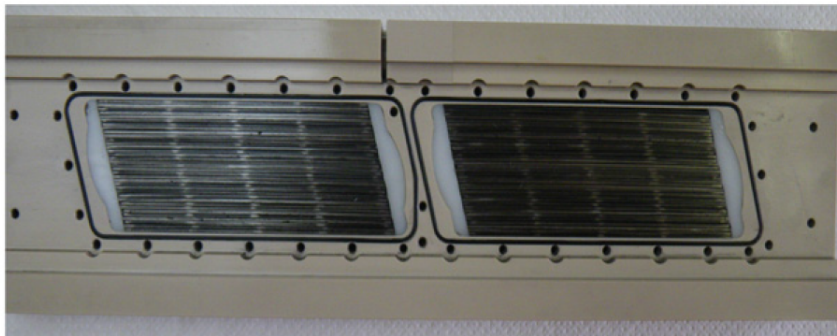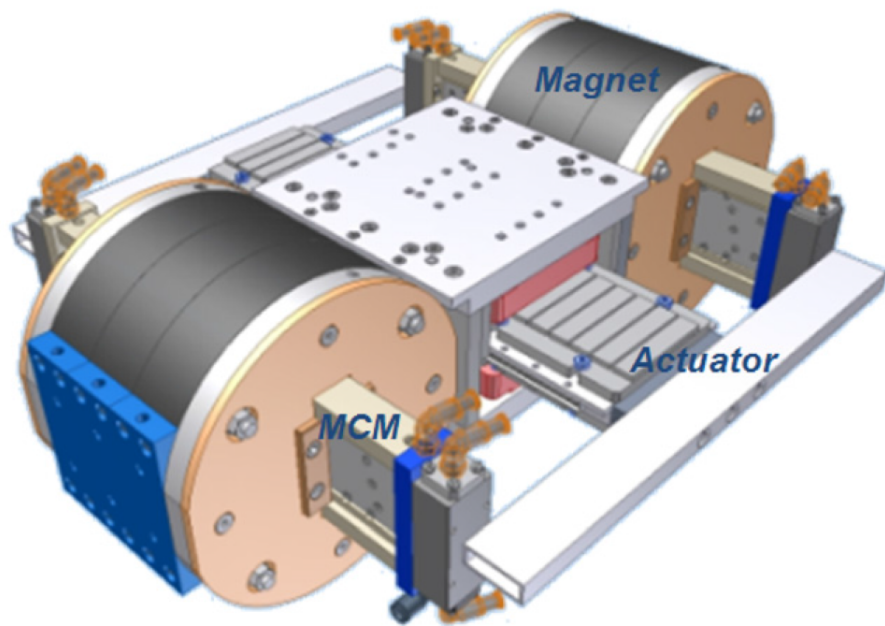
FIGURE 3.5: Balli et alt. linear prototype principle of operation. Picture taken from Balli et alt..[7]

Summary

- Since 1976 when the first magnetocaloric-based refrigeration prototype was made by Brown, improvements have been brought to the field. One may cite the discovery of giant magnetocaloric materials and the design of the first magnetic refrigerator using a permanent magnet instead of a superconducting one.

- There are two major types of magnetic prototypes, classified according to their motion: the reciprocating ones and the rotary ones. To assess the quality of a magnetic refrigerator, one can measure its no-load temperature span as well as its cooling power when this latter is null, then derive the coefficient of performance of the device.

- Numerous variations may be found in the literature concerning the magnetocaloric material used: this one can present under the form of small spheres or event powder, or can be shaped as plates. Packed beds have a higher energy density but, as in the case of gadolinium, powders can be toxic and the use of sheets is preferred. Sometimes one might event think of using a layered bed in order to fully catch the MCE of the different materials.

- Usually the magnets used present a field of around 1 or 2 T. The no-load temperature span and cooling power achieved by the prototype really depend on the quantity of raw material which is used. The operating frequency is however always really slow, that is comprised between less than 1 and a few Hz. The working fluid is most of the time water of a type of oil, but liquids are preferred to gases since they exhibit the best thermal properties.

References

[1] A. Kitanovski, J. Tušek, U. Tomc, U. Plaznik, M. Ožbolt, and A. Poredoš, *Magnetocaloric Energy Conversion*. Switzerland: Springer, 2015.

[2] G. V. Brown, "Magnetic heat pumping near room temperature," vol. 47, pp. 3673–3680, 1976.

[3] X. Bohigas, E. Molins, A. Roig, J. Tejada, and X. X. Zhang, "Room-temperature magnetic refrigerator using permanent magnets," vol. 36, no. 3, pp. 538–544, 2000.

[4] A. Lebouc, F. Allab, J.-M. Fournier, and J.-P. Yonnet, "Réfrigération magnétique," 2005.

[5] P. Clot, D. Viallet, F. Allab, A. Kedous-Lebouc, J. M. Fournier, , and J. P. Yonnet, "A magnet-based device for active magnetic regenerative refrigeration," vol. 39, no. 5, pp. 3349–3351, 2003.

[6] K. Engelbrecht, C. Bahl, and K. Nielsen, "Experimental results for a magnetic refrigerator using three different types of magnetocaloric material regenerators," vol. 34, pp. 1132–1140, 2011.

[7] M. Balli, O. Sari, C. Mahmed, C. Besson, P. Bonhote, D. Duc, and J. Forchelet, "A pre-industrial magnetic cooling system for room temperature application," vol. 98, pp. 556–561, 2012.

> ⌒─────── *Nomenclature* ───────⌒
>
> | | | |
> |---:|:---|:---|
> | T | (K) | temperature |
> | $\vec{H}$ | (A m^{-1}) | magnetic field |
> | $\vec{F}$ | (A m^{-1}) | magnetic force |
> | e | (m) | thickness |
> | ℓ | (m) | width |
> | L | (m) | length |

4

THERMAL STUDY

Before designing the prototype, a brief thermal study should be conducted in order to evaluate the powers involved, for e.g. choosing the hydraulic pumps that will be used, and so forth. As a reminder, the device will consist in Gadolinium plates immersed in a fluid that performs the heat transfers between a hot and a cold sources. Because of the configuration of the problem, the study will only be carried for one of these plates. One might also use the molecular field theory in order to assess the properties of Gadolinium such as the adiabatic temperature change or the specific heat capacity. In page 74 one will eventually find a summary of the chapter.

1. Governing equations

First, the problem studied will be described, as well as the simplifying hypotheses made in order to compute all the desired quantities, namely the temperature of the plates, the heat transfers occurring between the sheets and the fluid and the coefficient of performance of the device. One will derive the equations governing the situation before nondimensionalizing and finally discretize them in order to solve them in MATLAB. In particular, the well-known ε-NTU method will be exploited.

1.1 Geometry of the problem

The studied situation is drawn in Fig. 4.1. As already mentioned, it consists in a simple solid plate exchanging heat with a fluid flowing in a direction parallel to the length of the plate, in this case x. The dimensions indicated in the picture are the following ones: L is the length of the sheet, ℓ its width and e its thickness, whereas d represents the space between two sheets. For an assembly of N plates, the total height H is thus equal to $Ne + (N-1)d$.

The numerical values of all these quantities are respectively: $L = 10$ cm, $\ell = 2.5$ cm, $e = 1$ mm, $N = 10$, $d \simeq 4.44$ mm and $H = 5$ cm. Obviously these dimensions are not the exact ones that will be used for making the prototype itself, as it will be detailed in the following chapter. One may notice in Fig. 4.1 that other plates are drawn in gray but the study only concerns the first one, which could be the top one as represented in the picture or any one of them.
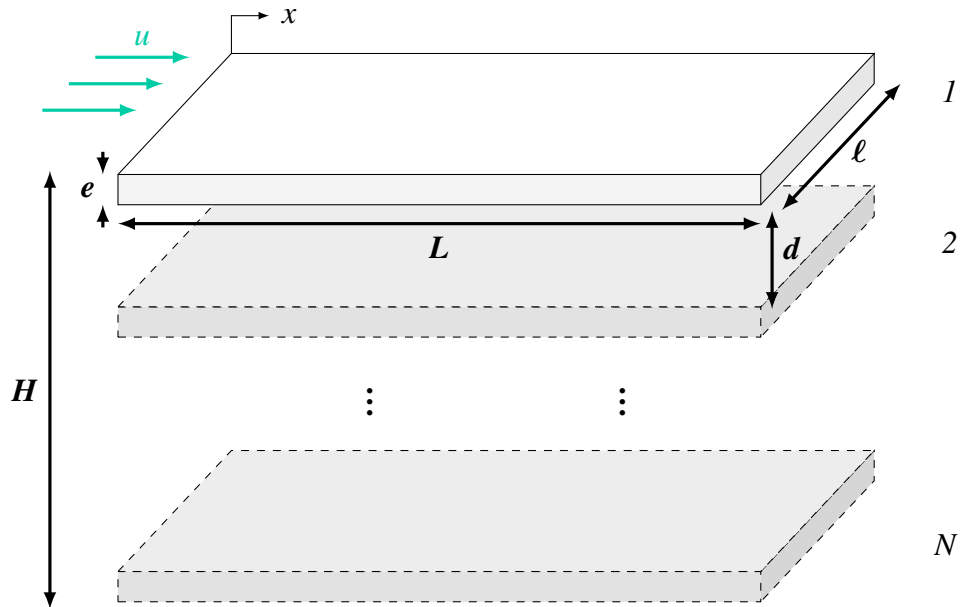
FIGURE 4.1: Geometry of the system.

1.2   Simplifying assumptions

Some hypotheses must be made in order to model the system and be able to solve the equations afterwards. They are all listed hereafter:

- The heat transfer between the plate and the fluid is supposed to occur only thanks to convection ; the transverse conduction is neglected both in the fluid and in the solid. This latter hypothesis will be checked later on by computing the Biot number. However, conduction along the plate must occur in order to create a thermal gradient, as explained previously in Chapter 2.

- It is also assumed that there is no radiative heat transfer between the plates.

- One supposes that the device is well thermally insulated from its surroundings so there are no heat leaks.

- The flow is assumed perfectly parallel to the plate and laminar in such a way that turbulence and secondary flows are neglected. This hypotheses are valid for sufficiently low Reynolds numbers and will also be verified later on.

- In a first approximation, one also forget about the roughness of the plates and all the other effects such as a sudden section change that might cause a pressure drop in the channels.

- The sheets are supposed to be homogeneous and isotropic so that the heating occurs uniformly.

- Hysteresis and effects such as eddy currents that might also cause the MCM the heat up are neglected. Only the MCE is taken into account and it is furthermore supposed reversible

- All the (de)magnetization processes are assumed to occur so quickly that only the time taken to perform heat transfers between the fluid and the solid has to be considered. Experience indicates indeed that the magnetization of the plate reaches almost instantly its final value, and that it increases a little bit more afterwards but this delayed contribution is negligible. The same holds of course for the demagnetization.

1.3 Equations

First of all one should note that all quantities X with index X_f refer to the **f**luid whereas those with index X_s state for the **s**olid Gadolinium plate.

One assumes first that the Gadolinium plate was just submitted to magnetization and that as a consequence, its temperature has increased. The convective heat transfer may be modelled by a thermal resistance R depending on the convection transfer coefficient of the fluid, h, as follows:

$$R = \frac{1}{hA} = \frac{1}{UA} \qquad (4.1)$$

where A is the heat transfer area, namely the surface of the plate. In the latter expression, U is called the overall heat transfer coefficient. Because there is only one sort of transfer considered, one has $U = h$.

The convective heat transfer per unit surface, $\dot{q}$ (W m^{-2}) from the solid to the fluid may be computed in this case as

$$\dot{q} = h\,(T_s - T_f). \qquad (4.2)$$

If the process considered was the demagnetization of the plate and that the temperature was decreasing, the heat transfer would occur from the fluid towards the solid and would simply be equal to $-\dot{q}$.

The internal energy equation for a fluid flowing at a velocity u in the x direction reduces to[?]

$$\rho_f c_{p,\,f} V_f\,(\partial_t T_f + u\,\partial_x T_f) = \dot{q}A \qquad (4.3)$$

where the dissipative term on the right-hand side is simply equal to the convective heat transfer per unit surface multiplied by the exchange area A. In the former relation, ρ_f is the fluid density, $c_{p,\,f}$ its specific heat capacity at constant pressure, V_f its volume and T_f its temperature. The volume is simply given by

$$V_f = L\,\ell\,d \qquad (4.4)$$

while the exchange area A is defined as

$$A = L\,\ell. \qquad (4.5)$$

Moreover, if $\dot{m}$ designates the mass flow rate one gets for the fluid velocity

$$u = \frac{\dot{m}_f}{\rho_f\,\ell\,d}. \qquad (4.6)$$

On the other hand, from the heat equation one finds for the solid that

$$\rho_s c_{\vec{H},s} \partial_t T_s = k_s \Delta T_s - \frac{\dot{q}}{L}. \tag{4.7}$$

In this relation, ρ_s designates the Gadolinium density, $c_{\vec{H},s}$ its specific heat capacity at constant magnetic field, k_s its thermal conductivity and T_s its temperature.

The unknowns of the problem are thus the temperature fields in the fluid T_f and in the solid T_s, as well as the convective heat transfer per unit surface $\dot{q}$. All of these depend on the time t and the space variable x since the situation is unidimensional.

1.4 Input parameters

If one aims at computing a problem numerically, the values of the input parameters appearing in the equation previously obtained must be looked for. They are all gathered in Table 4.1 in the next page and will be used in the following sections.

The convective heat transfer coefficient h depends on the geometry of the case considered and must be computed, as it will be done in the next section. The mass flow rate $\dot{m}_f$ of the incoming flow must be chosen and can be made to vary. The parameters k_f and ΔT_{ad} do not appear in the former equations but will be used in the following.

The first one of them is the thermal conductivity of the fluid. The second represents the adiabatic change of temperature of the material (see Chapter 2), assumed constant for now because it does not vary much around the ambient temperature for Gadolinium.

1.5 Nondimensionalization

Nondimensionalizing the equations previously written allows to assess the balance between the different input phenomena occurring in the system.

Starting from Eqs (4.3) and (4.7), one may nondimensionalize them by inserting the following quantities:

$$\xi = \frac{x}{L}, \qquad\qquad \theta_f = \frac{T_f}{\Delta T_{ad}},$$

$$\tau = \frac{t}{\dfrac{\rho_f c_{p,f} L^2}{k_f}}, \qquad\qquad \theta_s = \frac{T_s}{\Delta T_{ad}}.$$

Looking at these equations, it should be noted that the definition of the reduced time τ could differ according to whether one uses instead of k_f the solid conductivity or the convective heat transfer coefficient, but the choice made above allows the appearance of suitable dimensionless numbers for the present problem.

L (cm)	ℓ (cm)	e (mm)	H (cm)	d (cm)	N
10	2.5	1	5	4.44	8

MATERIAL PARAMETERS FOR THE WATER

$\rho_{\mathbf{f}}$ (kg m^{-3})	$\mu_{\mathbf{f}}$ (kg m^{-1} s)	$c_{p,\mathbf{f}}$ (J kg^{-1} K)	$k_{\mathbf{f}}$ (W m^{-1} K)
999.8	4185	10^{-3}	0.6

MATERIAL PARAMETERS FOR THE GADOLINIUM

$\rho_{\mathbf{s}}$ (kg m^{-3})	$c_{\overrightarrow{H},\mathbf{s}}$ (J kg^{-1} K)	$k_{\mathbf{s}}$ (W m^{-1} K)	$\Delta T_{\mathbf{ad}}$ (K)
7901	240 – 320	10.6	5

TABLE 4.1: input parameters used for solving the equations.

One obtains then for the first equation

$$\rho_f c_{p,\,f} \, L \, \ell \, d \left(\frac{\Delta T_{ad}}{\dfrac{\rho_f c_{p,f} L^2}{k_f}} \frac{\partial \theta_f}{\partial \tau} + \frac{\dot{m}_f}{\rho_f \, \ell \, d} \frac{\Delta T_{ad}}{L} \frac{\partial \theta_f}{\partial \xi} \right) = h \, L \, \ell \, (\theta_s - \theta_f) \, \Delta T_{ad}, \qquad (4.8)$$

or, after rearranging the terms,

$$\frac{\partial \theta_f}{\partial \tau} + \frac{\dot{m}_f c_{p,f} L}{k_f \ell d} \frac{\partial \theta_f}{\partial \xi} = \frac{hL^2}{k_f d} (\theta_s - \theta_f). \qquad (4.9)$$

The former relation may be revised as

$$\frac{\partial \theta_f}{\partial \tau} + \frac{1}{Le} \frac{\partial \theta_f}{\partial \xi} = Nu \frac{L}{d} (\theta_s - \theta_f) \qquad (4.10)$$

where two well-known dimensionless numbers appear, the first being the Nusselt number related to the flow, that is,

$$Nu = \frac{hL}{k_f}. \qquad (4.11)$$

On the other hand, one also finds the Lewis number, namely,

$$Le = \frac{k_f \, \ell \, d}{\dot{m}_f \, c_{p,\,f} \, L}. \qquad (4.12)$$

Proceeding in the same manner for Eq. (4.7)

$$\rho_s c_{\vec{H},s} \frac{\Delta T_{ad}}{\dfrac{\rho_f c_{p,f} L^2}{k_f}} \frac{\partial \theta_s}{\partial \tau} = k_s \frac{\Delta T_{ad}}{L^2} \frac{\partial^2 \theta_s}{\partial \xi^2} - \frac{h \Delta T_{ad}}{L} (\theta_s - \theta_f) \qquad (4.13)$$

after rearranging the terms,

$$\frac{\rho_s}{\rho_f} \frac{c_{\vec{H},s}}{c_{p,\,f}} \frac{\partial \theta_s}{\partial \tau} = \frac{k_s}{k_f} \frac{\partial^2 \theta_s}{\partial \xi^2} - Nu \, (\theta_s - \theta_f) \qquad (4.14)$$

1.5.1 Nusselt number

The ratio of Eq. (4.11) compares the heat transferred by convection and by conduction across the fluid.

The Nusselt number might be used to compute the value of the convective heat transfer coefficient h because this latter depends on the geometry of the problem. One easily finds in handbooks values already calculated for Nu as a function of the case treated, here a simple rectangular plate. From Incorprera et alt.[1], one has

$$Nu = 3.39.$$

60

In some problems the Nusselt number may depend e.g. on the position x, but in the present case it can be considered constant all along the plate. Therefore, one can deduce the value of the fluid convective transfer coefficient, namely

$$h = 10.17 \, \text{W} \, \text{m}^{-2} \, \text{K}.$$

Looking at the value of Nu which is greater than 1, one deduces that the transfer of heat carried by the fluid occurs mainly through convection. The conduction inside the fluid may thus be neglected.

1.5.2 Lewis number

This number is originally defined as follows, with D ($\text{m}^2 \, \text{s}^{-1}$) a proper diffusive coefficient,

$$\text{Le} = \frac{k_\text{f}}{\rho_\text{f} \, D \, c_{p,\,\text{f}}} \qquad (4.15)$$

Nevertheless, when looking at the product $\rho_\text{f} D$, it might be noticed that its units ($\text{m}^2 \, \text{s}^{-1} \times \text{kg} \, \text{m}^{-3}$) match the ones of the ratio $\dot{m}_\text{f}/l$ ($\text{kg} \, \text{s}^{-1} \times \text{m}$), if l simply designates some length. This shows the relevance of the definition obtained in Eq. (4.12) for the Lewis number.

Such a quantity characterizes the balance between heat and mass transfers. When computing its inverse, one finds the value of

$$\frac{1}{\text{Le}} = 46\,500,$$

which indicates that the transfer occurring mostly is the heat transfer whereas the mass one is negligible, as one would expect it in view of the considered situation. This means that one can neglect any inertia effect that would arise.

It should be noted that the Lewis number may be simply written as the ratio of the Schmidt and the Prandtl numbers, the first one being used in diffusive flows and the second appearing in most heat transfer problems.

1.5.3 Reynolds number

The Reynolds number Re does not appear in the former relations but is important in fluid mechanics since it allows to check whether or not a flow shows turbulence at some point, therefore permitting to verify a previously made assumption. It is defined as

$$\text{Re} = \frac{\rho_\text{f} u D_\text{h}}{\mu_\text{f}}, \qquad (4.16)$$

with u the characteristic velocity of the flow, D_h a characteristic length and μ_f the dynamic viscosity of the fluid. In the present case, although one may simply perform the global study for a flow along a plate, it is more appropriate for computing the Reynolds number to consider the fact that the flow occurs inside a rectangular pipe formed by two parallel plates and the closures

on the sides. Therefore the length to use is the hydraulic diameter D_h, given by

$$D_h = 4 \cdot \frac{A_{cs}}{P_w} \tag{4.17}$$

with A_{cs} the cross-section area and P_w the wetted perimeter of the pipe. A_{cs} is simply equal to the product $\ell \cdot d$ whereas P_w is given by $2(\ell + d)$. Knowing the values of Table 4.1 and using for instance a mass flow rate of 10^{-2} kg s^{-1} which would correspond to a fluid velocity of around 6.67 cm/s, the hydraulic diameter is equal to 0.48 mm. Therefore, one obtains

$$\text{Re} = 588.82,$$

that is, the flow is well laminar since for a pipe the critical Reynolds number is about 3000.

1.5.4 Biot number

The Biot number allows to verify the hypothesis made on the transverse conduction inside the solid, which has been neglected up to now. It is defined as

$$\text{Bi} = \frac{hL^*}{k_s}, \tag{4.18}$$

where L^* is the ratio between the volume and the exterior surface of the solid, namely in this case

$$L^* = \frac{L\ell e}{2\,(L\ell + \ell e + Le)}. \tag{4.19}$$

The Biot number looks like the Nusselt one, but the thermal conductivity of the solid is used instead the fluid one because one wants to compare the influence of the convection in the fluid and the conduction inside the plat. The convective heat transfer coefficient was computed in section 1.5.1 above.

Inserting the numerical values of Table 4.1 into the former relations, one finds $L^* = 4.76 \cdot 10^{-4}$ mm. Hence, one gets

$$\text{Bi} = 9.44 \cdot 10^{-3}$$

such that transverse conduction is negligible inside the solid and does not need to be taken into account.

1.5.5 Characteristic time

Different definitions might be used for the characteristic time of the system, according to their dimensions. But only one of them should be correct from a physical point of view. Denoting this time τ, one writes

$$\tau = \frac{\rho_s c_{\vec{H},s} d}{2h} \tag{4.20}$$

whose dimension is that of a time. With the former parameters one finds a value of

$$\tau = 27.07\ s.$$

This represents the time needed by the system that was just submitted to an adiabatic change of temperature to evacuate the heat by convection and reach $1/e \simeq 36.78\%$ times the value of its initial state. The temperature is indeed decreasing exponentially over time.

The physical parameters that seem best suited for characterizing the relaxation time are the convective heat transfer coefficient, the density of the solid, its specific heat capacity and a characteristic length of the pipe. The coefficient h is used rather than a conductive coefficient because the transfer occurs mostly by convection. On the other hand, the properties of the solid are used because it is inside the solid that the temperature is increased. The factor 1/2 accounts for the fact that only half a period is considered.

1.6 ε-NTU method[1]

The effectiveness-NTU method is used in heat exchanger analysis in order to evaluate its performances when e.g. the outlet temperature of the fluid remains unknown. The effectiveness ε is defined as the ration between the actual heat transferred in the heat exchanger q and the maximum possible one q_{max}, namely

$$\varepsilon = \frac{\dot{q}}{\dot{q}_{max}}. \tag{4.21}$$

In the former relation, the maximum heat rate that may be transferred is given by

$$\dot{q}_{max} = C_{min} \left(T_{h,\,in} - T_{c,\,in} \right) \tag{4.22}$$

where C_{min} is the minimum specific heat rate (namely the specific heat multiplied by the mass flow rate) among the two materials involved. The material possessing the smallest specific heat is indeed the one less requiring the least of heat to see its temperature increase, and will thus undergo the greatest change of temperature. $T_{h,\,in}$ and $T_{c,\,in}$ are respectively related to the warmer side and the cooler one, at the very entrance of the heat exchanger. The actual heat transfer occurring in the exchanger is thus given by

$$\dot{q} = \varepsilon \dot{q}_{max}, \tag{4.23}$$

where it can be shown that

$$\varepsilon = f \left(NTU, \frac{C_{min}}{C_{max}} \right). \tag{4.24}$$

NTU states for **N**umber of **T**ransfer **U**nits, whose definition is

$$NTU = \frac{AU}{C_{min}} \tag{4.25}$$

with U the overall heat transfer coefficient, A the transfer area. U was already computed in Eq. (4.1) from page 57. In the present case it is simply equal to h. On the other hand, C_{min} is given as

$$C_{min} = \dot{m}_f\, c_{p,\,f}. \tag{4.26}$$

The specific heat rate C being defined as the specific heat capacity multiplied by the mass rate, for the solid plate C is null because there is no flow of mass occurring. Therefore, one uses the

specific heat rate of the fluid.

The effectiveness depends on the type of heat exchanger and empirical data can be found in many handbooks. For a heat exchanger comprising a material in its solid phase, the relation between ε and NTU is given in e.g. Incroprera et alt.[1] as

$$\varepsilon = \left(1 - \exp\left(-\text{NTU}\right)\right). \tag{4.27}$$

Inserting this relation into Eq. (4.23), it becomes for $\dot{q}$

$$\dot{q} = \varepsilon\, \dot{m}_f\, c_{p,\,f}\left(T_s - T_f\right) \tag{4.28}$$

$$= \left(1 - \exp\left(-\text{NTU}\right)\right) \dot{m}_f\, c_{p,\,f}\left(T_s - T_f\right) \tag{4.29}$$

$$= \left(1 - \exp\left(-\frac{AU}{\dot{m}_f c_{p,\,f}}\right)\right) \dot{m}_f\, c_{p,\,f}\left(T_s - T_f\right) \tag{4.30}$$

and hence

$$\dot{q} = \underbrace{\left(1 - \exp\left(-\frac{Ah}{\dot{m}_f c_{p,\,f}}\right)\right) \dot{m}_f\, c_{p,\,f}}_{C_{\text{NTU}}}\left(T_s - T_f\right). \tag{4.31}$$

In the latter expression, a constant C_{NTU} is defined for the seek of simplicity in the calculations coming in the next sections.

Taking into account the previously detailed ε-NTU method, one eventually finds the following governing equations of the situation:

$$\rho_f c_{p,\,f} V_f \left(\partial_t T_f + u\, \partial_x T_f\right) = C_{\text{NTU}} A \left(T_s - T_f\right), \tag{4.32}$$

$$\rho_s c_{\vec{H},s} \partial_t T_s = k_s \partial_{xx}^2 T_s - \frac{C_{\text{NTU}}}{L}\left(T_s - T_f\right). \tag{4.33}$$

2. Discretization and numerical scheme

After having established the equations governing the studied situation and discussed the balance between the terms appearing in them, one now wants to solve them. However, this must be done numerically due to the time and spatial derivatives that show up in these relations. A discretization of the domain will first be made, then the equations themselves will be discretized using an implicit Euler approach.

2.1 Discretization of the domain

The spatial domain is rather simple since it consists in a rectangular plate. One discretize it by dividing the sheet into small steps Δx along the x-direction, as depicted in Fig. 4.2 hereafter.

The number of subdivision is denoted μ_L and is equal to

$$\mu_L = \frac{L}{\Delta x}.$$ (4.34)

The variable i designates the number of a subdivision, with i varying between 1 and μ_L.
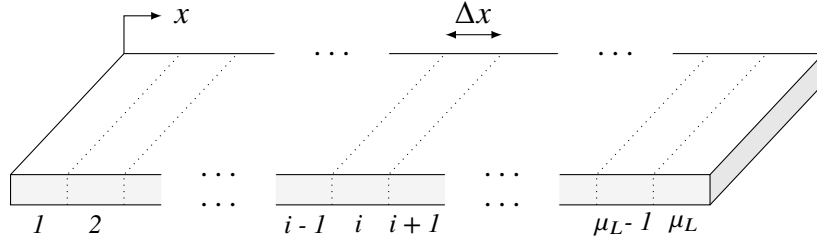

FIGURE 4.2: Geometry of the system.

On the other hand, the time period $\mathcal{T}$ taken for performing one heating/cooling of the MCM process is divided into $\nu_{\mathcal{T}}$ intervals of length Δt, in such a way that

$$\nu_{\mathcal{T}} = \frac{\mathcal{T}}{\Delta t}.$$ (4.35)

The magnetocaloric device will however perform a certain amount of cycles, this number being called K. The period taken by the system to perform a cooling and a heating steps is $2\mathcal{T}$. One assumed indeed that the (de)magnetization processes were instantaneous compared to the time needed for the heat transfers to occur between the plate and the fluid. The number of the cycle is represented by the variable k with $k \in [1, K]$, and the time step by n, with $n \in [1, 2K\nu_{\mathcal{T}}]$. A time scale summarizing all of this is drawn just below in Fig. 4.3.
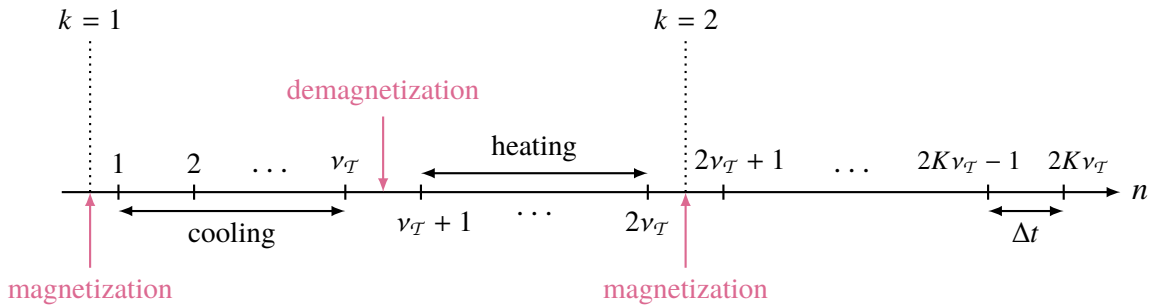

FIGURE 4.3: Time scale related to the system.

The temperature will thus be computed not for every possible (x, t) but only in a certain amount of points. The discrete version of the temperature at point $i\Delta x$ and after a time $n\Delta t$ then writes as

$$T(x = i\Delta x, t = n\Delta t) \rightarrow T_i^n.$$ (4.36)

2.2 Discretization of the equations

In order to discretize the equations previously obtained, different numerical schemes might be utilized. Here the choice was made on an implicit Euler method for approximating the time derivative, that is,

$$T^n = f(T^{n+1}). \tag{4.37}$$

The temperature after the nth time step is thus computed as a function of the temperature after the $(n + 1)^{\text{th}}$ one. For a first order time derivative, the easiest way to achieve this is to write

$$\partial_t T \rightarrow \frac{T^{n+1} - T^n}{\Delta t}. \tag{4.38}$$

On the other hand, for the first order spatial derivative, one can use the following approximation

$$\partial_x T \rightarrow \frac{T_{i+1} - T_{i-1}}{2\,\Delta x}. \tag{4.39}$$

For the second order derivative, the centered-in-space scheme will be utilized, namely,

$$\partial_{xx}^2 T \rightarrow \frac{T_{i+1} - 2T_i + T_{i-1}}{\Delta x^2}. \tag{4.40}$$

One may note that the first order spatial derivative could also have been approached by an upwind method.

Inserting these approximations into the governing equations of the problem and using the ε-NTU method for rewriting the heat transfer rate, one finds

$$\rho_{\text{f}} c_{p,\text{f}} V_{\text{f}} \left(\frac{T_{\text{f},i}^{n+1} - T_{\text{f},i}^n}{\Delta t} + u \frac{T_{\text{f},i+1}^{n+1} - T_{\text{f},i-1}^{n+1}}{2\,\Delta x} \right) = C_{\text{NTU}} A \left(T_{\text{s},i}^{n+1} - T_{\text{f},i}^{n+1} \right), \tag{4.41}$$

for the fluid part and for the plate one has

$$\rho_{\text{s}} c_{\vec{H},\text{s}} \left(\frac{T_{\text{s},i}^{n+1} - T_{\text{s},i}^n}{\Delta t} \right) = k_{\text{s}} \frac{T_{\text{s},i+1}^{n+1} - 2T_{\text{s},i}^{n+1} + T_{\text{s},i-1}^{n+1}}{\Delta x^2} - \frac{C_{\text{NTU}}}{L} \left(T_{\text{s},i}^{n+1} - T_{\text{f},i}^{n+1} \right). \tag{4.42}$$

It should be emphasized that because the scheme is implicit, the temperatures are all evaluated at the $(n + 1)^{\text{th}}$ step whereas the unknown one is T^n.

Rearranging the terms of Eq. (4.41), one gets the following relation

$$T_{\text{f},i}^n = \left(1 + C_{\text{f},1} \right) T_{\text{f},i}^{n+1} + C_{\text{f},2} T_{\text{f},i+1}^{n+1} - C_{\text{f},2} T_{\text{f},i-1}^{n+1} - C_{\text{f},1} T_{\text{s},i}^{n+1} \tag{4.43}$$

with the constants $C_{\text{f},1}$ and $C_{\text{f},2}$ defined as

$$C_{\text{f},1} = \frac{C_{\text{NTU}} A \Delta t}{\rho_{\text{f}} c_{p,\text{f}} V_{\text{f}}} \qquad \text{and} \qquad C_{\text{f},2} = \frac{u \Delta t}{2 \Delta x}.$$

For the solid, rewriting Eq. (4.42) yields to

$$T_{s,i}^n = \left(1 + C_{s,1} + 2C_{s,2}\right) T_{s,i}^{n+1} - C_{s,2}T_{s,i+1}^{n+1} - C_{s,2}T_{s,i-1}^{n+1} - C_{s,1}T_{f,i}^{n+1} \tag{4.44}$$

where

$$C_{s,1} = \frac{hA\Delta t}{\rho_s V_s c_{\vec{H},s}} \qquad \text{and} \qquad C_{s,2} = \frac{k_s \Delta t}{\rho_s c_{\vec{H},s} d\Delta x[2}.$$

with V_s the material volume, simply given by $V_s = L \cdot \ell \cdot e$.

3. Coding

To get an operational piece of code, one needs first to add initial and boundary conditions to the problem, reviewed hereafter. The actual connection with Chapter 2 is made afterwards. Finally, the convergence of the code is examined.

3.1 Matrix presentation

The equations obtained in the previous section may also be written under a matrix form. Such a presentation has a considerable advantage because the problem will be solved using MATLAB, a software optimized for matrix computations.

The temperatures of the fluid and the solid are presented in a vector of length $2\mu_L$. This vector will be updated at each time step after having performed the appropriate calculations. Inside this vector, the first μ_L elements correspond to the temperature of the fluid flowing in one direction or the other, that is when going from the cold reservoir side to the hot sink or conversely. The last μ_L elements represent the plate temperature.

Rewriting Eqs (4.43) and (4.44) under a matrix with this notation and taking into account the aforementioned initial and boundary conditions, one eventually gets the matrix from the following page.

3.2 Initial and boundary conditions

In order to perform calculations numerically, one needs to add enough initial and boundary conditions to close the problem. The initial condition is pretty direct and simply consists in assuming that at the beginning of the simulation, the fluid and the plate have the same temperature everywhere, respectively denoted $T_{f,0}$ and $T_{s,0}$.

Concerning the boundary conditions, one might use first the fact that at the entrance of the channel the fluid temperature should come from either the cold or hot exchanger, and thus has a temperature very close to one of theirs. The same holds for the end of the channel, and the opposite occurs when the fluid changes its direction. One can thus write in the case of a fluid flow from the cold to the hot side, in a mathematical point of view,

$$T_{f,1}^n = T_f^{\text{CHEX}} \quad \forall n, \tag{4.45}$$

$$T_{f,\mu_L}^n = T_f^{\text{HHEX}} \quad \forall n, \tag{4.46}$$

and in the opposite case,

$$T_{\text{f}, 1}^n = T_{\text{f}}^{\text{HHEX}} \quad \forall n, \tag{4.47}$$

$$T_{\text{f}, \mu_L}^n = T_{\text{f}}^{\text{CHEX}} \quad \forall n. \tag{4.48}$$

Temperatures for the hot and cold heat exchangers having a physical meaning will therefore have to be chosen properly.

Then one can consider that at the start of a new period (which does not especially need to be a new cycle), both the fluid and solid temperatures are equal to those at the end of the previous period, namely

$$T_{\text{f}, i}^{k \nu_T + 1} = T_{\text{f}, i}^{K \nu_T} \quad \forall i, \forall k, \tag{4.49}$$

$$T_{\text{s}, i}^{k \nu_T + 1} = T_{\text{s}, i}^{K \nu_T} \quad \forall i, \forall k, \tag{4.50}$$

$$\tag{4.51}$$

One may also use an adiabatic boundary conditions at both ends of the material because this latter was assumed perfectly insulated from its surroundings. This means that the derivative of the temperature as a function of the length equals 0, however this derivative as formerly computed involves points that should be outside the domain when computed in $i = 1$ or $i = \mu_L$. One might instead use the following definition which includes the two closest neighbours in only one direction and uses a different weights as

$$\partial_x T \rightarrow \frac{3T_i - 4T_{i-1} + T_{i-2}}{2 \, \Delta x}. \tag{4.52}$$

This might be applied to the solid temperature at both edges, which yields

$$\frac{3T_{\text{s}, \mu_L}^{n+1} - 4T_{\text{s}, \mu_L-1}^{n+1} + T_{\text{s}, \mu_L-2}^{n+1}}{2 \, \Delta x} \tag{4.53}$$

and

$$\frac{-3T_{\text{s}, 1}^{n+1} + 4T_{\text{s}, 2}^{n+1} - T_{\text{s}, 3}^{n+1}}{2 \, \Delta x} \tag{4.54}$$

where the change of sign is due to the change in direction of the derivative.

3.3 Including the MCE

In order to take the magnetocaloric effect exhibited by the material, as it was previously explained (de)magnetization steps are produced inside the code. To do so, the data obtained for the adiabatic change in temperature from Chapter 2 are utilized. To include this to the code, it suffices to look at the temperature inside the solid and check to what value of the adiabatic change of temperature it corresponds. Depending on whether the step is a magnetization or a demagnetization, one simply add or remove this latter value from the current temperature of the material.

$$
\begin{bmatrix}
T_{\mathrm{f},1}^{n+1} \\
T_{\mathrm{f},2}^{n+1} \\
T_{\mathrm{f},3}^{n+1} \\
\vdots \\
T_{\mathrm{f},\mu_L-1}^{n+1} \\
T_{\mathrm{f},\mu_L}^{n+1} \\
T_{\mathrm{s},1}^{n+1} \\
T_{\mathrm{s},2}^{n+1} \\
T_{\mathrm{s},3}^{n+1} \\
\vdots \\
T_{\mathrm{s},\mu_L-1}^{n+1} \\
T_{\mathrm{s},\mu_L}^{n+1}
\end{bmatrix}
=
\begin{bmatrix}
1 & 0 & 0 & \cdots & 0 & 0 & 0 & 0 & \cdots & 0 \\
-C_{\mathrm{f},2} & 1+C_{\mathrm{f},1} & C_{\mathrm{f},2} & \cdots & 0 & 0 & -C_{\mathrm{f},1} & 0 & \cdots & 0 \\
0 & -C_{\mathrm{f},2} & 1+C_{\mathrm{f},1} & C_{\mathrm{f},2} & 0 & 0 & 0 & -C_{\mathrm{f},1} & 0 & \cdots & 0 \\
\cdots & & \ddots & \ddots & \cdots & & \cdots & 0 & \ddots & \cdots \\
0 & 0 & -C_{\mathrm{f},2} & 1+C_{\mathrm{f},1} & -C_{\mathrm{f},2} & 0 & 0 & 0 & -C_{\mathrm{f},1} & \cdots \\
0 & 0 & & 1 & 0 & 0 & 0 & 0 & \cdots & 0 \\
0 & 0 & 0 & \cdots & 0 & -3 & 4 & -1 & & 0 \\
0 & -C_{\mathrm{s},1} & \cdots & \cdots & 0 & 0 & -C_{\mathrm{s},2} & 1+C_{\mathrm{s},1}+2C_{\mathrm{s},2} & -C_{\mathrm{s},2} & 0 \\
0 & 0 & -C_{\mathrm{s},1} & \cdots & 0 & 0 & 0 & -C_{\mathrm{s},2} & 1+C_{\mathrm{s},1}+2C_{\mathrm{s},2} & -C_{\mathrm{s},2} \\
\cdots & & \ddots & \ddots & \cdots & & \cdots & & \ddots & \ddots \\
0 & 0 & \cdots & -C_{\mathrm{s},1} & 0 & 0 & 0 & 0 & -C_{\mathrm{s},2} & 1+C_{\mathrm{s},1}+2C_{\mathrm{s},2} & -C_{\mathrm{s},2} \\
0 & 0 & \cdots & \cdots & 0 & 0 & 0 & 0 & 1 & -4 & 3
\end{bmatrix}
\begin{bmatrix}
T_{\mathrm{f},1}^{n} \\
T_{\mathrm{f},2}^{n} \\
T_{\mathrm{f},3}^{n} \\
\vdots \\
T_{\mathrm{f},\mu_L-1}^{n} \\
T_{\mathrm{f},\mu_L}^{n} \\
T_{\mathrm{s},1}^{n} \\
T_{\mathrm{s},2}^{n} \\
T_{\mathrm{s},3}^{n} \\
\vdots \\
T_{\mathrm{s},\mu_L-1}^{n} \\
T_{\mathrm{s},\mu_L}^{n}
\end{bmatrix}
\tag{4.55}
$$

3.4 Change in $c_{\vec{H},s}$

As it was seen in Chapter 2, the heat capacity of gadolinium around its Curie temperature experiences a λ anomaly and changes abruptly when temperature goes from below to above T_C. Therefore, to account simply for this behaviour one may use the value $c_{\vec{H},s} = 320\,\text{J kK}^{-1}$ below the Curie point and $c_{\vec{H},s} = 240\,\text{J kK}^{-1}$ above it. Inside the code, this is achieved by updating the values of the constants whenever needed during the calculations.

3.5 Improvements

Some improvements could be brought to the code already written in order to get a better understanding of the behaviour of the system.

3.5.1 Including the HEX's

First, one could take into account the heat exchanges occurring inside the cold and hot heat exchangers instead of just assuming their temperatures are constant over time. This may be done by adding similar equations as the ones derived for the heat transfer inside the fluid but by adapting the parameters and temperatures considered. Such an adding could permit to have a preliminary design of the heat exchangers that should be used to accompany the prototype.

3.5.2 Pressure drop

Because of the roughness of the pipe, a pressure drop might appear as the water is flowing inside the system. The Darcy-Weisbach relation for a pressure drop Δp inside a pipe is given by

$$\frac{\Delta p}{L} = f \frac{\rho_f}{2} \frac{\langle u \rangle^2}{D_h} \tag{4.56}$$

with the aforementioned hydraulic diameter

$$D_h = 4 \frac{A_{cs}}{P_{wetted}}. \tag{4.57}$$

In the former equation A_{cs} is the cross-section area, equal to $A_{cs} = \ell\, d$, and P_{wetted} the wetted perimeter, given by $P_{wetted} = 2\,(\ell + d)$.

Another parameter appears: f is the fouling factor computed as

$$f = \frac{64}{\text{Re}}, \tag{4.58}$$

with Re the Reynolds number reminded in the beginning of the chapter.

Including this pressure drop is another amelioration that might be brought to the code.

3.5.3 Convergence of the code

A convergence once the difference in temperatures computed between two consecutive cycles does not overcome a certain ϵ value, that can be arbitrary set to e.g. $\epsilon = 10^{-3}$ K. This criterion would ensure that the system is no longer in its transient regime and has reached the stationary one. It can be written as

$$\left| T_s^{(k+1)\nu_T} - \underline{T}_s^{k\nu_T} \right| \leq \epsilon. \tag{4.59}$$

Otherwise the backward-Euler, centered-in-space method is known to be unconditionally stable for the heat equation thus any steps Δt and Δx may be utilized for performing the calculations.

The main issues in obtaining results showing a physical sense arise from the choice in the temperatures used for the limit conditions, the period of the cycle $\mathcal{T}$ and the mass flow rate $\dot{m}_f$.

4. Results

In this section the results obtained using the numerical scheme from the previous paragraphs will be presented and discussed.

4.1 Temperature in the AMR bed as a function of time

In Fig. 4.4 is shown a simulation using for the mass flow rate the value of $\dot{m}_f = 3.5 \cdot 10^{-5}$ kg/s, which corresponds to a fluid velocity of 0.23 mm/s. The temperatures used for the limit conditions are: $T_{f,0} = 293.15$ K, $T_{s,0} = 293.15$ K, $T_f^{HHEX} = 298.15$ K and $T_f^{CHEX} = 288.15$ K. The period was set to $\mathcal{T} = 10$ s and the number of cycles displayed K to 50 (note that this is not the number of cycles after which the system is stationary). The steps used were $\Delta t = 0.001$ and $\Delta x = 0.001$.

One sees in Fig. 4.4 the hottest and coldest parts of the AMR bed. After each magnetization of demagnetization step, the flow occurs and the temperature decreases exponentially over time, as it would be expected for such a system. One sees that the envelope of the curves increases or decreases over time depending on the side of the AMR bed, until it reaches a stable shape when the system is stationary.

One sees that the active magnetic regeneration cycle is operating since the temperatures reached after a few cycles are comprised in a larger interval than the cold and hot heat exchanger temperatures. The largest temperature attained is 299.18 K and the lowest one is 286.17 K.

4.2 Temperature span ΔT_s along the AMR bed

One can compute the difference between the temperatures attained on each side of the bed, that is the temperature span reached by the system when the AMR is working. To do so one simply subtract the coldest temperatures from the highest ones. The maximum temperature span achieved is 6.86 K.

One may draw this gradient as a function of time, which is done in Fig. 4.5. The curve is however not correct compared to what is usually obtained in the literature. It should be more

smooth and should not present the peaks that are visible in Fig. 4.5. However, the global shape of the curve is still correct, and one sees how the temperature span should increase over time.

Compared to the adiabatic change of temperature experienced by the material which reaches a maximum of 4.75 K and during the simulations, the temperature span achieved here reaches a maximum value of 6.86 K.
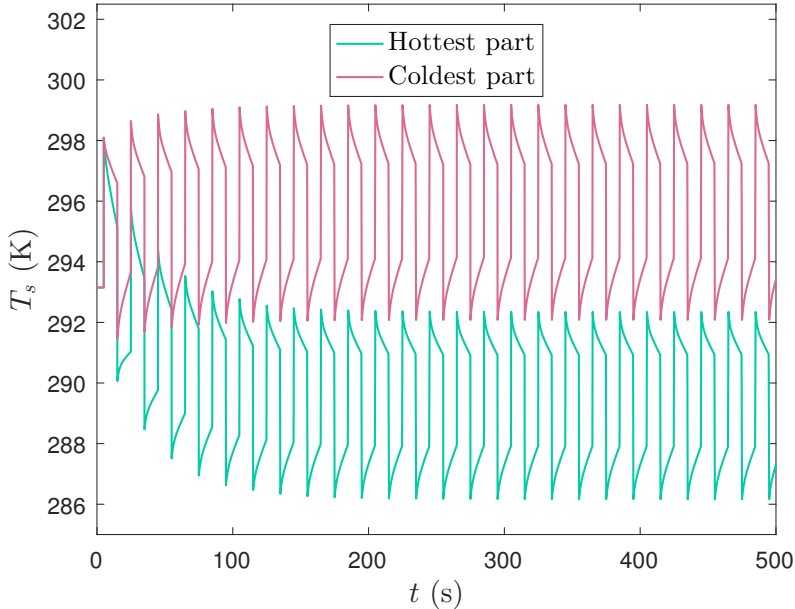

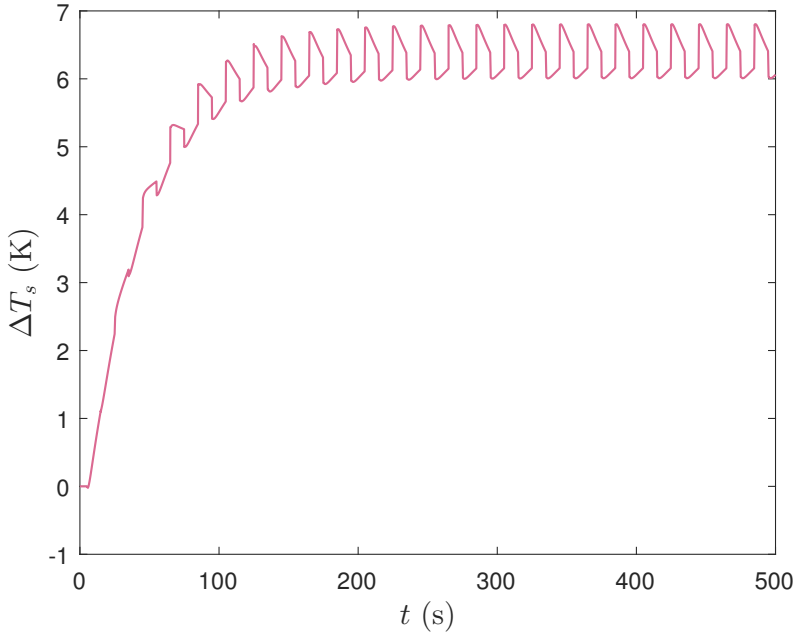FIGURE 4.4: Temperature in the hottest and coldest parts of the bed with respect to time.

FIGURE 4.5: Temperature span along the bed as a function of time
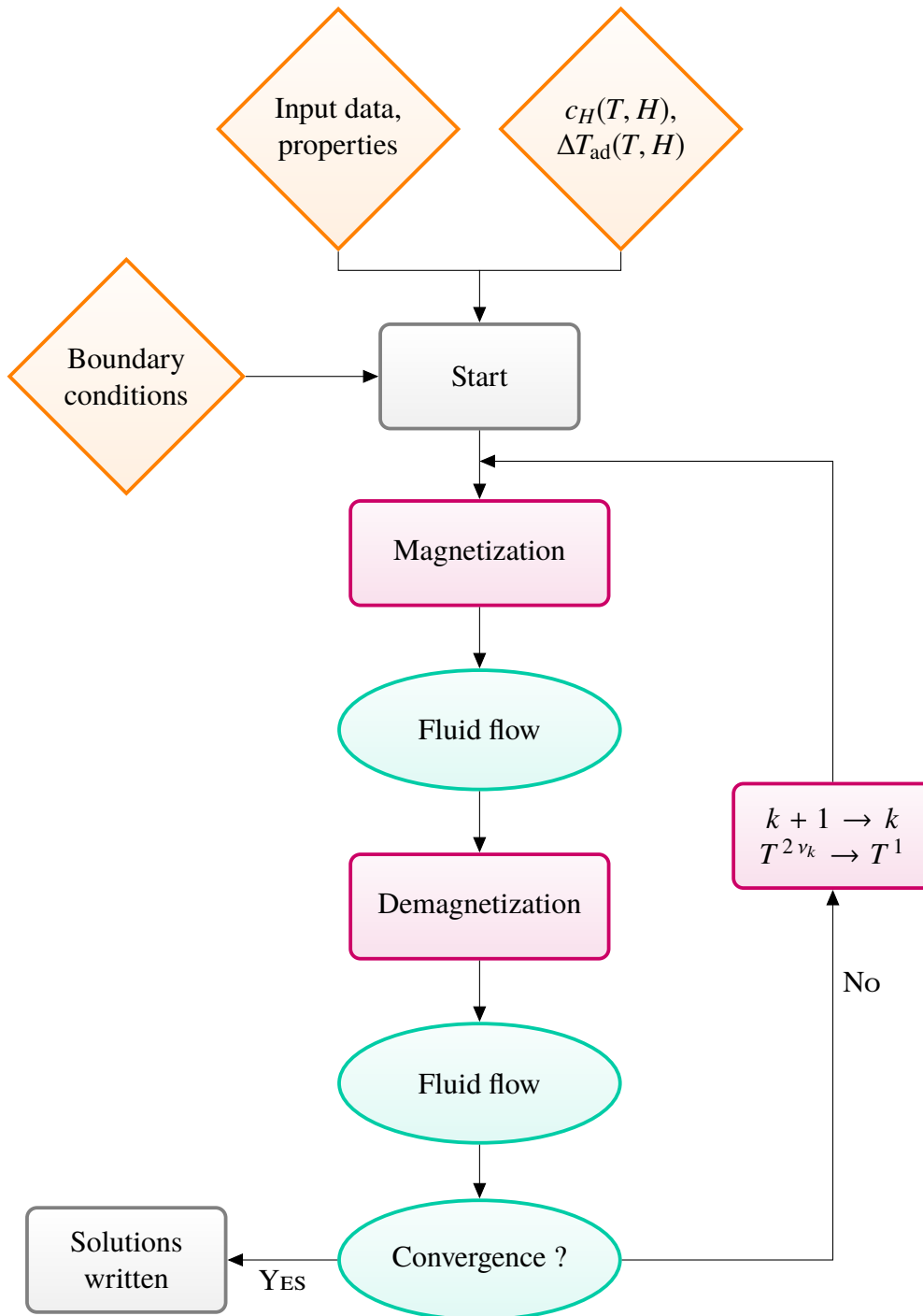
FIGURE 4.6: Chart of the final coding

Summary

- In the case of a fluid flowing along a rectangular plate, one finds that a convective heat transfer $\dot{q}$ occurs between them according to the following system of equations:

$$\rho_{\mathrm{f}} c_{p,\,\mathrm{f}} V_{\mathrm{f}}\, (\partial_t T_{\mathrm{f}} + u\,\partial_x T_{\mathrm{f}}) \;=\; \dot{q} A,$$

$$h\,(T_{\mathrm{s}} - T_{\mathrm{f}}) \;=\; \dot{q},$$

$$\rho_{\mathrm{s}} c_{\vec{H},\,\mathrm{s}} \partial_t T_{\mathrm{s}} \;=\; k_{\mathrm{s}} \Delta T_{\mathrm{s}} - \frac{\dot{q}}{L}.$$

- A dimensional analysis of the former set of equations allows to see that the conduction inside the solid is negligible. The flow is also found to be laminar and the characteristic time of the system for a given number of plates equal to 8 is 27.07 s.

- The convective heat transfer can be computed using the ε−NTU method which is typical for the design of heat exchangers. After what the spatial and temporal domains as well as all the equations obtained may be discretized. The method used for discretizing the equations is the backward-Euler, centered-in-space one, whose convergence is unconditionally stable.

- After what the MCE is included inside the code by using the data derived in Chapter 1. One also needs to add the change in the value of the heat capacity of the material below and above its Curie point, as well as suitable initial and boundary conditions and convergence criterion to the problem. A flowchart of the final code is drawn in Fig. 4.6. Some improvements such as taking into account the pressure drop inside the channel could be taken into account.

- When plotting the temperature in the hottest and coldest parts of the AMR bed, one gets the expected behaviour of a transient regime where the temperature span increases, followed by a stationary one. After each (de)magnetization step, the fluid flow occurring makes the temperature decrease or increase exponentially.

- The temperature span achieved at the end of the simulation is greater than the adiabatic change in temperature experienced by the material. The AMR cycle is thus working well. However, a bug in the code remains and does not allow to get the expected curve of the temperature span as a function of time. Nevertheless its global behaviour was still caught.

References

[1] F. P. Incropera, D. P. Dewitt, T. L. Bergman, and A. S. Lavine, *Foundations of Heat Transfer*. John Wiley & Sons, Inc., sixth ed., 2013.

[2] H. R. E.-H. Bouchekara and M. Nahas, *Magnetic Refrigeration Technology at Room Temperature, Trends in Electromagnetism - From Fundamentals to Applications, Dr. Victor Barsan (Ed.)*. InTech, 2012.

[3] J. Tusek, A. Kitanovski, I. Prebil, and A. Poredos, "Dynamic operation of an active magnetic regenerator (amr): Numerical optimization of a packed-bed amr," vol. 34, pp. 1507–1517, 2011.

[4] F. Allab, *Étude et conception d'un dispositif de réfrigération magnétique basé sur l'effet magnétocalorique géant*. PhD thesis, Institut National Polytechnique de Grenoble, May 2008.

[5] U. Legait, *Caractérisation et modélisation magnétothermique appliquée à la réfrigération magnétique*. PhD thesis, Institut National Polytechnique de Grenoble, July 2011.

<div style="text-align:center">

Nomenclature

</div>

T	(K)	temperature
$\vec{H}$	(A m^{-1})	magnetic field
$\vec{B}$	(T)	inductive magnetic field
$\vec{M}$	(A m^{-1})	magnetization
$\vec{F}_{\mathrm{mag}}$	(A m^{-1})	magnetic force
e	(m)	thickness
ℓ	(m)	width
L	(m)	length

5

DESIGN OF THE PROTOTYPE

In this chapter, the design of the prototype will be explained step by step. Because the Gadolinium plates are ferromagnetic, once they approach or leave the magnet yoke, a large magnetic force act on them. The prototype must then be conceived knowing the value of this force since this one must be countered in order to move the plates in and out of the magnet. Another important part is the design of the housing that will contain the plates and should thus fit perfectly their dimensions. Finally, one also needs to think about the supports required e.g. to hold the magnet in place or to attach all the pieces together.

1. Conception of the device

In this section, all the stages leading to the construction of the prototype will be briefly described. Basically, it consists in a magnetocaloric material moving through the variations of a magnetic field. This leads, thanks to the magnetocaloric effect, to temperature variations in the material.

As already explained in Chapter 2, the material best indicated for exploiting the MCE around ambient temperature is Gadolinium. The magnet used is a Halbach cylinder array whose nominal value is 1.05 T. As described in Fig. 5.1, this magnet has an inner radius of 5 cm and an outer one of 20 cm, while it is 10 cm long. A picture of the magnet is visible in Fig. 5.2.

In order to properly exploit the variations of temperature appearing in it, one may use either plates or powder of Gadolinium. But even though the powder presents a higher energetic density, its toxicity oriented the choice of the raw material towards 1 mm-thick sheets of Gd. These ones are also all 10 cm long and 2.5 cm wide in order to fit the dimensions of the magnet

FIGURE 5.1: Halbach cylindrical magnet and its dimensions (in cm).

yoke. In order to avoid the appearance of a torque on the plates, they should be placed in parallel with the main direction of the magnetic induction field, as depicted in turquoise in Fig. 5.1. Two plates are presented as example in the picture of Fig. 5.3 hereafter.

The plates are fixed in a case which is itself placed in a tube that may slide into the magnet yoke. Heat transfers are then performed by a suitable hydraulic circuit connected to the container.

The heat transfer fluid chosen is simply tap water which can circulate between a hot and a cold heat exchangers.

The container of the plates should fit inside the magnet yoke while containing all the plates and a tube must be able to surround it, thus the dimensions of the housing are fixed and, in the end, the best deal is to use eight plates at a time.

On the other hand, the motion of the tube inside and outside the magnet yoke is achieved using a linear guidance system provided by the LRJ company. This former will be described in details in a section below. It will be attached to the tube using simple aluminum bars. Obviously in the present case, it is important to avoid using materials such as e.g. cast iron for the device support, otherwise there might be trouble appearing because of its interaction with the magnetic field. A motor taken from the Leclercq Energy company, fixed to the guidance system, insures the motion of the whole system. As it will be explained later on, the magnetic force acting on the plates once they enter the field is such that the guidance system and the motor should be able to resist a force of at least 80 N, that is a weight of around 8 kg. One also needs to take into account the weight of the hydraulic circuit, the water inside it as well as the tube and its supports. The former value might thus by security be fixed to 10 kg.

The magnet must also be supported in order to be at the right height for the tube to move through its gap. The tube is already attached to the guidance system but it could be even more sustained for ensuring safety. Additional aluminum bars attached outside the prototype itself may be used in order to provide this additional support and make sure the tube and its initial fixations will not bend under the action of the force.

As already mentioned, all those stages will be described in more details afterwards. But first one needs to know exactly how the gadolinium plates behave inside the magnet and what value the force acting on them takes.

FIGURE 5.2: Picture of the Halbach cylindrical magnet used.
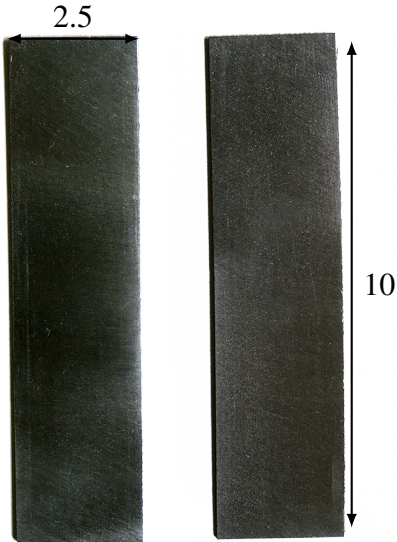
FIGURE 5.3: Two Gadolinium sheets and their dimensions (in cm).

2.   Magnetic field

The cylindrical Halbach magnet used for the prototype provides an inductive field $\overrightarrow{B}$ oriented mainly along the y axis of Fig. 5.1 whose nominal value is 1.05 T. However, this field is not uniform throughout the yoke of the magnet ; it is smaller close to the edges and greater at the center. The graph of Fig. 5.5 was drawn by Jean-François Fagnard at the lab.

One might indeed see it in the graph of Fig. 5.5 hereafter which represents the components of $\overrightarrow{B}$ along the three axes of Fig. 5.1, B_x, B_y and B_z. The y axis is actually represented on the top surface of the magnet, as the picture of Fig. 5.2 shows it. The graph of Fig. 5.5 exhibits the field components as a function of the distance from the center along the z axis, at different (x, y) locations which are drawn in blue in Fig. 5.4. This latter is simply a top view of the magnet. Points 1, 2 and 3 lie in a plane corresponding to any z value and respectively have the coordinates expressed in millimeters: $(0, 0)$, $(20, 0)$ and $(0, 20)$.
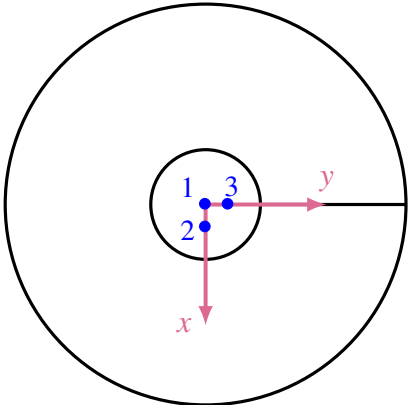
FIGURE 5.4: Top view of the magnet.

One notices in the graph below that the value of the B_y component reaches its greatest around the very center of the magnet yoke, whereas it diminishes as the distance from the center increases. This behaviour is nearly the same in locations 1, 2 and 3. The value taken by the inductive field is just a little bit higher in 3 at the center and smaller close to the edge.
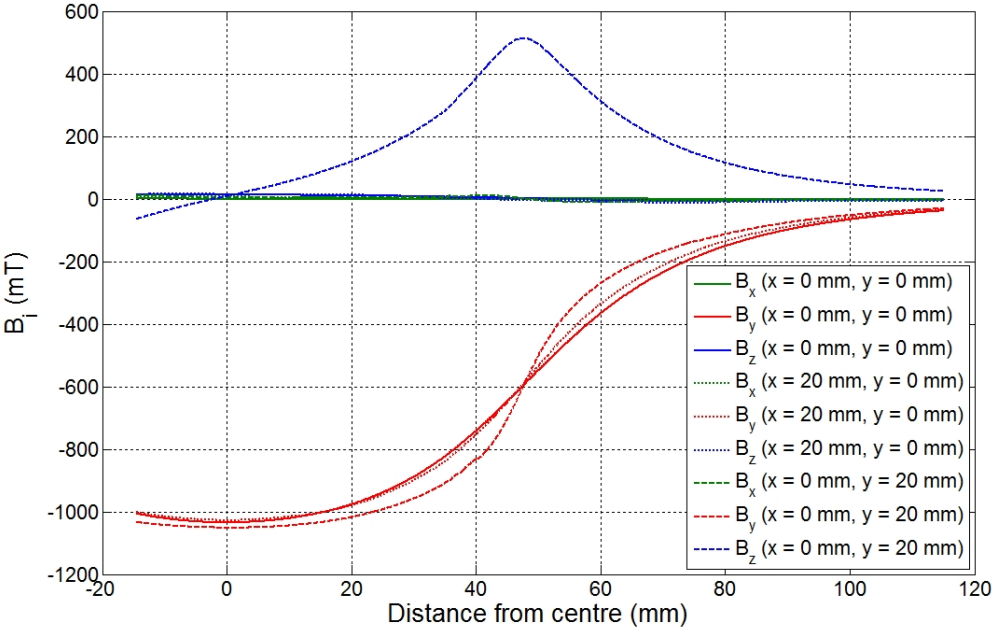
FIGURE 5.5: Variation of the magnetic inductive field as a function of the distance to the center of the magnet, in directions x, y and z, at locations 1, 2 and 3.

On the other hand, one sees that B_x is almost null everywhere, so is B_z except in point 3. At this location, the component of the field varies and reaches a maximum around the distance of 5 cm from the center. This one corresponds to the end of the magnet yoke.

It should be noted that the graph of Fig. 5.5 was only drawn for measurements made on half the length of the magnet. One might assume that the field behaves the same way on the other half, that is, it is mostly oriented along the y direction, remains quite high close to the center and decreases near the edge.

3. Magnetic force

The force acting on the sheets when put inside the magnet yoke will be first estimated theoretically, then it will be measured for different numbers of plates and at several distances from the center of the magnet. Knowing the values taken by this force allows to choose an adequate guidance system for moving the tube containing the sheets in and out of the magnet.

3.1 Theoretical calculation

The magnetic force $\overrightarrow{F}_{mag}$ acting on the Gadolinium plates might be computed thanks to the following formula. This one links the magnetization inside the plates, $\overrightarrow{M}$, to the divergence of the magnetic field $\overrightarrow{H}$, inside the volume $\mathcal{V}$ of the magnet yoke as

$$\overrightarrow{F}_{mag} = \mu_0 \int_{\mathcal{V}} \left(\overrightarrow{M} \cdot \nabla \right) \overrightarrow{H} \ \mathrm{d}\mathcal{V}. \tag{5.1}$$

If the magnetic field inside the gap was perfectly uniform, its gradient would cancel. But as it was discussed in the previous section, the magnetic inductive field $\overrightarrow{B}$ is non uniform, and thus so is $\overrightarrow{H}$. One indeed knows, since these fields act in air, that $\overrightarrow{B} = \mu_0 \overrightarrow{H}$.

In a first step, the value of the force in Eq. (5.1) may be roughly estimated using this latter relation between $\overrightarrow{B}$ and $\overrightarrow{H}$, which allows to write

$$F_{mag} \simeq MBd^2 \tag{5.2}$$

where d represents a characteristic length, e.g. the diameter of the magnet yoke. With $M = 4 \cdot 10^3$ A m^{-1} (cfr. Fig. in page), $B \simeq 1$ T and $d = 5$ cm, one finds for one plate

$$F_{mag,\ 1} \simeq 4000 \times 1 \times 0.05^2 = 10 \text{ N}$$

which yields for eight plates

$$F_{mag,\ 8} \simeq 80 \text{ N}.$$

On the other hand, the weight of one plate G_1 is

$$G_1 = \rho_m \mathcal{V} g = 7901 \times 0.1 \times 0.025 \times 0.001 \times 9.81 = 0.02 \times 9.81 \simeq 0.2 \text{ N},$$

and for all the plates

$$G_8 = 8 \times G_1 = 8 \times 0.2 \simeq 1.6 \text{ N}.$$

The magnetic force is therefore around 50 times bigger than the weight of all the 8 plates.

3.2 Measurements

The magnetic force acting on the Gadolinium sheets was then measured for different configurations and the results obtained will be presented in the following section. As aforementioned, the magnetic field is not uniform throughout the yoke of the magnet. One might thus expect that the force will also vary within the magnet gap and depending on whether the plates are more or less centered. This force is also expected to increase with an increasing number of plates. Moreover, it should reach a maximum when the plates are half entered inside the magnet in the z direction, and to cancel once they reach the center of the yoke. If the plates are at the center of the gap where the field is maximum, there is indeed no reason for them to be more attracted by one side or another thus they will naturally remain in this equilibrium position.
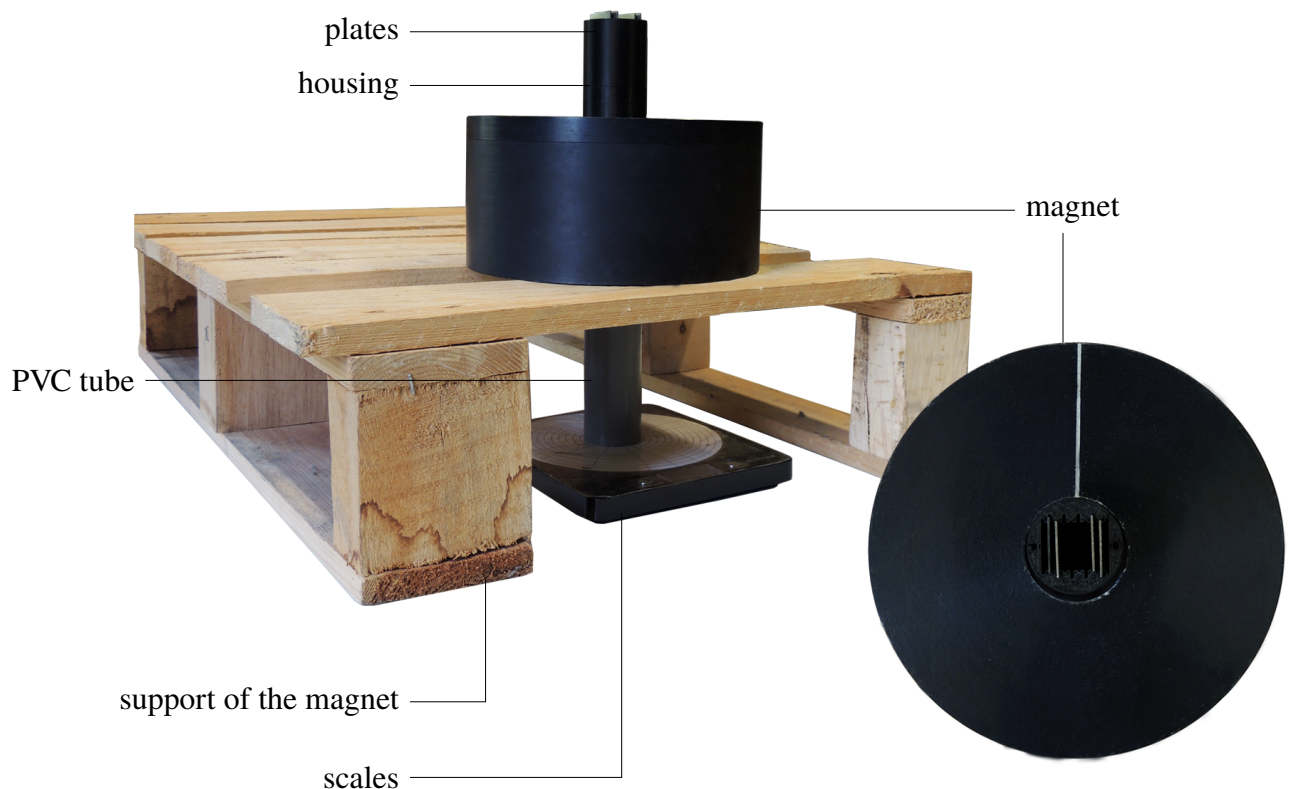
FIGURE 5.6: Measuring system with the 22 cm-long tube and four sheets.

Measurements were made by fixating the magnet and by placing the sheets inside it at different distances, along z, from its center. The number of sheets used was made to vary. Other measurements were also taken by placing the plates either at the very center of the yoke or by positioning them closer to the edges, namely by changing their (x, y) coordinates. The plates

were however always parallel to the main direction of the magnetic field, indicated in turquoise in Fig. 5.1 because they naturally oriented themselves along this direction, no matter where they were placed inside the gap.

3.2.1 Measuring method

Measuring a force can be done in many distinct ways. Here the easiest one was to simply weigh the sheets outside the magnetic field and under its influence with a simple scales. In the second case, if the plates are placed adequately, the vertical force exerted downwards will be either greater or smaller depending on whether they are approaching the magnet center or moving away from it.

But if one drops a ferromagnetic plate inside the gap of a 1 T-magnet, the force acting on it will be high enough so that the plate will naturally stay in the center of the magnet. This position is indeed the one minimizing the energy of the overall system. It is therefore required to prevent the sheet from reaching the center of the magnet to be able to measure the force acting on it at different positions. In the present case, simple PVC tubes of different lengths were used in order to be able to adapt the location of the plates during the measurements. This is illustrated in the picture of Fig. 5.6 below.

Because of the configuration of the measuring system, when trying to put the sheet beneath the center of the magnet yoke, this one does not stay in place and rises up due to the attraction by the magnetic field. Therefore one may simply add weights on top of the plate so that it cannot move upwards. This supplementary weight is then simply removed from the value measured in order to know the actual magnetic force.

3.2.2 Different configurations

The positioning of the plates depends on their number, their distance with respect to the center of the magnet and the way they are placed compared to each other.
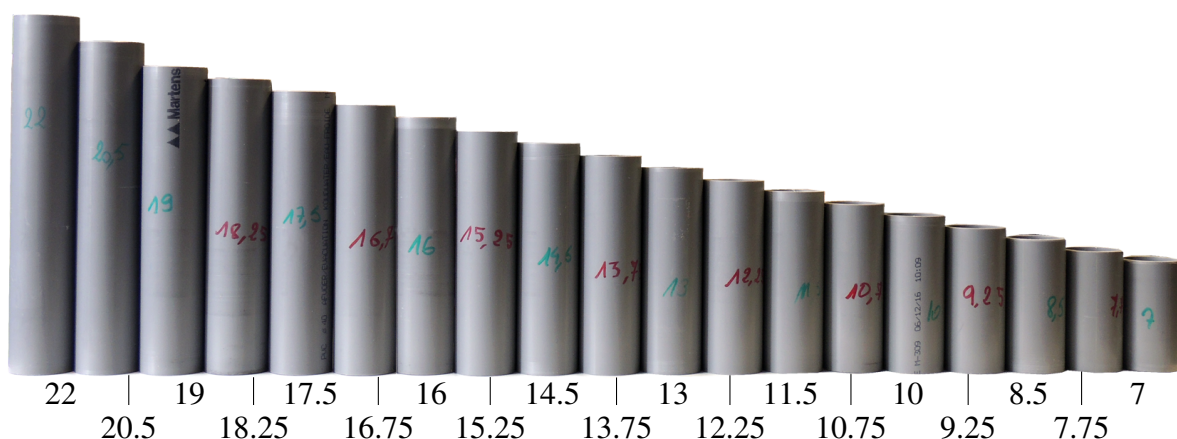
FIGURE 5.7: PVC tubes used for holding the plates and their respective lengths (in cm).

- **Number of Gadolinium sheets**

The number of sheets used vary between one and eight. Because they look alike each other without being exactly the same, one needs to perform the measurements with distinct plates in order to account for the fact that the thickness or even the weight of a plate could possibly have an influence over the force acting on it. Moreover, the plates may be combined in different manners in the housing ; this will be explained in more details below.

- **Distance from the center of the magnet**

As it can be seen in the sketches from Figs 5.8 and 5.9 in the next page, the housing containing the plates is placed along the axis z of the magnet. The center of this latter was defined as the origin of the framework drawn in the diagram of Fig. 5.1. In Figs 5.8 and 5.9, this central point is drawn in pink. When the plates are placed above it their distance with respect to it will be considered positive, and negative when they lie below it. This distance is taken from the center of mass of the housing.
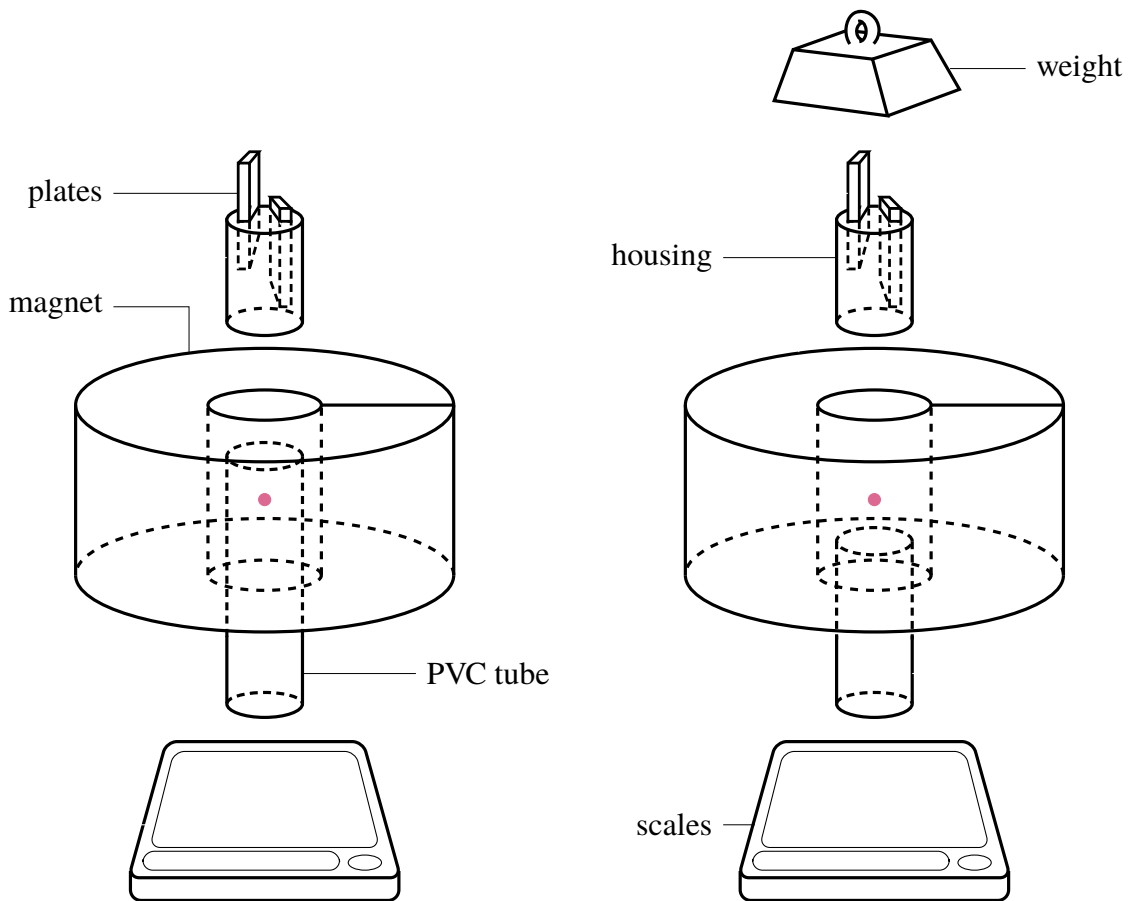
FIGURE 5.8: Measuring device layout: case of a positive distance.

FIGURE 5.9: Measuring device layout: case of a negative distance.

The case is put on top of a PVC tube in order to hold still at a fixed distance during the measurements. This tube is then placed onto the scales so that the magnetic force added to the weight of the whole set may be measured. This is also illustrated in Figs 5.8 and

5.9. Once this total force is known, one simply has to subtract the weight to obtain the magnetic force acting on the plates.

The PVC tubes used have lengths varying every 0.75 cm between 7 cm and 19 cm, and two additional tubes with lengths of 20.5 and 22 cm. They are all visible in the picture from Fig. 5.7 where they were placed like a Pan flute.

As already mentioned, when the sheets are placed at a negative distance from the center they will tend to rise up and remain positioned at the center of the magnet yoke. To counter this issue one just needs to add some extra weight on top of the housing containing the plates, then to subtract it from the total force measured. This situation is depicted in Fig. 5.9.

Whereas it is not drawn in the sketches of Fig. 5.8 and 5.9, the magnet is supported by a wooden pallet and lies thus at a distance of 12 cm from the scales. One wants to know the actual distance between the center of the magnet yoke being 5 cm upwards, and the center of mass of the housing containing the sheets. This latter is also located 5 cm above the end of the tube. For a given length of the tube, the distance looked for, denoted d, should then be given by simply subtracting 12 cm from this length. Consequently, the interval of distances used for the measurement is the following:

$$d \in \Big\{ -5,\ -4.25,\ -3.5,\ -2.75,\ -2,\ -1.25,\ -0.5,\ 0.25,\ 1,$$
$$1.75,\ 2.5,\ 3.25,\ 4,\ 4.75,\ 5.5,\ 6.25,\ 7,\ 8.5,\ 10 \Big\}\ \text{cm}.$$

One should note at this point that the bottom of this container which is about 3 mm thick was neglected here and this additional thickness simply added to the height of the scales. Together they have a total length of 12 cm, as aforementioned.

- **Combinations of the plates**

The plates may be placed, for a given number of them, in different configurations. Pictures of the housing containing four sheets under different angles might be seen in Fig. 5.10 hereafter.

In particular, because there are eight available locations inside the container, the number of combinations for n plates is given by the well known binomial coefficient as

$$\binom{n}{8} = \frac{8!}{n!\,(8-n)!}, \quad n \in [1, 8].$$

This yields a total of 255 combinations for all the values of n. Knowing that the sheets will be positioned at 17 distinct distances from the center of the magnet, one should perform 4335 measurements if all the possibilities are explored. But in the present case, because one mostly wants to find an order of magnitude of the magnetic force in order to choose an adequate guidance system for the prototype rather than being very precise, this number is not justified. Therefore, the amount of different combinations for each number of plates n

FIGURE 5.10: Caption

at each distance d is lowered to eight, except for the cases of $n = 7$ where only two combinations are exploited and $n = 8$ (this latter for obvious reasons). This reduces the number of measurements by four. Hence, when measuring for instance the force as a function of the distance for a given n, one has several values for each d, which allows to perform averages and to avoid mistakes, but not too many for this amount to be completely pointless. This choice will be furthermore justified later on.

A drawing of the housing containing the plates is visible in Fig. 5.12, and a top view is sketched in Fig. 5.11.
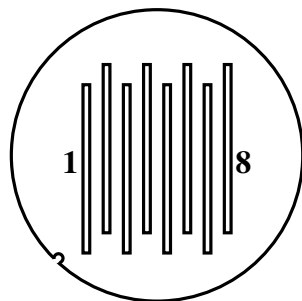
FIGURE 5.11: Top view of the housing.
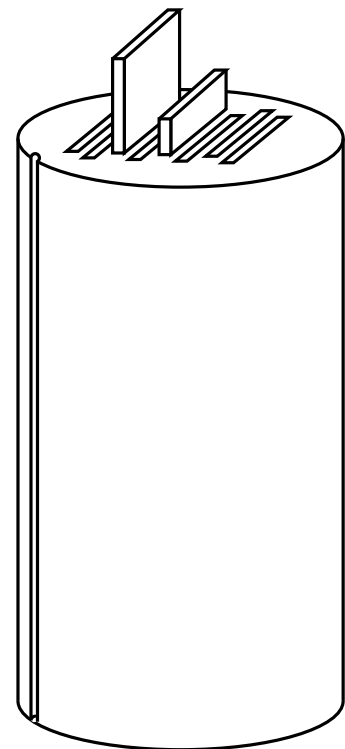
FIGURE 5.12: Side view.

It was made cylindrical in order to fit the magnet gap. Its design will be discussed later on in details. The important point is that its height is 10 cm, its diameter 4.3 cm and it can hold up to eight plates at the same time. The cuts made for the sheets are 2.5 cm wide and
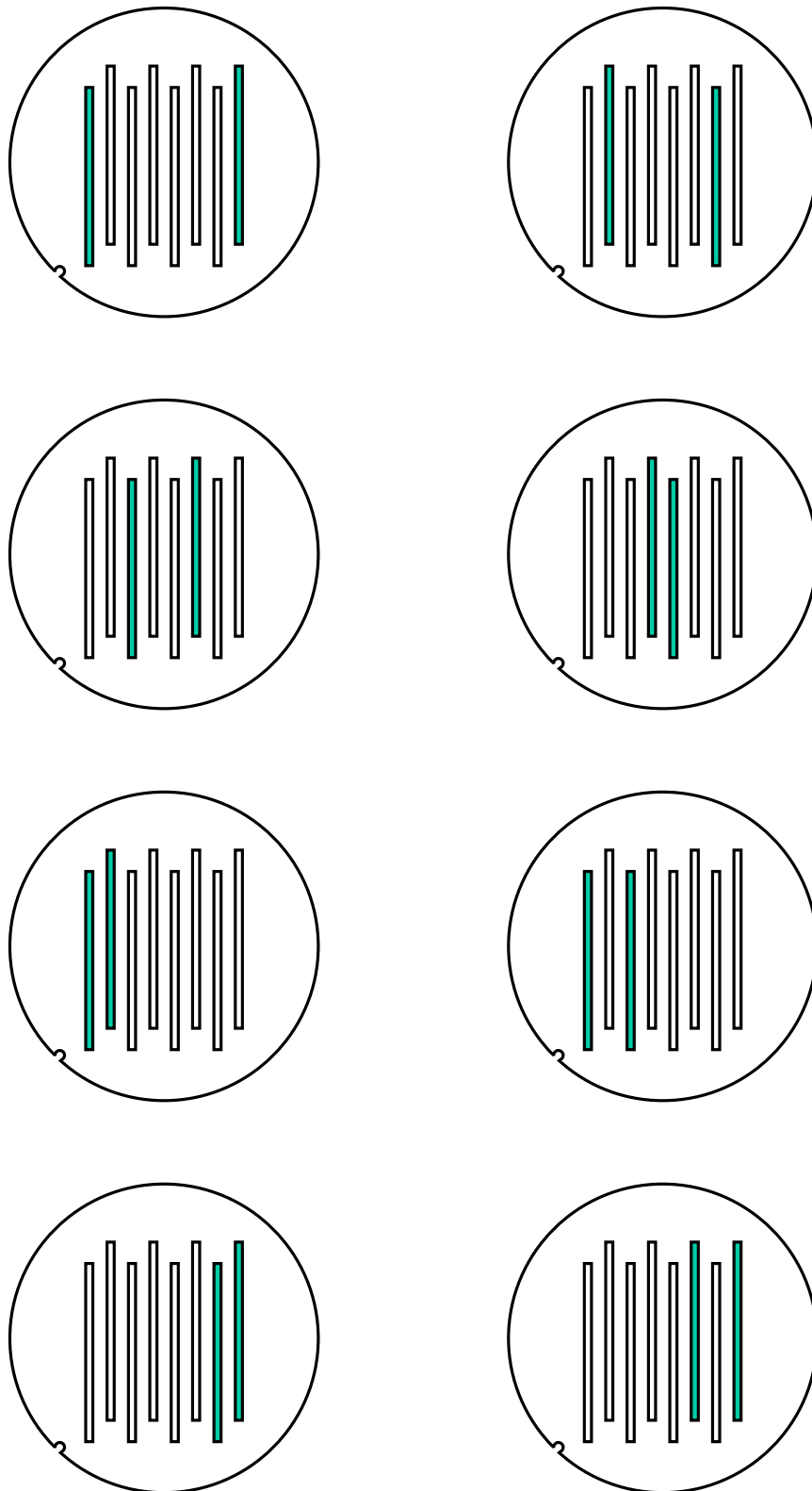
FIGURE 5.13: Eight different plates configuration in the case of two sheets of gadolinium put inside the housing.

and 1 mm thick and have been placed in a staggered arrangement due to precision of the 3D printer. Different views of this case with two plates inside are presented in Fig. 5.13. As aforementioned, for a given number of plates n, only eight out of all the possible combinations are explored during the measurements and the pictures from Fig. 5.13 show the ones explored with two plates.

Looking at the top view picture of the container, the small notch appearing on the edge because of the 3D printer and drawn in the illustrations allows to define positions inside the container going from 1 to 8. The housing is always put in the same manner inside the magnet in order not to inverse these positions. It is placed such that the plates are parallel to the $y-$direction and that the line indicating this direction is on the top (see Fig. 5.4), namely the "1" lies in the negative x values and the "8" in the positive ones.

3.2.3 Environmental observations and constraints

When performing the measurements, some constraints appear and the influence of some environmental parameters may be observed, all listed hereafter.

- Obviously the number of plates that fit at a time inside the magnet cannot overcome eight. This is dictated by the dimensions of this one.

- The measurements depends on the temperature inside the room since the material used exhibits the MCE which is a temperature-dependent phenomenon. But because the experience was performed in the basement the temperature was more or less always of 22 °C.

- When the plates are positioned in the magnet, at first the value indicated by the scales is not stabilized and takes some time to remain still. This might be due to the change in temperature or because the domains inside the gadolinium need some time to align themselves on the main field which yields a transient state in the beginning of the measurement.

- Once the sheets are put inside the magnet, the container gets more attracted on the side of the positive y values.

- Other parameters such as relative humidity might have an influence too on the measurements and could be more investigated.

All these effects can possibly affect the measurements that should thus be performed and analyzed with great precaution.

3.3 Results

The results obtained will be presented in this section. First the force as a function of the distance taken between the center of mass of the plates and that of the magnet will be reviewed and analyzed. Then the influence of the position of the plates inside the housing will be examined. Finally, some physical parameters that might also have an influence on the force will be studied too.

3.3.1 Force as a function of the distance

In this first subsection the distance between the plates and the center of the magnet yoke will be made to vary, for a fixed number of plates. Results are presented here in the case of one, two, four and eight plates placed inside the container. The curves obtained for three, five, six and seven plates are visible in the Appendices, from pages 121 to 123.

- **One plate**

  Fig. 5.14 displays the force acting on one plate as a function of the distance. For each distance the plate was placed at every possible position inside the container and then the average was made in order to get the force value. Several plates were used for each point in order to get the widest possible sample. It should be noted once again that measurements were not taken for symmetrical distances.
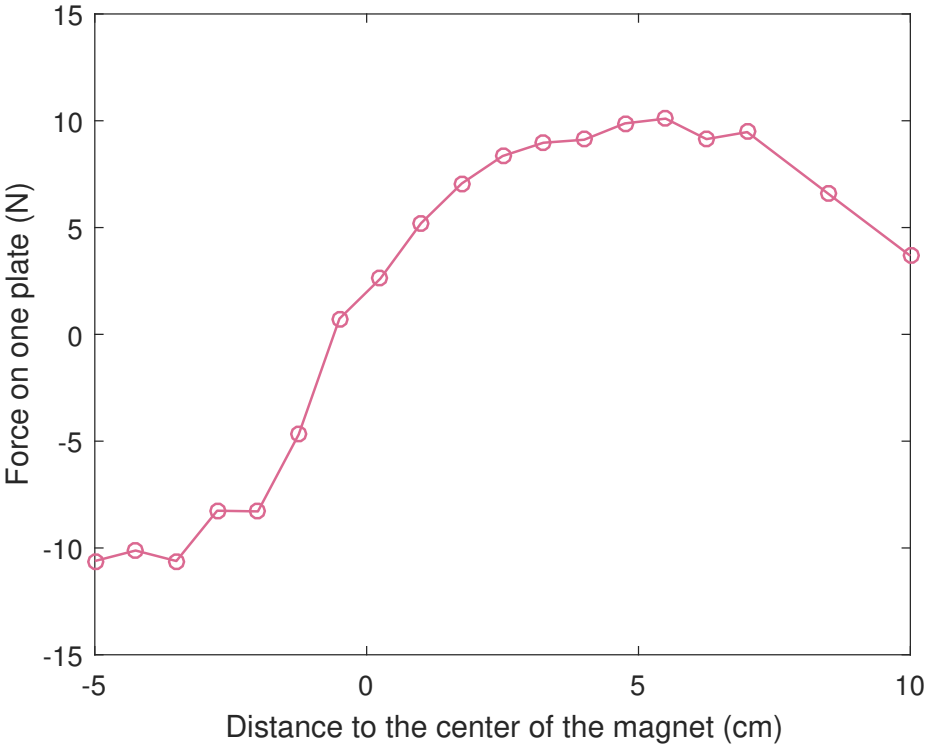
FIGURE 5.14: Force acting on one plate as a function of the distance of the housing from the yoke center.

One sees in the chart that at a distance of 10 cm above the magnet center, the force acting on the plate is positive. It increases as the plate is brought closer to the center of the magnet gap. Around the value of 5 cm, the force reaches a maximum then starts decreasing as the plate gets closer to the center. Close to this very center the force appears to cancel, then to increase again once the plate is placed farther and further from the magnet center, but its sign has changed and it is now negative. In around −5 cm, the force seems to reach a minimum whose absolute value is of the same order of magnitude as the maximum.

The fact that the force acting on the plates cancels at the center of the magnet gap makes perfect sense ; at this position, there is no reason for the plate to be attracted more on one side of the magnet than on the other. At this spot the plate remains in equilibrium. Moreover, the plate orients itself along the main direction of the field in order to stay aligned with it, direction that is drawn in Fig. 5.4 in page 79. One should indeed remain that the force is due to a gradient of magnetic field, thus at the center this gradient cancels and so does the force. It can be seen in the graph of Fig. 5.5 when the field along the y-direction is maximal close to the center, hence it has a null derivative.

On the other hand, the extrema of the force show up at the most unstable positions of the plate inside the magnet, namely when the gradient takes its highest values. The change of sign is due to the fact that the magnetic field gradient and the force simply change their direction ; as the plate pass beyond the center, it is attraced towards this one in the other direction.

Concerning the values of these extrema, one finds out that they are equal to 10.100 N and -10.612 N. This corresponds to what was evaluated in a first approximation in Section 3.1 from page 80.

- **Two plates**

In Fig. 5.15 one sees the force measured in the case of two plates put inside the container. Once again several combination were tested and the average was made in order to get the data in the graph. The observations that can be drawn from this chart are exactly the same as for the previous one, except for the fact that the force takes greater values.

One expects the force acting on two plates to have more or less twice the value of the force obtained with only one plate. It may be considered that the magnetic fields appearing because both plates are magnetized will not have an influence on each other nor on the Halbach magnet field either and that the main field acting on the plates is this latter. Consequently, the system should behave linearly and adding more and more plates should simply yield a force equal to the number of plates times the force obtained for only one plate.

Looking at the graph from Fig. 5.16 which compares the double of the force on one plate and the force acting simultaneously on two plates, one deduces that the behaviour of this latter is the same as the addition of the forces acting each on separate plates.

The maximum and minimum values taken by the force in the case of two plates together are respectively 20.249 N and -21.445 N, that is, more or less the double of the extrema obtained for one plate (respectively 20.199 N and -21.224 N).
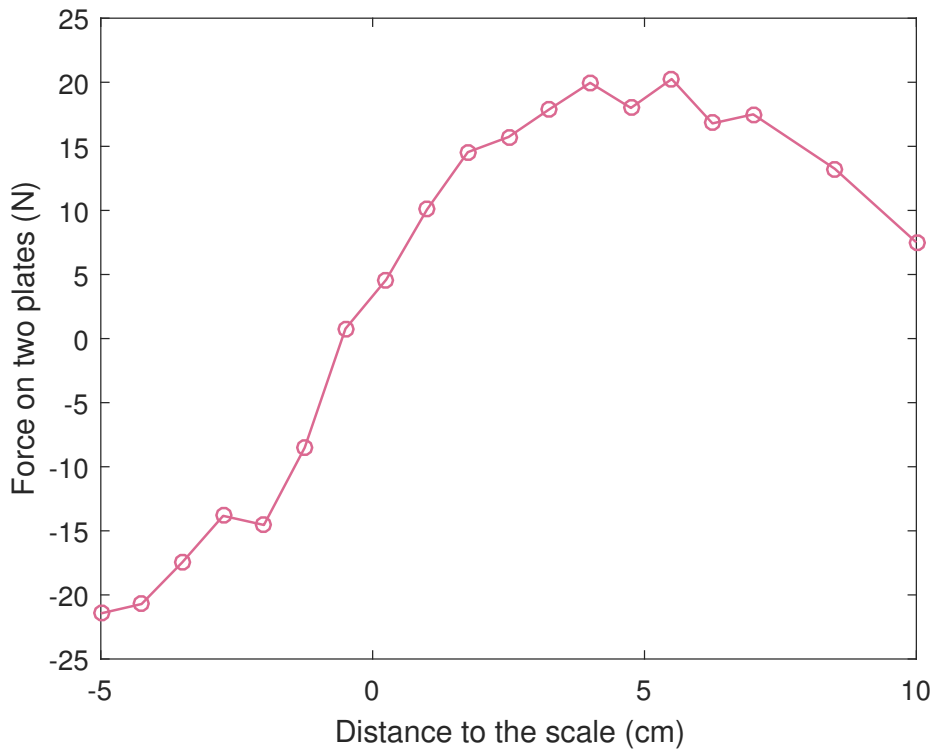
FIGURE 5.15: Force acting simultaneously on two plates as a function of the distance of the housing from the yoke center.
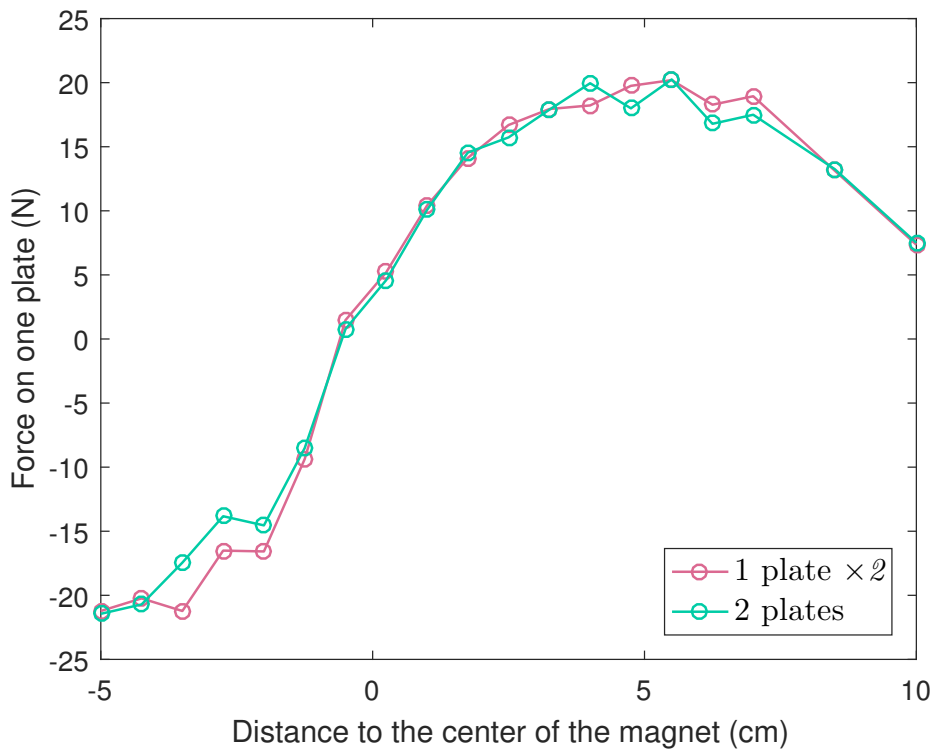

FIGURE 5.16: Comparison between the double of the force acting on one plate and the force acting on two plates simultaneously as a function of the distance of the housing from the yoke center.

- **Four plates**

  Fig. 5.17 displays the results obtained for the force that the magnet exerts on four plates at the same time. Once again the shape of the curve looks exactly like the previous graphs.

  The maximum value taken by the force is in this case 38.600 N, and the minimum one -39.959 N. One sees that it is, as expected, more or less four times bigger than the value reached for only one plate.
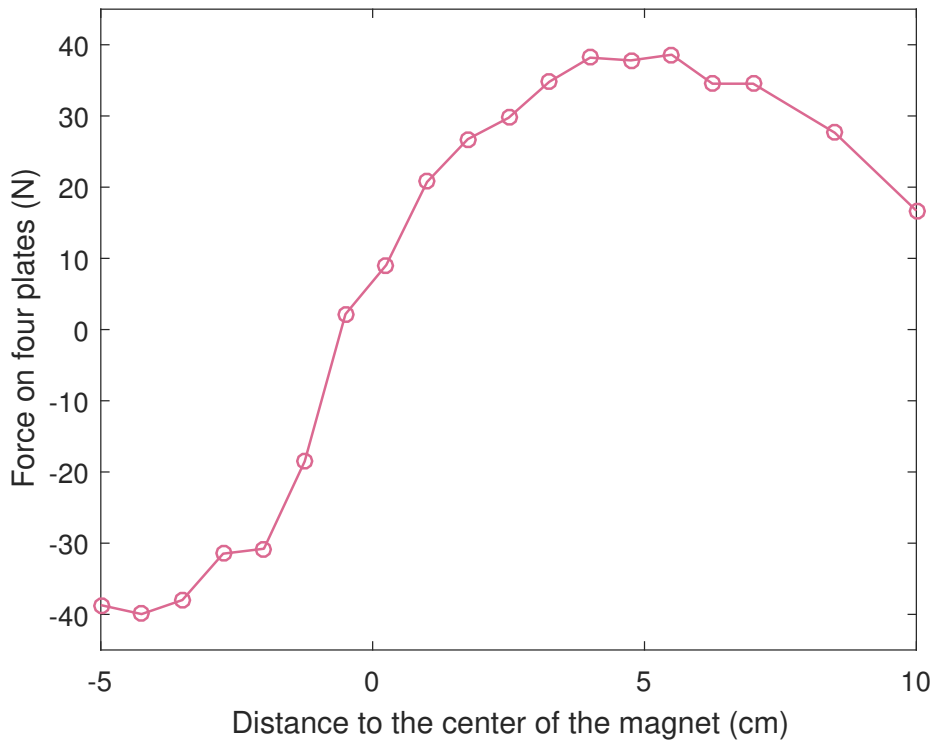
FIGURE 5.17: Force acting simultaneously on four plate as a function of the distance of the housing from the yoke center.

- **Eight plates**

  In Fig. 5.18 one sees the force that eight plates put inside the container are subjected to at the same time as a function of the distance to the magnet center. The curve follows the same behaviour as in the precedent cases.

  The highest value taken by the force is 76.508 N, while the smallest one is -76.371 N. Looking at the values taken by all the extrema as the number of plates increase, one sees that it is close to but not exactly n times the values obtained for only one plate. In the case of two plates one gets values a little bit greater/smaller, and the opposite for four or eight plates. With eight other plates out of the twenty available ones, the result would certainly have been different. This comes from the fact that not all plates are exactly the same, and some of them may experience a higher or lower force depending on their physical parameters. This will be investigated in more details in the following sections, where the force acting on different plates will be compared and where the influence of the thickness, weight and other parameters of the plates will be analyzed.

As already mentioned, the purpose of these measurements is to be able to dimension the guidance system as well as the motor that should be used for actually making the prototype. Because only eight plates will be used due to the constraints appearing on the dimension of the container, the values obtained for the extrema in this case give the sought order of magnitude. The device should hence be able to resist a force of the order of around 80 N.
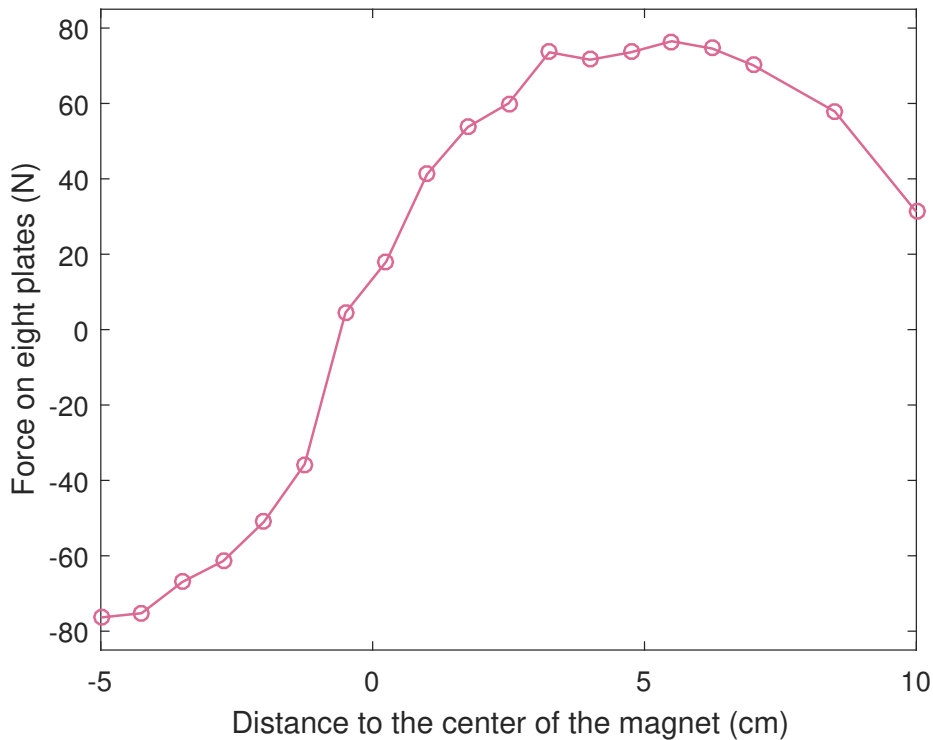

FIGURE 5.18: Force acting simultaneously on eight plates as a function of the distance of the housing from the yoke center.

- **Fit of the curves**

All the curves presented previously as well as the ones visible in the Appendices may be approached by a polynomial using the fitting tool of MATLAB. Fifth-order polynomial was used since above this order the polynomial is badly conditioned. Gathering the mean of all the coefficients obtained for each number of plates, one might plot the force as a function of the distance in order to get the value of the distance at which the force cancels or reaches maximal values. Obviously such a plot does not have any physical meaning except for the shape of the curve. It is only used here in order to find the zero and the extrema of the force.

Fig.5.19 displays this global force curve. In order to compute all the fitting polynomials, because the force should be antisymmetric but that the data were not obtained for symmetrical distances, one may add the opposite of the last few points before the first points measured, so that the curve is "completed". The values obtained should indeed be close to each other. Then the fit of the curve allows to find a antisymmetric function.

Because of the parity of the force, it is better to take a polynomial of odd order, here 5 as aforementioned.
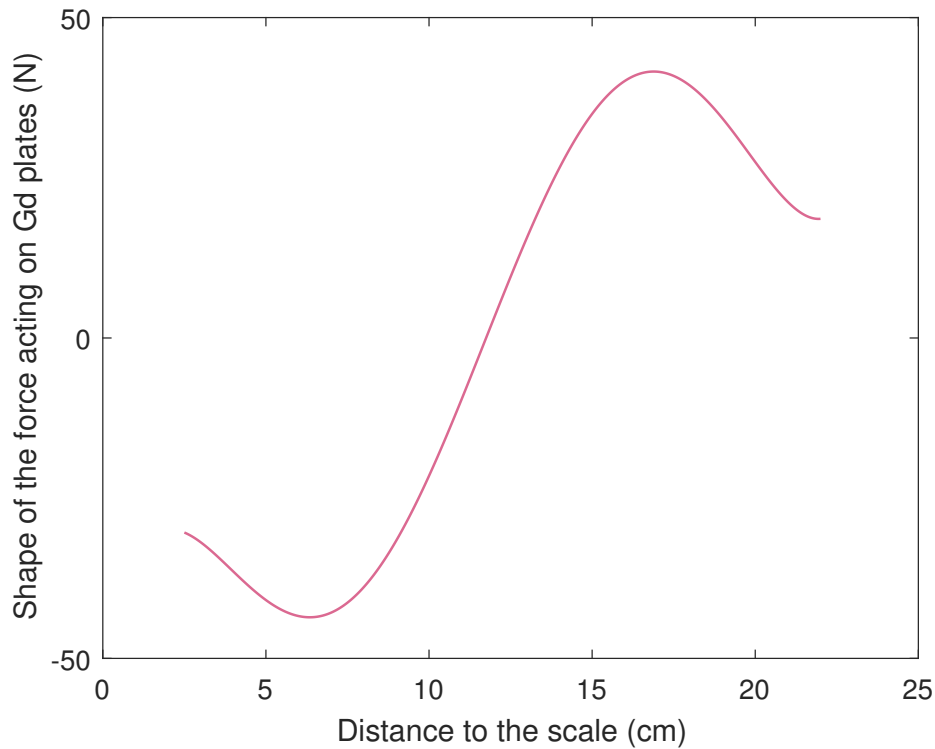

FIGURE 5.19: Mean plot.

- **Zero of the force**

  The curve previously drawn cancels at a distance of -0.25 cm. Looking at all the previous graphs, one sees that this is more or less what is obtained for each number of plates.

- **Extrema of the force**

  The maximum value reached by the force occurs at 5.40 cm above the magnet center. On the other hand, the force has a minimum for a distance of -4.21 cm below the center. Comparing these values, one sees that the maximum lies at 5.15 cm of the zero and the minimum at -3.96 cm. Once again these values seem in line with all the experimental curves obtained.

3.3.2 Force as a function of the position and the orientation of the plate(s)

Now the influence of the position of a plate inside the container will be observed and analyzed to see whether or not it has an influence on the force measured. The influence of the orientation of the plate will be tested as well, namely measurements will be performed by placing the plates in the case then by turning them by 180° and checking if the force is the same or not. A priori both these parameters should have very little influence on the measurements.

- **Position of one plate**

In order to study the influence of the position of one plate inside the container, one may place it in every possible spot and measure the force obtained. A chart may then be drawn of the force as a function of the location of the plate. This might also be done for different plates in order to repeat the measurements and get a wider span of values. During the experiment, the distance with respect to the center of the magnet should be set to a fixed value since this is not the studied parameter this time. It was chosen to be 10 cm and ten plates were picked randomly. To reach this distance, one uses the 22 cm PVC tube.

It is better to fix the distance away from the center because as one might see in the previous graphs it behaves almost linearly in this area. Around the center the force has more or less the same behaviour but changes of sign. Close to an extremum the force is no longer linear. Too far from the center the force would cancel but before that it would decrease more and more slowly thus it would no longer be linear either. The distance of 10 cm seems therefore appropriate for performing the measurements.

It is easier to assess the effect of the position on one plate only because if one puts e.g. two plates inside the container in several configurations, as drawn in Fig. 5.13 for instance, how can one tell the influence of the position of the plates on a simple graph ? To study both positions at a time one should draw a surface where the axes represent the position of the first and the second plates. Thus by rising the number of plates the dimension of the hypersurface should increase too and it becomes completely pointless to make such an analysis since data cannot be easily exploited.

Fig. 5.20 shows the force acting on one plate as a function of the position of this one. The position is denoted from 1 to 8 as in Fig. 5.11. Ten distinct plates were used and are represented by curves of different colors. One sees directly that the value taken by the force varies between 3.2 and 4.8 N, thus there is a factor of 3/2 between these two extremes. This explains why the extrema obtained e.g. for the force acting on eight plates simultaneously are not exactly equal to eight times the results for one plate alone.

It might be seen in the graph of Fig. 5.20 that the force on the sheets is a bit greater in the middle and smaller on the sides. In particular, the values are even lower on the right side than on the left one, namely close to the eighth position. This may come from the shape of the magnetic field inside the magnet gap. When taking a look at Fig. 5.5 in page 79, the $y-$component appears to dictate the shape of the force as a function of the distance to the center, but the other components, which vary much less, might have an influence too in the other directions.

The middle positions (4, 5) are indeed placed close to the point denoted 3 in Fig. 5.4, where the $z-$component becomes higher. Because it was observed experimentally that the plates are more attracted towards this point and that the force is greater in its direction, both these observations might be caused by such a field variation. However, nothing can be said about the fact that the force is observed to be a little bit higher on the first positions (1, 2) than on the last ones (7, 8) because information about the magnetic field in point 2 from Fig. 5.4 are available but not on its symmetrical location.
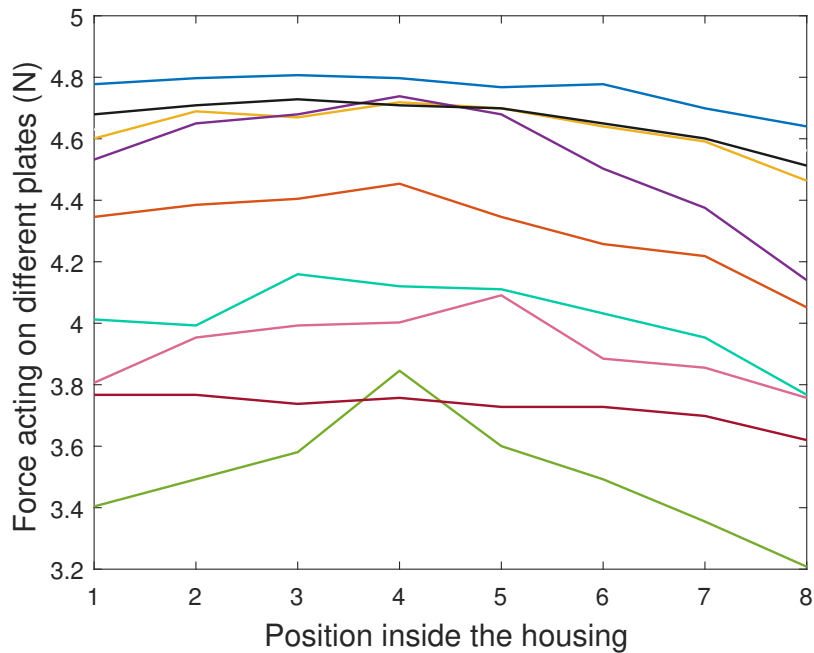
FIGURE 5.20: Force acting on different plates as a function of their position inside the container.

- **Force as a function of the orientation of the plate**

As aforementioned, the container is always placed in the same manner with the line drawn on the magnet above it such that the position 1 is on the left and the 8 on the right. One can examine if when the plates are put first in this peculiar way then turned and placed in the opposite manner the behaviour of the force as a function of the position is still the same or not. It should be but the experiment is worth being carried out.

The distance was once again fixed to 10 cm from the center of the magnet, namely the same PVC tube of 22 cm was used. Three different plates were randomly chosen and tested by being put in the housing in one sense then turned by 180° and tested again in all the possible positions.

Fig. 5.21 displays the results obtained for the three plates. The solid lines show the force acting on the plate when the first batch of measurements is taken, whereas the dotted lines represent the results one get by turning the plates. Each plate is associated to a particular color.

As one might see in the graph from Fig. 5.21, each couple of curves related to a plate are really close to each other, with some disparities due to the imprecision of the measurements. Nevertheless, the same behaviour is observed each time. One sees that the plates experience each a different force value, which can vary by around 1 N in this case. It enhances the importance of using several plates when performing the measurements.
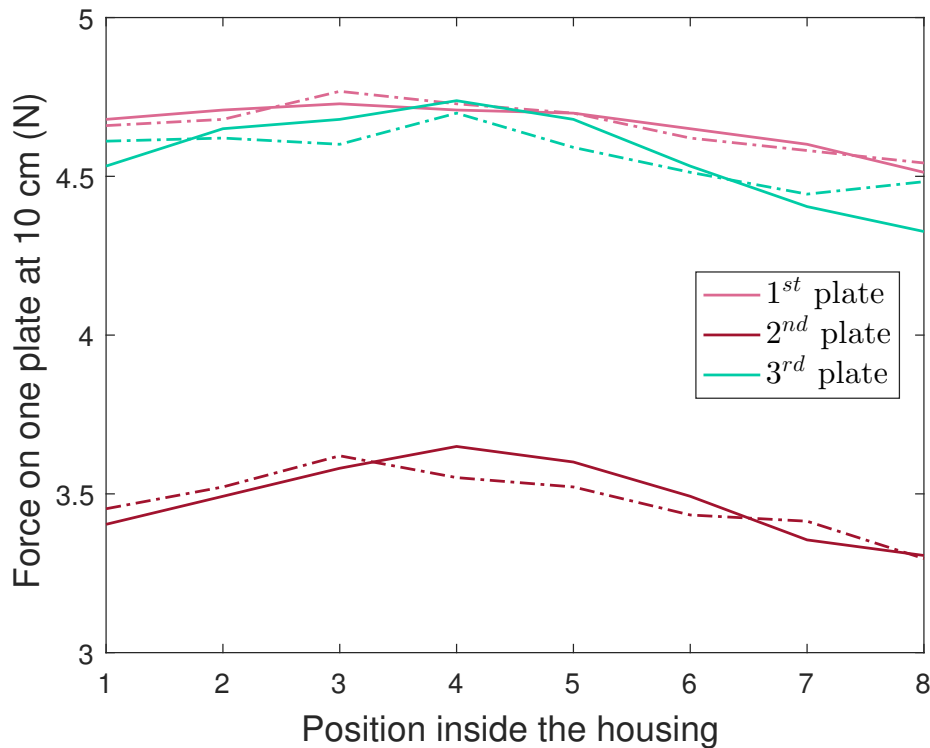
FIGURE 5.21: Force acting on different plates as a function of their position inside the container.

3.3.3 Force as a function of the physical parameters of the plate(s)

In this section, one will examine if the thickness and or the weight of the plates have an influence on the force acting on them. Other parameters could be investigated because some of the plates are not perfectly flat and some do not have a completely rectangular shape. The rugosity of the plates might be explored too. Nevertheless, these irregularities are not in a sufficient amount for these parameters to be relevant to analyze.

The twenty Gadolinium sheets present at the lab were used for this experiment. Because one tries to analyze another parameter than the distance at which the plate lies from the center of the magnet yoke, this one was chosen to be 6.25 cm and remained fixed during all the measurements performed. This peculiar distance actually corresponds to the 18.25 cm-long PVC tube. The center of mass of the sheets is thus separated by 6.25 cm from the center of the magnet yoke and the bottom of these sheets by 1.25 cm.

Each plate was weighted and its thickness measured with a digital caliper. Then the magnetic force acting on each sheet was measured for all the positions in the container, namely eight possibilities. The results are visible in Table 5.1 below. In this latter one sees the force measurements presented under the form *average value* $\langle F_{mag} \rangle$ ± *standard deviation* ΔF_{mag}. Note that the 10% rule was applied, which simply means that every digit whose contribution is smaller than 10% of ΔF is not taken into account.

First the influence of the thickness of the plate will be evaluated. To do so, one might simply use the tools of statistical inference which are the correlation coefficient and the drawing of a scatter plot or a histogram. For two given variables X, Y, if one has a sample of N measurements

Plate	Thickness e (mm)	Width ℓ (mm)	Length L (mm)
1	0.93	25.48	99.76
2	1.02	24.22	99.95
3	1.01	25.10	100.66
4	0.99	25.19	99.95
5	1.00	24.91	100.03
6	0.92	24.97	100.29
7	0.97	25.46	100.17
8	1.01	25.54	100.36
9	1.00	25.37	99.75
10	1.01	25.56	100.46
11	1.01	25.21	100.16
12	1.01	25.41	99.91
13	1.01	25.07	100.94
14	1.02	25.18	101.02
15	1.00	25.27	100.32
16	1.01	25.05	100.15
17	1.00	25.42	100.17
18	0.98	25.62	100.13
19	1.00	25.11	100.16
20	1.00	25.21	99.88

TABLE 5.1: Dimensions of all the Gd plates: thickness (in mm), width (in mm), length (in mm) and volume (in m^3).

Plate	Mass m (g)	Density ρ (kg m^{-3})	Force F_{mag} (N)
1	19.39	8202.36	9.280 ± 0.050
2	20.45	8282.02	10.760 ± 0.080
3	20.26	7939.40	11.787 ± 0.048
4	19.76	7927.58	11.477 ± 0.046
5	18.58	7456.61	11.060 ± 0.049
6	18.57	8060.24	8.680 ± 0.040
7	20.03	8096.79	9.530 ± 0.060
8	20.53	7930.23	9.470 ± 0.050
9	20.11	7946.55	8.780 ± 0.050
10	20.47	7893.01	8.780 ± 0.040
11	20.34	7975.58	11.130 ± 0.060
12	20.21	7881.91	9.300 ± 0.038
13	20.25	7922.93	9.089 ± 0.007
14	20.23	7797.09	9.030 ± 0.068
15	20.15	7948.47	8.970 ± 0.060
16	20.37	8039.17	10.870 ± 0.390
17	20.27	7960.50	9.050 ± 0.040
18	20.53	8166.19	10.420 ± 0.060
19	20.24	8047.66	10.949 ± 0.079
20	20.21	8026.29	10.100 ± 0.360

TABLE 5.2: Characteristics of all the Gd plates: mass (in g), density (in kg m^{-3}, average on the position in the housing of the magnetic force acting on it (in N).

of values x_i and y_i for $i = 1, \ldots, N$, the correlation coefficient $r_{X,Y}$ is obtained by dividing the covariance of the two variables by the product of their standard deviations as

$$r_{XY} = \frac{\displaystyle\sum_{i=1}^{N} (x_i - \langle x \rangle)(y_i - \langle y \rangle)}{\sqrt{\displaystyle\sum_{i=1}^{N} (x_i - \langle x \rangle)^2 \sum_{i=1}^{N} (y_i - \langle y \rangle)^2}} \in [-1, 1]. \qquad (5.3)$$

The brackets $\langle \ldots \rangle$ represent the mean value of a variable. Applying this to the values measured for the thickness of the plates e and the force acting on them F_{mag}, one finds that

$$r_{eF_{mag}} = 0.267.$$

The closer the correlation coefficient is to 1 or -1, the more correlated are the two variables, but only in the case where the conditional mean of Y given X is linear. Therefore, a visual aid is required to see at which point these two variables are correlated or not. One might draw a scatter plot of both variables and see if there seems to be any kind of relation between them. Sometimes several linear relations can for instance be derived from one scatter plot, indicating that there are different types of behaviours appearing in one physical system.

In Fig. 5.22 is drawn a scatter plot of the two variables e and F_{mag}, given by the software MATLAB. As one may see it in the graph, most points are located in the northeast part of the first quadrant but some of them can be found a little bit lower. Hence, there does not seem to be a strong correlation existing between both variables.

Figs 5.23, 5.24 and 5.25 display respectively the scatter plots obtained when drawing the force as a function of the length, the width and the volume of the plates. Each correlation coefficient associated is written in the graph. One sees that for the force vs. the length of the plate, one gets a coefficient of -0.163, whereas in the case of the width one has -0.392. For the volume, one obtains a value equal to 0.059. Hence, the force acting on the plate does not seem to be correlated to its volume nor its length or width.

In Figs 5.26 and 5.27, one sees the force drawn respectively as a function of the mass and the density of the plate. The corresponding correlation coefficients are respectively equal to 0.047 and -0.026, and looking at the curves one sees that there is no link between the force and the mass or the density.

No correlation between the force and the physical parameters studied here seems to arise. However, as it is the most visible in the graph of Figs 5.23 and 5.25, each time the points obtained appear to split into two distinct groups ; one might see that for very close width and even volume values, the force may be comprised between 8.5 and 9.5 N, or between 10.5 and 11.5 N. This can be seen in the other charts too, but it is less obvious.

In order to further investigate this behaviour and its possible origin, one should extend the sample to more than 20 plates and search for other parameters that may influence the force acting on the plates, such as the already mentioned rugosity of these. Environmental causes might play a role too, such as the relative humidity in the room or the ambient temperature. Perhaps this division into subgroups is simply due to the peculiar sheets used and has no physical meaning.
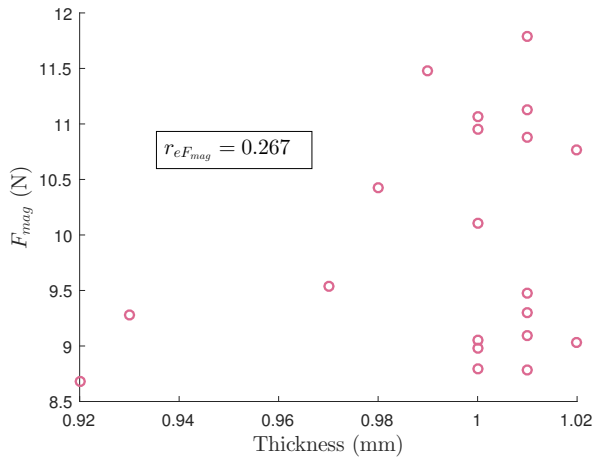
FIGURE 5.22: Scatter plot: magnetic force acting on one plate vs. thickness of the plate.
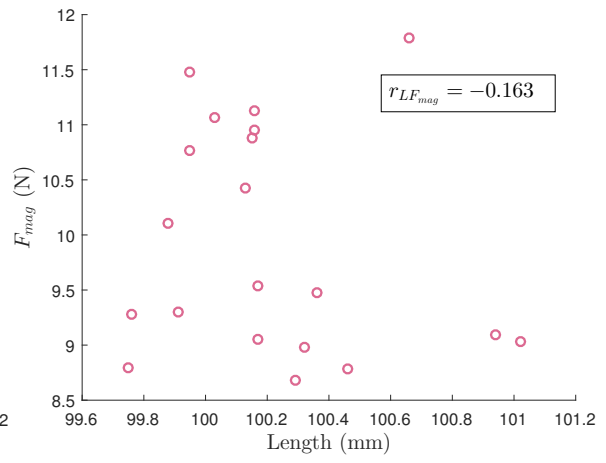

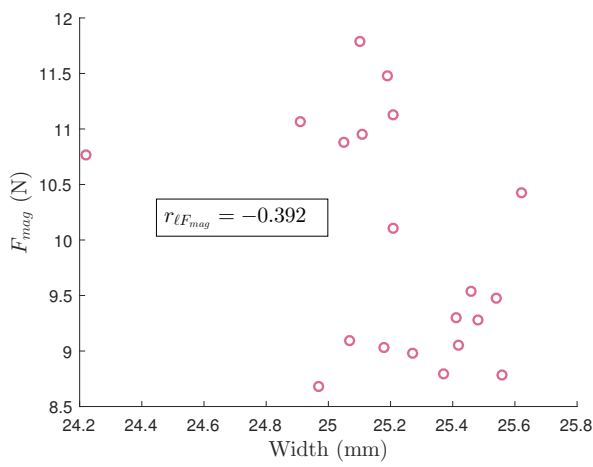FIGURE 5.23: Scatter plot: magnetic force acting on one plate vs. length of the plate.

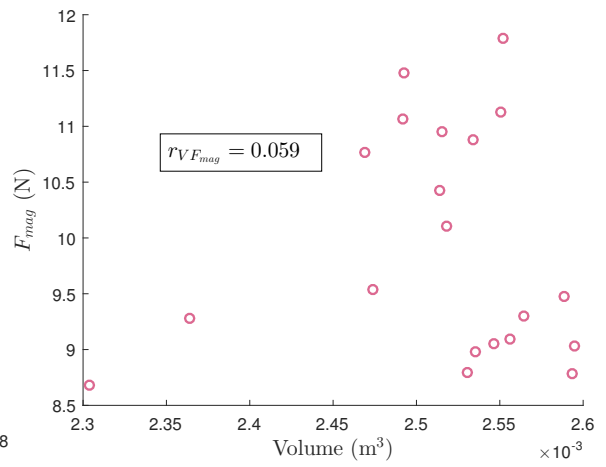FIGURE 5.24: Scatter plot: magnetic force acting on one plate vs. width of the plate.

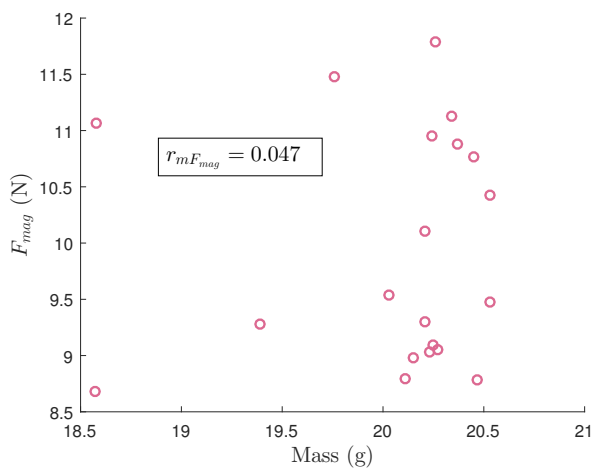FIGURE 5.25: Scatter plot: magnetic force acting on one plate vs. volume of the plate.

FIGURE 5.26: Scatter plot: magnetic force acting on one plate vs. mass of the plate.
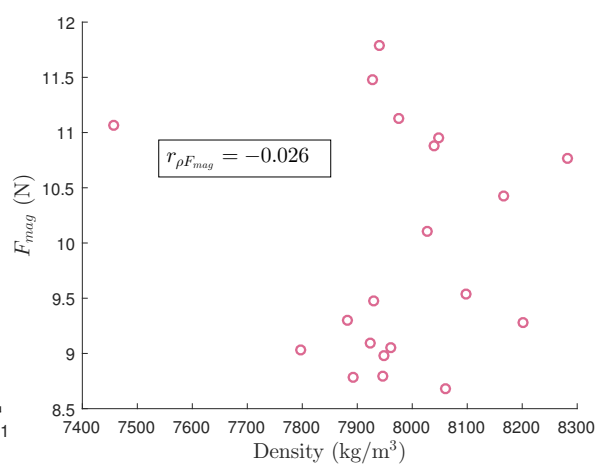

FIGURE 5.27: Scatter plot: magnetic force acting on one plate vs. density of the plate.

3.3.4 Improvements

Some improvements could be made in order to get more accurate measurements and to perform them easily in a greater amount, listed here after.

- First of all the scales mostly utilized was limited to measuring weights under 5 kg, but the values reached up to 8 kg, so another scales was needed. A simple bathroom scales was used but it had less precision and was difficult to use because the weight was not printed for a long time on the screen.

- The main issue is certainly the fact that PVC tubes were used to hold the housing and the plates in place, but they are neither modular, nor perfectly steady as the measurements are performed. Another system should be thought of in order to get more values easily.

- The measurements were not symmetrical, but it would be interesting to get the complete curve to see if there is one side where the force is a little bit greater, and so forth.

- One would also have had to take measurements further away from the center of the magnet. In this case they stopped at 5 cm above the center, but the force does not cancel yet at this distance. It would be of interest to see at which exact distance from the magnet center its influence on the gadolinium sheets is no longer measurable.

- The plates were held in a staggered arrangement inside the container, meaning that some of them were a few mm closer to one edge than to the other, and conversely. The force acting on them could thus be slightly modified because of this issue.

- Finally, to fully describe the force a magnet exerts on gadolinium, the sample used should be expanded ; one could for instance use several magnetic field values. Different configurations could also be explored: the magnet could have another shape than being cylindrical, powder or spheres of gadolinium could be used instead of plates, plates of distinct sizes could also be taken,... The possibilities are numerous.

Designing an experimental setup is not an easy task, and sometimes one must deal with the shortage possibilities that the lab offers. All these improvements could yield to better, more accurate measurements.

3.4 Conclusions

In this section the force acting on the gadolinium sheets was measured as a function of several parameters. The aim of making such measurements is to evaluate the order of magnitude of the force that should resist the motor and the guidance system that will be used for the prototype.

First a rough estimation of the force acting on the eight plates that will serve at a time gave a value of around 80 N, which is 50 times greater than the weight of all the plates.

After what the force was measured for a different number of sheets placed simultaneously inside their case, for a batch of distinct distances between the center of the magnet and the center of mass of these sheets. The average was made on all the positions for several arrangements. Distances were made to vary between -5 and 10 cm. One could observe that the force cancels

close to the center of the magnet, changes its sign when crossing it whereas it reaches a maximum at around 5 cm above the center and a minimum at around -5 cm below this latter. Away from the center the force is assumed to cancel once again.

For one plate only, the maximum value attained by the force is around 10 N. As the number of plates placed in the container is increased to n, the value taken by the force is more or less multiplied by n, and this might be especially seen by computing the extrema. However, because the plates are not all exactly the same, sometimes the force acting on them is a little bigger or smaller and this affects the global behaviour obtained for n plates at a time.

Then the force as measured for one sheet as a function of its orientation and its position inside the housing. As expected, both these parameters do not have a strong influence on the results obtained. However, as the plate is oriented in one side than in the other, slight differences appear because of the lack of accuracy of the measuring method. Concerning the position, one could observe that the force was lightly higher on one side than on the other, and most of the time even greater at the center of the container. This behaviour might be attributed to magnetic field which is not uniform for a given distance to the center of the magnet yoke.

Several physical parameters related to the sheets and that may influence the force were finally studied. The dimensions and the volume of the plates, as well as their mass and density, were investigated, yet nothing could have been said on the existence of a possible correlation between one of these parameters and the value taken by the force. The only observation made was that two clouds of points seem to appear on each scatter plot that was drawn. However, no one can tell with the sample used if this is simply due to the peculiar plates given by the factory or if it is an actual behaviour gadolinium may exhibit. At the very least this short study allowed to know the exact dimensions and weight of the plates.

Some improvements could be made in order to understand better how gadolinium reacts to the influence of an external magnet ; the measuring system could especially be enhanced. Moreover, other materials could be tested in order to compare them, as well as different magnet values. There are many other possibilities that may be investigated in order to best design a magnetocaloric prototype. The following section talks about the instrumentation that should accompany the operation of the demonstrator, then the final design of this latter is described in the last section.

4. Instrumentation

This section presents the instrumentation needed to highlight the performances of the prototype. To assess the quality of the device, temperature measurements are required at several locations along the AMR bed and at the HHEX and the CHEX. They can be taken using thermocouples ; those utilized here will be first described and tested. An acquisition card and a Labview program will be utilized to collect temperature data.

4.1 Principle : the Seebeck effect

To perform temperature measurements, different sensors can be used but the easiest method is to utilize thermocouples that can be quickly handmade and allow measurements in a large temperature range. They are also cheap, but they are limited in accuracy compared to other

temperature sensors. They typically allow to measure temperatures with up to a 0.1 K precision. However, this is not especially a problem in this case because the temperatures obtained while the device is working should vary by a few degrees.

In the present case, type T thermocouples have been chosen ; they are constituted of Copper and Constantan, an alloy of Copper and Nickel with a high resistance. The basic principle of working of a thermocouple is indeed the Seebeck effect, which consists in the appearance of a voltage difference due to a temperature gap between two dissimilar materials. In any conducting material, a temperature gradient ΔT yields a voltage gradient ΔV and both are linked through a proportionality coefficient as

$$\Delta V = -S(T)\Delta T, \tag{5.4}$$

with $S(T)$ the Seebeck coefficient, depending on temperature. It typically varies in $\mu V/K$ and is characteristic for each material.

4.2 Two-junction thermocouples

Fig. 5.28 shows a diagram of a two-junctions thermocouple of type T, that is, two Copper wires connected on one end to a Constantan wire and on the other end to the entries of a voltmeter allowing to read the voltage difference appearing as the temperature varies. As one may see, four spots are denoted from A to D and represent the different contacts in the electrical circuit. Using the previous relation of Eq. (5.4), one may decompose the voltage difference appearing at the terminals of the voltmeter, ΔV, as follows

$$
\begin{align}
\Delta V &= V_A - V_D \tag{5.5} \\
&= V_A - V_B + V_B - V_C + V_C - V_D \tag{5.6} \\
&= -S_1\left(T_{ref} - T_1\right) - S_2\left(T_1 - T_2\right) - S_1\left(T_2 - T_{ref}\right) \tag{5.7} \\
&= \left(S_1 - S_2\right)\left(T_1 - T_2\right) \tag{5.8} \\
&= \left(S_1 - S_2\right)\Delta T. \tag{5.9}
\end{align}
$$

This relation can be extended for infinitesimal variations of voltages and temperatures, that is,

$$\mathrm{d}V = \left(S_1 - S_2\right)\mathrm{d}T. \tag{5.10}$$

Integrating the former equation between two voltage values V_i and V_f, and two temperature values T_i and T_f, one finds

$$\Delta V = V_f - V_i = \int_{T_i}^{T_f} \left(S_1(T) - S_2(T)\right)\mathrm{d}T \tag{5.11}$$

The relation obtained in Eq. (5.9) is actually true only for small temperature variations which may be approximated as linear. For the Copper-Constantan thermocouple, $\Delta S = S_1 - S_2$ has a value of 40 $\mu V/K$ at ambient temperature.
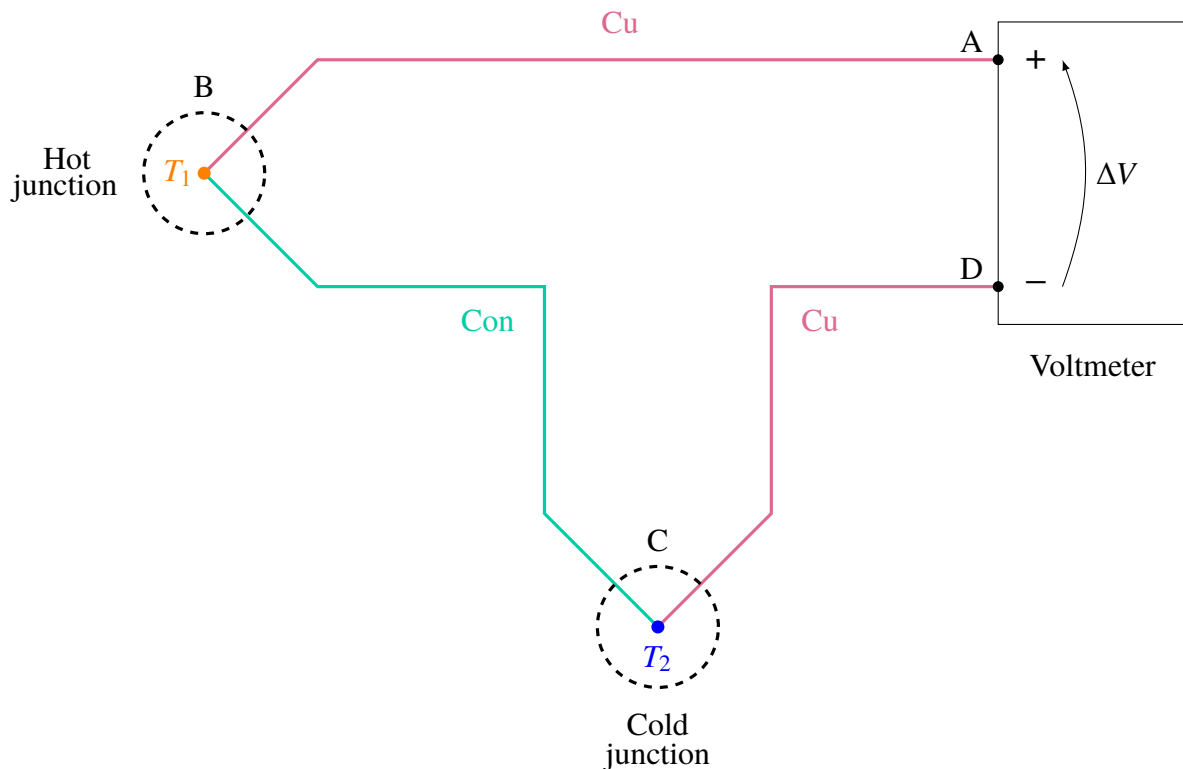
FIGURE 5.28: Example of a two-junction thermocouple of type T.

4.3   Manufacturing the thermocouples and using them

In order to actually make the thermocouples, one simply needs Copper and Constantan wires of around the same diameter, here chosen to be 0.2 mm for the Copper and 0.15 mm for the Constantan. The length is around 1.6 m in total, in order to reach the prototype placed on a table next to the measuring bench. Then the insulating material wrapped around the wires must be scratched a little in order to weld them together. The wires should not be too thick ; if it is the case, they will turn into caloduc and conduct heat in addition to the electric signal. To avoid most of the noise that could be taken into account if the wires are making a loop, they are tightly interlaced.

Five thermocouples were fabricated. Each thermocouple can be connected to an operational amplifier fixed to an acquisition card. The exit of each operational amplifier is then joined to a National Instruments cDAQ-9172 chassis. This one can receive eight modules allowing to perform analog or digital measurements. One module has a capacity of three pairs of inputs and outputs. The whole set is then connected to a computer with a simple USB 2.0 cable, and a LABVIEW program allows to collect and save all the voltage data easily after they are amplified. The acquisition card was handmade by Philippe Laurent at the Montefiore Institute.[1]

In order to measure a temperature with a thermocouple, one needs to put the cold junction at a reference temperature and keep it at this precise temperature during all the measurements.

---

[1] I forgot to take pictures but I assume that everyone has already seen an acquisition card and thermocouples and that this is not a big deal.

In this case, the chosen reference is the ambient temperature but the junctions could as well all be placed in a cold bath of ice. Once the other junction experiences a variation of temperature, a voltage difference should appear at the other terminals of the thermocouple. Then using a reference table, one finds the temperature corresponding to the value of the voltage difference measured.

T (°C)	0	10	20	30
0	0.000	0.391	0.790	0.196
1	0.039	0.431	0.830	1.238
2	0.078	0.470	0.870	1.279
3	0.117	0.510	0.911	1.320
4	0.156	0.549	0.951	1.362
5	0.195	0.589	0.992	1.403
6	0.234	0.629	1.033	1.445
7	0.273	0.669	1.074	1.486
8	0.312	0.709	1.114	1.528
9	0.352	0.749	1.155	1.570

TABLE 5.3: Temperature (in °C)−voltage (in mV) correspondence for a type-T thermocouple.

However, the actual temperature value is not the one of the exact voltage measurement : this latter should be augmented by the voltage difference that corresponds to the ambient temperature if one uses a table taken for a reference temperature of $0\,°C$. An example of such a table is visible in Table 5.3

Finally, the data obtained are treated than filtered with MATLAB. A low-pass filter was used with a cutoff frequency of 10 Hz. The voltage recorded are indeed continuous signals.

4.4 Measurements

The thermocouples will be tested in the following cases: measuring ambient temperature and the human body one. Their accuracy can be checked by using a reference thermometer which was not handmade. In the following, the thermocouples are designated by the names "T 1", "T 2", ..., "T 5".

4.4.1 Room temperature

As aforementioned, the ambient temperature inside the lab can be measured using the five thermocouples and be compared to a reference temperature, T_{ref}. The temperature of the lab is

given by a commercial thermometer to be 22.3 °C. Fig. 5.29 displays the temperature registered during 2 s using LABVIEW then treated with MATLAB.

Table 5.4 shows the average value measured by the five thermocouples, as well as the offset between these and the actual temperature that should have been measured. One sees that all the values recorded by the thermocouples are smaller than this reference. Thermocouples T 3 and T 5 have the worst offsets, respectively equal to −1.34°C (6.01 % of error) and −1.44°C (6.46 % of error). The three other thermocouples present a smaller relative error comprised between only 2 and 3 %.

In Fig 5.29 one sees that the thermocouple values obtained all seem pretty stable as time is passing. As their average values indicated it, they all measure temperatures slightly below the actual value that should be obtained, and thermocouples T 3 and T 5 are the further away from this latter.

	T 1	T 2	T 3	T 4	T 5
$\langle T \rangle$ (°C)	21.81	21.67	20.96	21.71	20.86
ΔT (°C)	-0.49	-0.63	-1.34	0.59	-1.44
$|\Delta T| / T_{\text{ref}}$ (%)	2.19	2.82	6.01	2.65	6.46

TABLE 5.4: Maximal body temperatures measured by the five thermocouples.

4.4.2 Human body temperature

The temperature of a human neck, which is a little lower than the temperature taken e.g. inside the mouth, was recorded during 14 s using all the five thermocouples and the results obtained are presented in Fig. 5.30. Measurement using a commercial thermometer indicates that the temperature denoted T_{ref} should[2] be of 32.8 °C.

As one might see in the chart from Fig. 5.30, all thermocouples react in the same time and relaxes in more or less the same time too after the measurement is taken. However, the relaxation time is much longer. One also notices that three thermocouples reach the same measurement value, but thermocouples x and y always display values a little bit smaller.

When computing the exact maximum reached by all thermocouples, one gets the values presented in Table 5.5. In this Table, one also sees the difference between the reference temperature and the maximum, that can be considered as offsets existing for each thermocouples. Thermocouples T 3 and T 5 thus have the worst offsets of respectively −2.09 °C (6.37 % of error) and −1.10 °C (3.35 % of error). All the three others give measurements close to the reference with an error of less than 1 %.

The relative errors made on the measurements is not the same as the ones computed in the previous case. This might be due to the fact that the thermometer used for having a reference

---

[2]My body temperature does not overcome 36 °C so this value must be accurate.
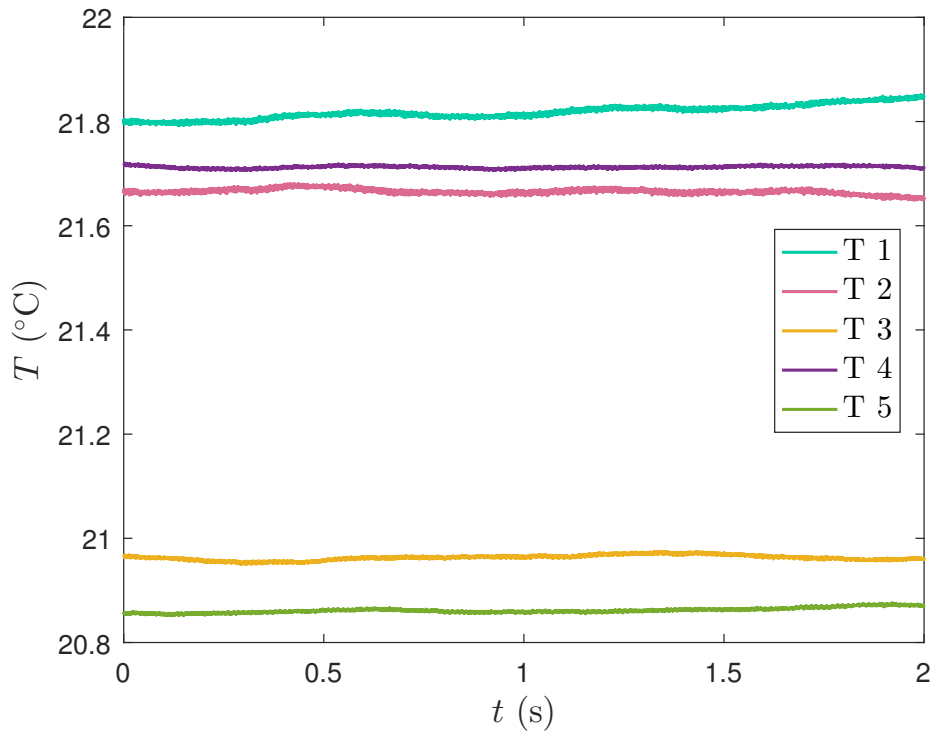
FIGURE 5.29: Room temperature measured by the five thermocouples, on a period of 2 s.

temperature was either more accurate or not as much as the one utilized in the present case. For measuring the ambient temperature in the lab it was a mercury thermometer ; for recording the body temperature it was a digital thermometer.

	T 1	T 2	T 3	T 4	T 5
T_{max} (°C)	32.83	32.61	30.71	32.91	31.70
ΔT (°C)	0.03	-0.19	-2.09	0.11	-1.10
$\lvert \Delta T \rvert / T_{ref}$ (%C)	0.09	0.58	6.37	0.34	3.35

TABLE 5.5: Maximal body temperatures measured by the five thermocouples.

4.4.3 Conclusions

All five handcrafted thermocouples have been proven to work, despite the fact that compared to the actual temperature they should measure, they present a small offset. For thermocouples T 1, T 2 and T 4, the relative error made on the measurements because of this offset was less than 3 %. On the other hand, thermocouples T 3 and T 5 present a larger offset and always record values inferior to the reference ones.
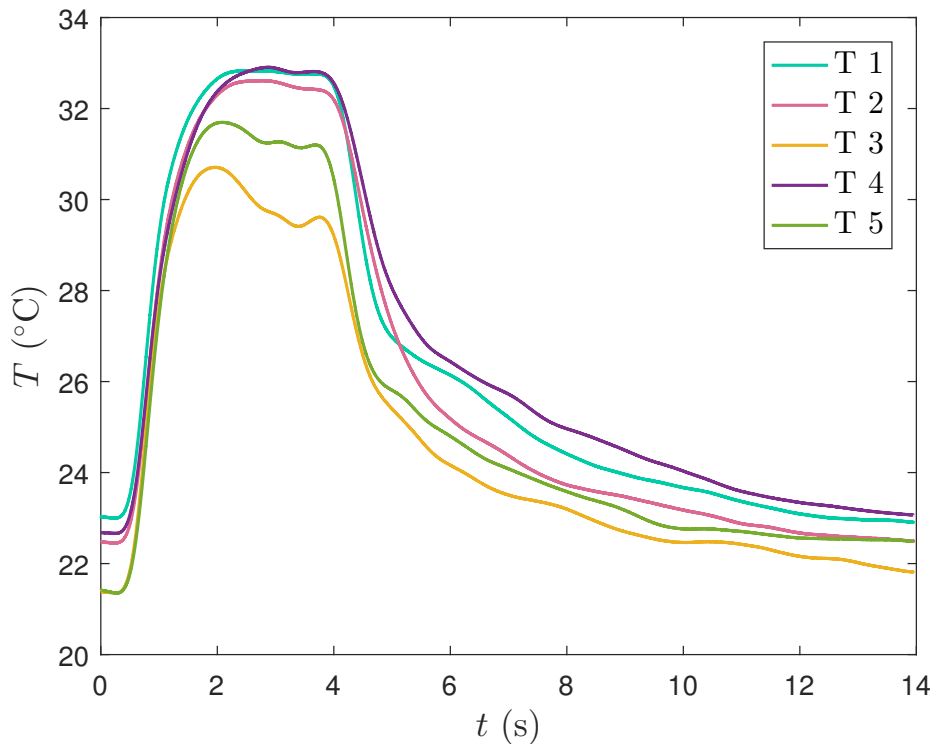
FIGURE 5.30: Temperature of a human neck measured by the five thermocouples, on a period of 14 s.

5. Final design of the device

This last section aims at presenting the design of the prototype in more details. The container used to hold the plates in place will be described in more details, than the choice of the guidance system and the motor will be discussed. A word will then be said about the hydraulic circuit and the remaining parts of the device.

5.1 Choice of the magnet

In numerous papers people investigate how they could best optimize the magnet they will use for their demonstrator but here there was not a lot of options. The magnet utilized was already at the lab and seemed well suited for the present application when compared to what has already been made in the literature. Plus, its magnetic field has a typical value for magnetic refrigeration which actually makes it a very good candidate.

5.2 Choice of the material

The reason of the choice of gadolinium as the magnetocaloric material has already been explained in details in Chapter 2. One uses plates instead of e.g. powder because this latter is toxic. Small spheres could also have been used, and many papers make a comparison between them and the sheets, as e.g. in Tu[1].

The plates were chosen to be 100 mm long, 25 mm wide and 1 mm thick by looking at what was already been made in the literature, and by taking into account the fact that these plates should fit the magnet yoke dimensions.

5.3 Housing of the plates

As aforementioned, a PVC tube in which are found the gadolinium plates allows to move them in and out of the magnet to ensure the (de)magnetization processes and to perform the heat exchanges with the working fluid. To be able to hold the plates still inside the tube, one has to design a suitable housing that was 3D printed at the "Systèmes microélectroniques intégrés" (μsys) lab at the Montefiore institute, with the kind help of Gérald Colson. The template itself was done using the AutoCAD software. Some physical constraints must be taken into account, all listed hereafter.

- The container must first fit the magnet yoke, namely it should be cylindrical with a diameter a bit smaller than that of the magnet. Because one needs to place the housing in a tube to move it in and out of the magnet, the thickness of the tube also needs to be accounted for. The diameter of the housing was thus set to 43.3 mm, whereas the diameter of the magnet yoke is not exactly 50 but 45 mm. The PVC tube should thus be carved adequately in order for its inner and outer diameters to fit these dimensions.

- The housing should also be at least 100 mm long in order for the plates to be held on their whole length. But the plates need to be sustained at both ends so they will remain inside the housing, thus a cap is added on each side. This cap should however still be pierced in order for the fluid to be able to flow through the entire device.

- The plates are 1 mm thick and 25 mm wide. Hence, suitable apertures should be made in order to hold them. Not all the twenty sheets can fit the available space. Moreover, because the 3D printer has a limited accuracy of around 1 mm, to make sure that the device will not experience small fractures or failure during the printing process, the spacing between the plates was chosen to be 2 mm. This permits to place eight gadolinium plates at a time.

- Because of this limited precision of the 3D printer once again, the apertures made for the sheets are set to 1.2 mm. The machine will indeed be more likely to use a little more raw material than a bit less. The width of the holes left for the plates are set to 25 mm. On the other hand, the spacing left open so that the fluid may flow in between the sheets and perform heat transfer is only 20 mm thick.

- The apertures made for the sheets are, once again because of the printer accuracy, placed in a staggered arrangement. One can picture the ensemble as follows: there is a large, rectangular opening for the fluid in the middle of the housing, and the holes made for the plates exceed this latter on both sides but not in a symmetrical fashion. On one side the aperture will be 4 mm longer than the initial hole, and 1 mm (again set to 1.2 mm) on the other side. Then one simply alternates between the plates shifted more to the left or to the right of the central hole. This is visible in e.g. Figs 5.10 and 5.13 from pages 85 and 86 but it will be detailed afterwards.

- Finally, because the 3D printer would have trouble printing the 100 mm-long device at a time, it is split in four parts: two middle sections which actually hold the plates, and two caps to close the whole set. These pieces must be attached together and one might use screws to do so. A suitable hole is thus added on two sides of the housing, here having a 3 mm diameter but any screw could be used.

5.3.1 Thermocouples

In order for the thermocouples to be put in contact with the AMR bed, one should also pierce little holes on the side of the container and the tube holding it. In the present case five thermocouples were fabricated and can be placed along the sheets. This would allow to measure the temperature gradient appearing along the AMR bed during the operation of the device. They were not added to the template of the case because the precision of the 3D printer would not allow to make holes as tiny as the diameter of the thermocouples.

5.3.2 AutoCAD

Fig. 5.32 displays the middle section of the housing, with all its dimensions, that was drawn with AUTOCAD. Two of them were 3D printed, each having a length of 45 mm. On the other hand, Fig. 5.31 shows the cap used to terminate the container and hold the sheets in place. It has a total length of 8 mm, with 5 mm dedicated to hold the plates. The one draw in Fig. 5.31 as well as its symmetric were also 3D printed in order to close the container.
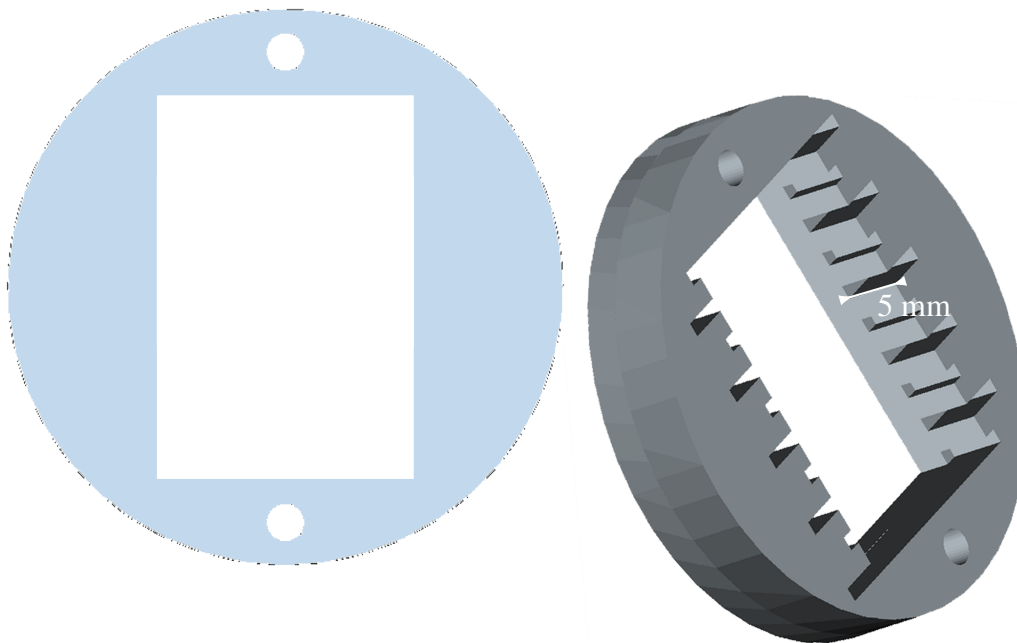

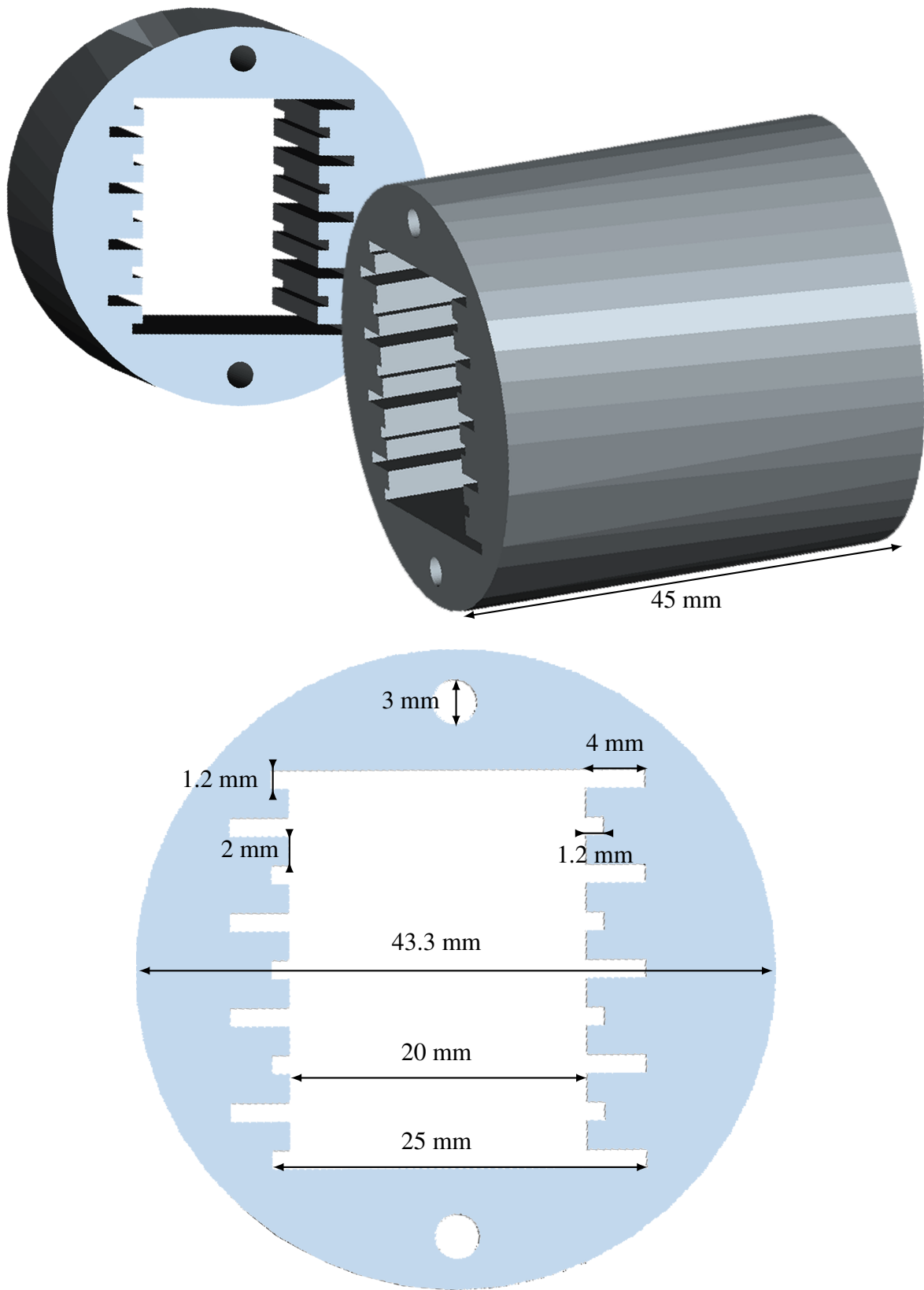
FIGURE 5.31: Cap of the housing drawn with AUTOCAD.

45 mm

3 mm

4 mm

1.2 mm

2 mm

1.2 mm

43.3 mm

20 mm

25 mm

FIGURE 5.32: Middle section of the housing of the plates and its dimensions, drawn with AutoCAD

5.4 Guidance system

As already explained, the main purpose when measuring the magnetic force acting on eight plates at a time in order to choose a proper guidance system and a motor. One found out that this force does not exceed 80 N.

The guidance system was fabricated by the Bosch Rexroth company but ordered at the LRJ sprl. The model chosen was the LF6C linear guidance system. It consists in a carriage gliding on a strap. The total length is of 1350 mm. The carriage itself has a length of 500 mm and a width of 90 mm.

The maximum admissible moment $M_{\text{adm, max}}$ the system can handle in the direction exerted by the magnetic force is of $0.4 \times A\,\text{N m}$, with A the length chosen for the carriage in mm. This

$$M_{\text{adm, max}} = 0.4 \times 500 = 200\,\text{N m}.$$

If the system is attached to the carriage at e.g. a distance of 50 cm, the force never overcoming 80 N, one finds that the maximum magnetic moment that could be exerted on the system, $M_{\text{mag, max}}$, is equal to

$$M_{\text{mag, max}} = 80 \times 0.5 = 40\,\text{N m},$$

namely one ensures that $M_{\text{mag, max}} < M_{\text{adm, max}}$.

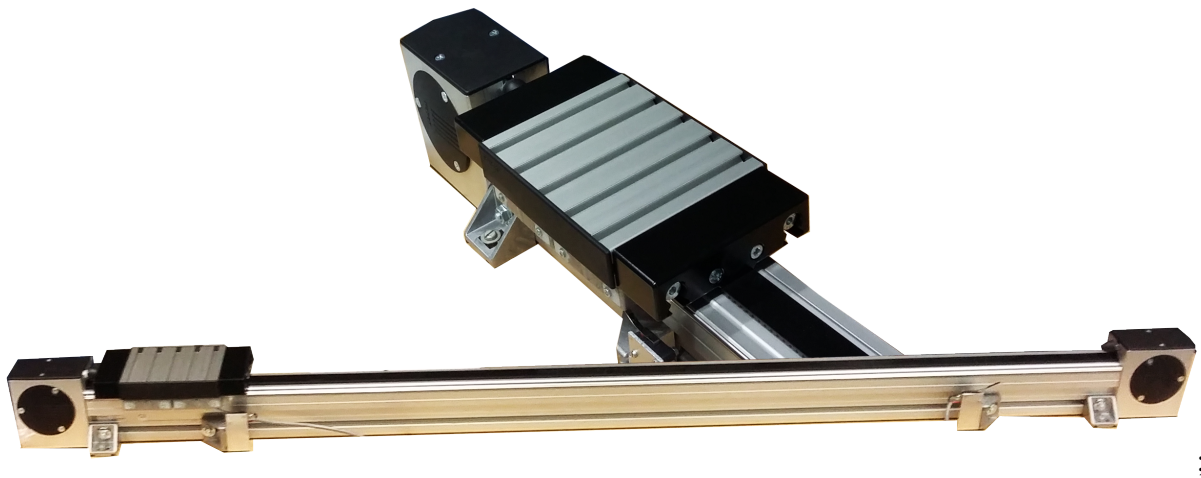A picture of the guidance system and of the carriage is visible in Fig. 5.33.

FIGURE 5.33: Linear guidance system provided by the LRJ company.

5.5 Motor

The motor was provided by Leclerq Energy. It consists in a screw motoreducer Motovario NMRV040-2AWAC71-02F, along with a mono-phase frequency dimmer and a reaction arm. Moreover, a controller allows to program the behaviour of the motor. Besides this motor, limit switches were to be added at each end of the guidance system to allow the back-and-forth motion of the ensemble.

A picture of the motor along with its controller unit is visible in Fig. 5.34. One also sees in this photo the way the motor was fixed to the guidance system.

FIGURE 5.34: Motor provided by the Leclercq Energy company.

5.6 Final design

In Figs 5.36 and 5.35 hereafter, one sees a sketch of the final design of the magnetic part of the prototype along with its dimensions. Some parts are still missing for the prototype to operate properly, such as the hydraulic circuit and the fixation of the ensemble.

5.6.1 Fixations and support

As one might see it in Fig. 5.36, an additional support should be added in order to prevent the tube from bending under the action of the magnet force. However, this support does not need to look like it is drawn in the picture and it would more likely consist in bearing fixed on the sides of the whole system.

One also needs to fix properly the tube to the carriage ; this might be done by using aluminum bars. Their length should not exceed $M_{\text{adm, max}}/F_{\text{mag, max}}$, namely $200/80 = 2.5$ m. Thus by taking bars which are 30 cm long for instance (available at the lab), one ensures the good working of the guidance system.

The final support required is the one needed to hold the magnet in place. It should be set at the perfect height so that the PVC tube containing the housing can move through its yoke.

5.6.2 Hydraulic circuit

The prototype cannot operate if the AMR does not exchange heat with a working fluid, which was chosen to be water. One thus still needs to design a hydraulic circuit comprising all the items of the subsequent list.

- Suitable tubing for transporting the fluid through the circuit, as well as an adequate support.

- A hot heat exchanger and a cold one to make sure that the refrigerator does not violate the second principle of thermodynamics.

- A pump in order to ensure the flow of water through the tubes.

- Appropriate connections between the hydraulic circuit and the housing containing the gadolinium plates.

- A water reservoir in order to fill the circuit.

- One also needs to think about the instrumentation required for measuring the temperatures at the entrance and the outlet of the heat exchangers.

Once this hydraulic circuit is designed, the ensemble may be put all together and one can then test if the prototype works properly or not and bring the necessary corrections if this is not the case.

- A - tube containing the Gadolinium plates;

- B - magnet;

- C - additional support for the tube;

- D - linear guide system;

- E - carriage;

- F - support fixed to the tube;
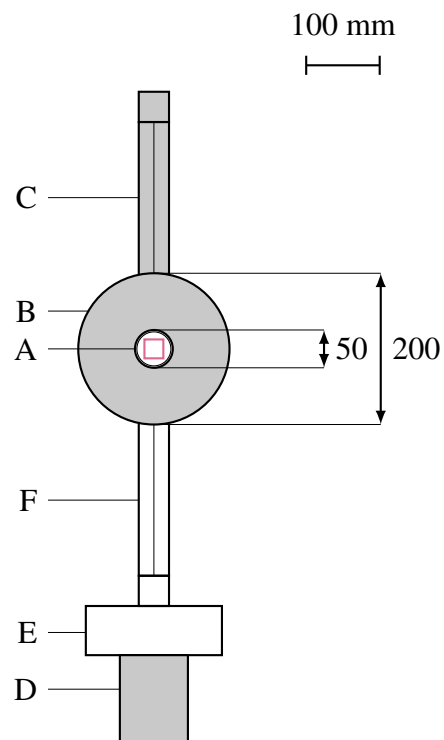
- F - motor attached tp the guidance system.

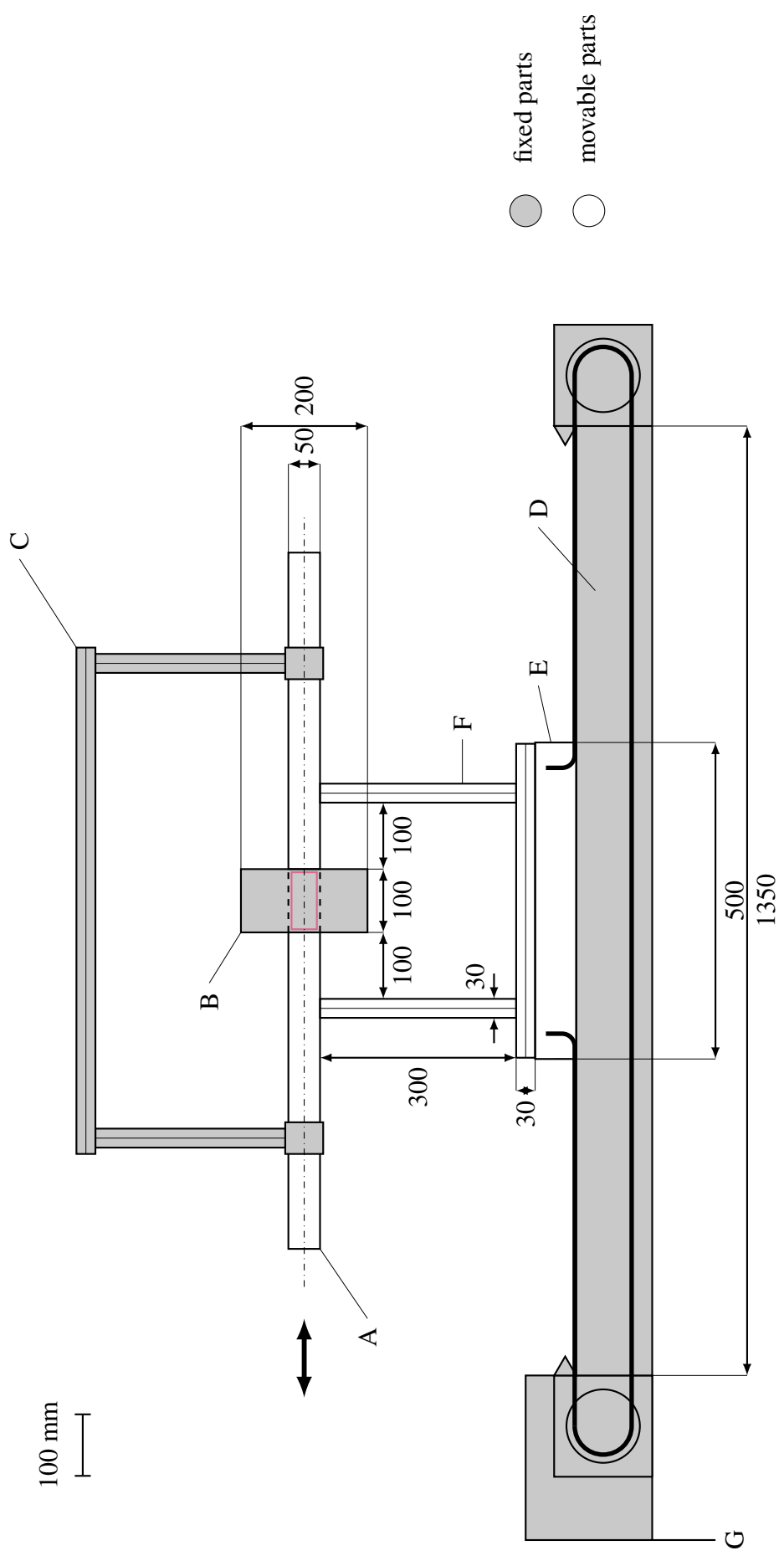FIGURE 5.35: Front view of the prototype.

FIGURE 5.36: Profile view of the prototype.

Summary (1/2)

- The prototype will consist in plates of Gd moving in and out of a cylindrical 1.05 T-magnet yoke in a reciprocating fashion. To ensure this motion one wants to use a linear guidance system. In order to properly choose this latter the magnetic force acting on the sheets as they enter the non uniform magnetic inductive field of the magnet must be evaluated.

- This magnetic force was studied for several number of sheets, different configurations of them and as they were placed at distinct distances from the center of the magnet. It was found out that when the 8 plates are located at the distance of .. cm from the center of the magnet yoke the force reaches a maximum value of .. N.

- Moreover, for every number of plates studied the curve showing the force as a function of the distance from the magnet center had more or less the same shape. This means that the force was null at the very center of the yoke, reached out a maximum (resp. minimum) at the top (bottom) edge of this one to diminish further away and cancel at the infinity.

- This force was also found out not to depend much on the physical properties of the sheets, nor their position or orientation, although the sample of only 20 plates may not be enough to assert such a behaviour or not. However the shape of the field inside the magnet gap has an influence of it since the force is greater at the center whereas it decreases a little bit closer to the edges. Finally, the magnetic force does not depend on the orientation of the plates inside the magnet yoke.

- The main issues when performing the measurements were the fact that the sheets are sensitive to environmental conditions and that the force needed from a few seconds to several minutes to stabilize. The conditions of measurements were in fact quite tenuous and prevented a good precision to be achieved. To analyze more precisely the behaviour of the plates inside the magnet gap one should ensure better measuring conditions.

- The housing containing the plates and that will be placed in a tube which will itself glide inside the magnet yoke was designed with AutoCAD and then 3D-printed. Some constraints were taken into account for doing so: the dimensions of the plates, the need for a coolant to pass through the system, the fact that some spacing had to be saved for placing some thermocouples. These latter will permit to analyze the performances of the prototype.

116

Summary (2/2)

- The linear guidance system chosen for the prototype was provided by the LRJ company and its carriage can handle a maximum moment of 200 N m. The motor along with its controlling unit, on the other hand, was furnished by the Leclercq Energy company, then fixed to the guidance system in order to make its carriage move along it.

- The supports of the tube, its fixation to the carriage and additional supports as well as a housing for the magnet still need to be built. The hydraulic circuit should also be designed and constructed in order for the prototype to be operating.

- The instrumentation, however, is already ready and functioning. Five type T thermocouples were made, that is thermocouples constituted of Copper and Constantan wires. They were tested and their offset evaluated. The relative error due to this offset is for two thermocouples of a few percents (between 3 and 6), but for the three other ones it is really small.

- Despite the fact that the demonstrator is not operational and could not be tested, a few things were learnt from the study of the magnetic force acting on the gadolinium and the influence of diverse parameters on it. There are some missing pieces to add so as to make the prototype actually work but at the very least the basis is already there.

References

[1] J. Tušek, A. Kitanovski, S. Zupan, and A. Poredoš, "A comprehensive experimental analysis of gadolinium active magnetic regenerators," vol. 53, pp. 57–66, 2013.

[2] A. Kitanovski, J. Tušek, U. Tomc, U. Plaznik, M. Ožbolt, and A. Poredoš, *Magnetocaloric Energy Conversion*. Switzerland: Springer, 2015.

[3] F. Allab, *Étude et conception d'un dispositif de réfrigération magnétique basé sur l'effet magnétocalorique géant*. PhD thesis, Institut National Polytechnique de Grenoble, May 2008.

[4] E. Brück, "Developments in magnetocaloric refrigeration," vol. 38, 2005.

6

CONCLUSION

The search for more environmentally-friendly refrigeration technologies keeps rising around the world in order to replace the steam compression technique which is nowadays still utilized but unfortunately involves nocive gases with global warming and ozone layer depletion potential. In this context, scientists have gained interest in the magnetocaloric effect-based refrigeration around room temperature during the past few years. The purpose of this master thesis was to design a prototype for magnetic refrigeration that uses linear, reciprocating motion between a 1.05 T-field cylindrical, Halbach magnet and gadolinium sheets.

In this work, at first the theory underlying the MCE was fully reviewed. Basic thermodynamic relations were derived and Weiss's theory of ferromagnetism was utilized in order to perform theoretical calculations on the effect appearing in gadolinium. This material is however not well suited for commercial application of the technology because of its expensive price. Other alloys that may be used for magnetic refrigeration were thus reviewed too. A survey of the possible cycles that can be performed in order for a refrigerator to work was also made, but the most utilized one is the active magnetic regeneration cycle.

After what a small tour of already existing prototypes was realized. The very first one was built in 1976 and improvements have been achieved since then. The discovery of materials presenting a giant MCE as well as the use of permanent magnets instead of superconducting ones were two major advances in the domain. Demonstrators already made around the world show other interesting ideas, such as the use of a layered AMR bed that allows to fully exploit MCE around the Curie point of each material involved. Another one is to utilize two beds placed side to side, moving in and out of the magnet so as to reduce the magnetic force and demagnetization effect appearing in the material, which can be problematic during the operation of the device.

Knowing what has already been achieved in the field, a thermal study was then conducted for the present prototype. First a dimensional analysis allowed to assess the relative importance of the physical phenomena arising and that can enter in competition with one another. Next, the heat exchanges appearing between the gadolinium sheets and the working fluid were numerically computed using Matlab, and analyzed in details. One used the $\varepsilon-$NTU method which permits to design heat exchangers, and to discretize the governing equations obtained in this way the well-known centered-in-space, backward-Euler method was chosen.

But a heat analysis alone is not sufficient for designing the prototype, and one needs to study the magnetic force acting on the gadolinium plates as they enter or leave the magnet. The influence of this one may be estimated in several manners: first the force as a function of the

distance between the sheets and the center of the magnet was measured and analyzed. Then the plates were positioned in different manners inside their support so as to see if the force acting on them varies in this case. The influence of the physical parameters was also evaluated, such as the density of the plates. The method used for performing all the measurements was quite simple and consisted in measuring the weight of the plates outside and inside the magnet ; the difference between both of them then gives the magnetic force acting on the plates.

Next, thermocouples were made and tested in order to measure temperatures and asses the performances of the prototype. The final step of the work was the description of the parts required for the good working of the device. A suitable housing that was 3D-printed holds the gadolinium plates in place. This container is put inside a PVC tube that is made to move in and out of the magnet yoke by being fixed to a linear guidance system provided by the LRJ company. The motion is then ensured by a motor bought at the Leclercq Energy company. A suitable hydraulic circuit to perform exchanges between the gadolinium sheets, the working fluid and two heat exchangers placed outside the device, a cold and a hot one, still needs to be constructed. This very last stage would allow to finish the mounting of the prototype and test it for good.

Despite the fact that the prototype was not fully terminated, this project was still an enriching experience in the sense that it reunited capacities a physicist engineer should acquire and enhance during his career, such as deriving numerical models, even very simple ones, or perform experimental measurements in order to assess the behaviour of something. The subject really acts as a bridge between different fields, gathering thermodynamics along with heat exchanges and ferromagnetism theory.

But beyond that, the magnetocaloric effect study is part of a process of scientific renewal. The current global consumption in electricity, especially the part dedicated to refrigeration, as well as global warming and ozone depletion, are part of an undeniable, sad reality that needs to be faced. The search for alternative technologies which will harm less our beautiful nature is now crucial, and it is more than ever required to find environmentally-friendly solutions.

APPENDICES

1. Magnetic force acting on Gadolinium plates
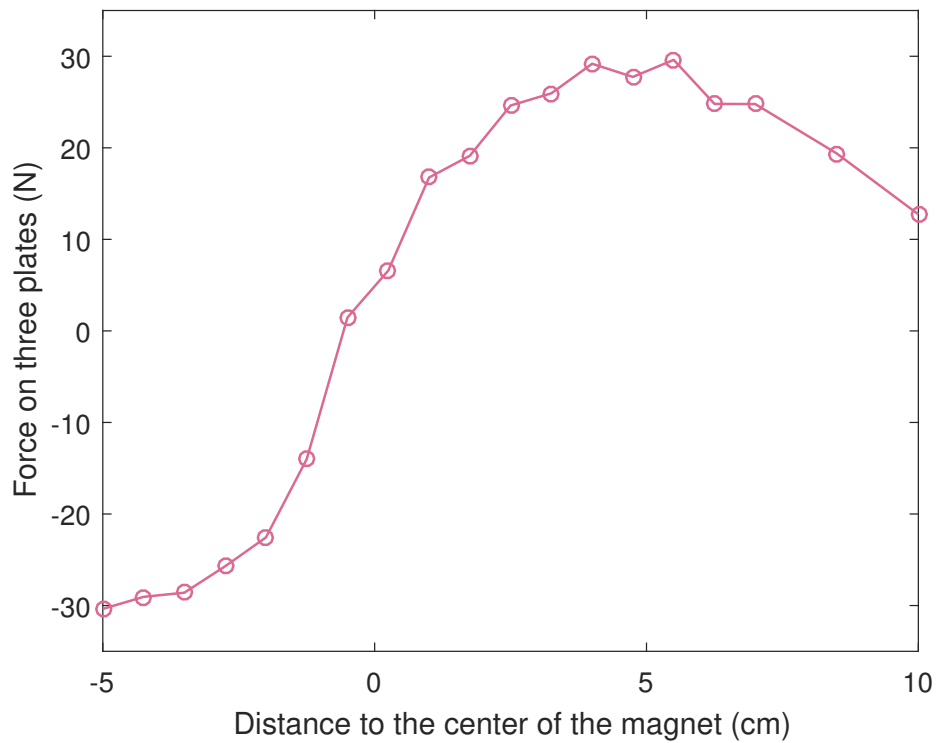
1.1 Three plates

FIGURE 1: Force acting on one plate as a function of the distance of the housing from the yoke center.
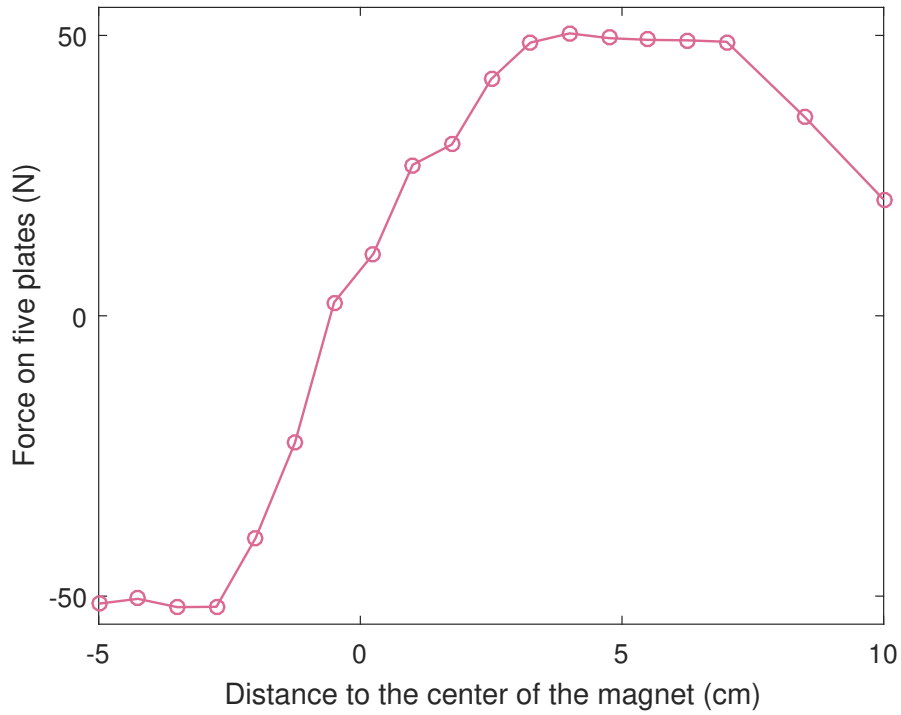
1.2   Five plates

FIGURE 2: Force acting on one plate as a function of the distance of the housing from the yoke center.
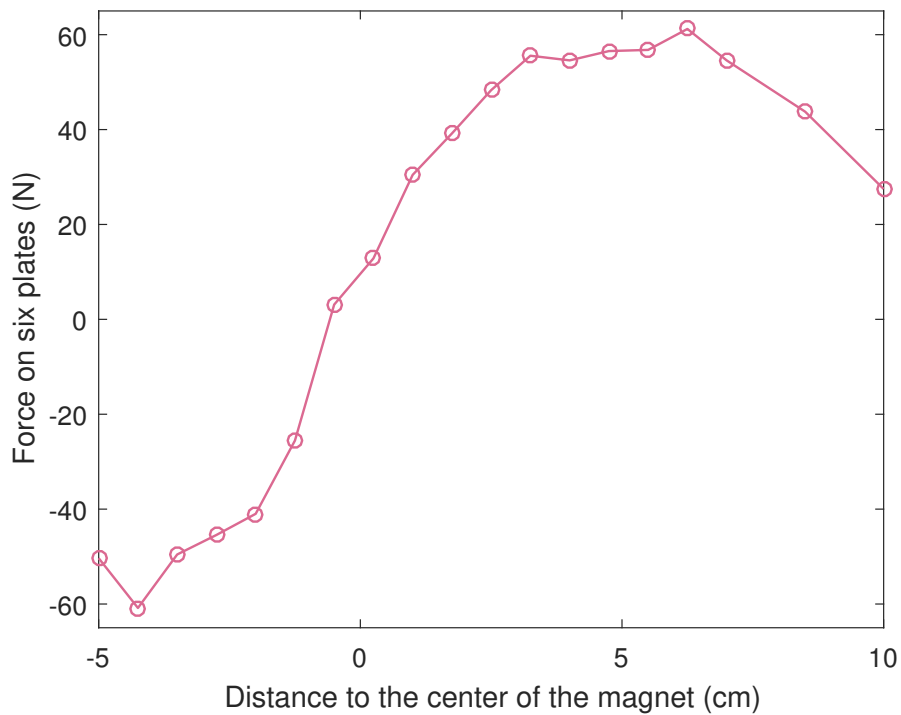
1.3   Six plates

FIGURE 3: Force acting on one plate as a function of the distance of the housing from the yoke center.
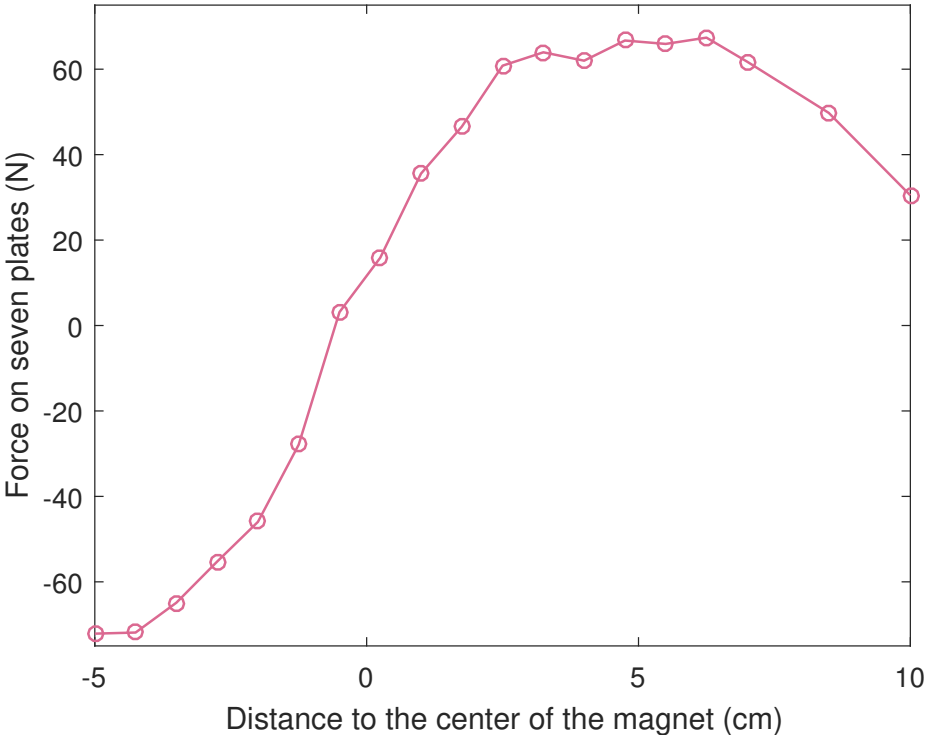
1.4 Seven plates

FIGURE 4: Force acting on one plate as a function of the distance of the housing from the yoke center.